POLISH ACADEMY OF SCIENCE
COMMITTEE FOR ELECTRONICS AND TELECOMMUNICATIONS

# ELECTRONICS AND TELECOMMUNICATIONS QUARTERLY

KWARTALNIK ELEKTRONIKI I TELEKOMUNIKACJI

VOLUME 53 — No 1

WARSAW 2007

Address of Editorial Office
00-665 Warszawa, ul. Nowowiejska 15/19 Politechnika, pok. 470
Instytut Telekomunikacji, Gmach im. prof. JANUSZA GROSZKOWSKIEGO

Editor-on-duty
Wednesdays and Fridays
From 2pm to 4pm
Phone number: (022) 234 77 37

Telephone numbers
Editor-in-Chief: 0607240533
Deputy Editor-in-Chief: 0502660096
Responsible Secretary: 0500044131

| | |
|---|---|
| Ark. wyd. 8,0 Ark. druk. 6,25 | Podpisano do druku w lutym 2007 r. |
| Papier offset. kl. III 80 g. B-1 | Druk ukończono w lutym 2007 r. |

Publishing
Warszawska Drukarnia Naukowa PAN
00-656 Warszawa, ul. Śniadeckich 8
Tel./fax: 628-87-77

KO — czł.
dr hab. inż.
dr hab. inż.
rof. dr inż.

# *IMPORTANT MESSAGE FOR THE AUTHORS*

The Editorial Board during their meeting on the 18th of January 2006 authorized the Editorial Office to introduce the following changes:

## 1. PUBLISHING THE ARTICLES IN ENGLISH LANGUAGE ONLY

Starting from No 1'2007 of E&T Quarterly, all the articles will be published in English only.

Each article prepared in English must be supplemented with a thorough summary in Polish (e.g. 2 pages), including the essential formulas, tables, diagrams etc. The Polish summary must be written on a separate page. The articles will be reviewed and their English correctness will be verified.

## 2. COVERING THE PUBLISHING EXPENSES BY AUTHORS

Starting from No'2007 of E&T Quarterly, a principle of publishing articles against payment is introduced, assuming non-profit making editorial office. According to the principle the authors or institutions employing them, will have to cover the expenses in amount of 760 PLN for each publishing sheet. The above amount will be used to supplement the limited financial means received from PAS for publishing; particularly to increase the capacity of next E&T Quaterly volumes and verify the English correctness of articles. It is neccessary to increase the capacity of E&T Quarterly volumes due to growing number of received articles, which delays their publishing.

In case of authors written request to accelerate the publishing of an article, the fee will amount to 1500 PLN for each publishing sheet.

In justifiable cases presented in writing, the editorial staff may decide to relieve authors from basic payment, either partially or fully. The payment must be made by bank transfer into account of Warsaw Science Publishers The account number: Bank Zachodni WBK S.A. Warszawa Nr 94 1090 1883 0000 0001 0588 2816 with additional note: "For Electronics and Telecommunications Quarterly".

Editors

Electron
Elektrotechn
The E&T
of Polish Ac
Quarterly is
theoretical,
recognised a
tronics, radi
The auth
young resea
The arti
critical estim
branch of t
mathematica
and ISO (In
All the
specialists w
The publish
*Science and*
The per
telecommun
Moreover it
Each au
distribution
author. The
accessible.
The artic
and the ed
publications
editorial off
The artic
office addre

# Dear Authors,

Electronics and Telecommunications Quarterly continues tradition of the "Rozprawy Elektrotechniczne" quarterly established 53 years ago.

The E&T Quarterly is a periodical of Electronics and Telecommunications Committee of Polish Academy of Science. It is published by Warsaw Science Publishers of PAS. The Quarterly is a scientific periodical where articles presenting the results of original, theoretical, experimental and reviewed works are published. They consider widely recognised aspects of modern electronics, telecommunications, microelectronics, optoelectronics, radioelectronics and medical electronics.

The authors are outstanding scientists, well-known experienced specialists as well as young researchers – mainly candidates for a doctor's degree.

The articles present original approaches to problems, interesting research results, critical estimation of theories and methods, discuss current state or progress in a given branch of technology and describe development prospects. The manner of writing mathematical parts of articles complies with IEC (International Electronics Commision) and ISO (International Organization of Standardization) standards.

All the articles published in E&T Quarterly are reviewed by known, domestic specialists which ensures that the publications are recognized as author's scientific output. The publishing of research work results completed within the framework of *Ministry of Science and Higher Education* GRANTs meets one of the requirements for those works.

The periodical is distributed among all those who deal with electronics and telecommunications in national scientific centres, as well as in numeral foreign institutions. Moreover it is subscribed by many specialists and libraries.

Each author is entitled to free of charge 20 copies of article, which allows for easier distribution to persons and institutions domestic and abroad, individually chosen by the author. The fact that the articles are published in English makes the quarterly even more accessible.

The articles received are published within half a year if the cooperation between author and the editorial staff is efficient. Instructions for authors concerning the form of publications are included in every volume of the quarterly; they may also be obtained in editorial office.

The articles may be submitted to the editorial office personally or by post; the editorial office address is shown on editorial page in each volume.

Editors

M. Kasznia
I. Olszewsk
A. Dobrogo
with a
K.M. Noga
M. Rawski:
F. Wysocka
approx
Information

CONTENTS

M. Kasznia: Dynamic parameters of synchronization signals ..... 7
I. Olszewski: On line routing of guaranteed bandwidth with restoration ..... 23
A. Dobrogowski, J. Lamperski, P. Stępczak: Analysis of properties of the multiwavelength source with an acousto-optic frequency shifter ..... 39
K.M. Noga, G.K. Karagiannidis: Characterization of Weibull fading channels ..... 47
M. Rawski: Efficient veriable partitioning method for functional decomposition ..... 63
F. Wysocka-Schillak: Design of 2-D FIR filters with real and complex coefficients using two approximation criteria ..... 83
Information for the Authors ..... 97

dyna
descr
time
comp

*Keyw*

Allan
be the qu
The para
signal to
The estin
using the
network i

The
posed by
Symposiu
This cha
of the ph
extended

ELECTRONICS AND TELECOMMUNICATIONS QUARTERLY, 2007, 53, no 1, pp. 7–22

# Dynamic parameters of synchronization signals

MICHAŁ KASZNIA

*Katedra Systemów Telekomunikacyjnych i Optoelektroniki*
*Politechnika Poznańska*
*ul. Polanka 3, 60-965 Poznań*
*mkasznia@et.put.poznan.pl*

*Otrzymano 2006.09.28*
*Autoryzowano 2006.11.22*

The paper presents the methods of characterization of synchronization signals using dynamic parameters. The idea of dynamic Allan deviation and dynamic time deviation is described. Then the procedures of calculating dynamic parameters are presented. Some time effective methods for computing dynamic parameters are proposed. The results of computation for different data series are presented and discussed.

*Keywords:* synchronization signal, Allan deviation, time deviation

## 1. INTRODUCTION

Allan deviation ADEV and time deviation TDEV are the parameters which describe the quality of synchronization signal in the telecommunication network [1, 2, 3]. The parameters allow the variations of time interval provided by the synchronization signal to be assessed and the type of phase noise affecting the signal to be recognized. The estimates of the parameters are calculated for a series of observation intervals, using the sequence of time error samples measured between two timing signals at the network interface.

The characterization of the timing signal using the dynamic parameter was proposed by L. Galleani and P. Tavella at the Joint Meeting of IEEE Frequency Control Symposium (FCS) and the European Frequency and Time Forum (EFTF) in 2003 [4]. This characterization with dynamic Allan deviation (DADEV) allows the variations of the phase noise affecting the analyzed signal to be recognized. This approach was extended by A. Dobrogowski and M. Kasznia at the 18$^{th}$ EFTF in 2004 [5]. The

dynamic time deviation (DTDEV) was introduced and the time effective methods of calculating the dynamic parameters were proposed.

The evaluation of timing signal using dynamic parameters consists in the calculation of the Allan deviation or time deviation values for the segments (slices) of a time error sequence, with a change of the initial point of calculation. The results of calculation are presented in the form of a three-dimensional graph as a function of observation interval $\tau$ and time $t$. Some changes affecting the data sequence (e.g. change of the noise level or change of the dominating phase noise type) may be recognized by the shape of the three-dimensional graph. We can distinguish the calculation for overlapping and non-overlapping segments of data. The arrangement of the segments depends on the number of segments, the time shift between the segments, their length and the length of the whole data sequence. This arrangement (resulting in a specific calculation procedure) influences the form of presented calculation result (i.e. we can obtain different forms of the 3D graphs for the same data sequence).

In the paper the identification of the phase noise changes in the synchronization signals, using dynamic deviations, is described. Then, the influence of the computation procedure (determined by the data segments arrangement) on the form of results obtained is analyzed. The results of DADEV and DTDEV calculation performed for several examples of time error sequences, using different calculation procedures (for overlapping and non-overlapping data segments), are presented and discussed. The multiplication of the computation procedures in the case of dynamic parameters causes an extension of the calculation time, compared with the computation time of the common Allan deviation or time deviation. Some time effective methods for computing the dynamic parameters [5] are presented. The relations between the length of a time error data sequence, data segments (slices) and maximum observation intervals, important for the reliable estimation of the parameter in the telecommunication applications (fulfilling the telecom standards and recommendations) are also discussed.

## 2. IDEA OF DYNAMIC PARAMETERS

The idea of dynamic parameters is simple. Instead of one curve representing the values of ADEV or TDEV as a function of observation interval $\tau$, a set of the curves plotted in the form of three-dimensional graph, as a function of observation interval $\tau$ and time $t$, is considered. As result, we can recognize the changes of the type of phase noise affecting analyzed timing signal. Changing slope of the parameter's curve indicates the changes of the noise type [4].

In order to obtain this form of graph, the following computation procedure is performed. First, the data sequence (time series of time error measured at some network interface) is divided into equal segments (slices) with the length of $T_s$. We can consider overlapping data segments (Fig. 1) and non-overlapping data segments (Fig. 2). The arrangement of the segments depends on the number of segments, their length and the length of the whole data sequence. Then, the calculation of the parameter's value for

a required range of observation intervals for each data segment is done. The results of calculation are plotted in the form presented in Fig. 3.

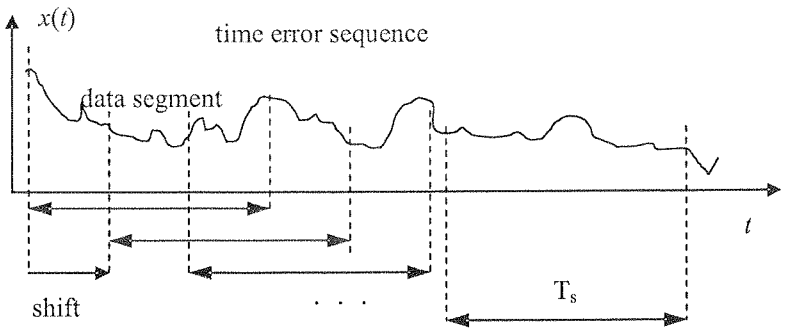


Fig. 1. Overlapping segments of time error sequence

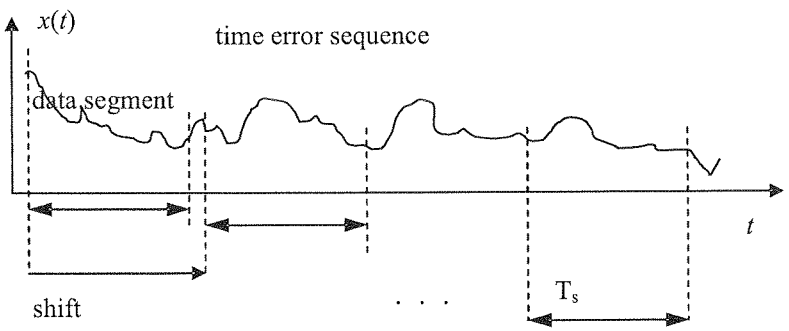


Fig. 2. Non-overlapping segments of time error sequence

The formulae for the estimators of the Allan deviation ADEV and the time deviation TDEV take the form:

$$A\hat{D}EV(\tau) = \sqrt{\frac{1}{2n^2\tau_0^2(N-2n)}\sum_{i=1}^{N-2n}(x_{i+2n} - 2x_{i+n} + x_i)^2} \tag{1}$$

$$T\hat{D}EV(\tau) = \sqrt{\frac{1}{6n^2(N-3n+1)}\sum_{j=1}^{N-3n+1}\left[\sum_{i=j}^{j+n-1}(x_{i+2n} - 2x_{i+n} + x_i)\right]^2} \tag{2}$$

where $\{x_i\}$ is a sequence of $N$ samples of time error function $x(t)$ taken with interval $\tau_0$; $\tau = n\tau_0$ is an observation interval.

The procedure of dynamic ADEV and dynamic TDEV calculation depends on the set of quantities. These are: the length of the whole data series T, the length of the data

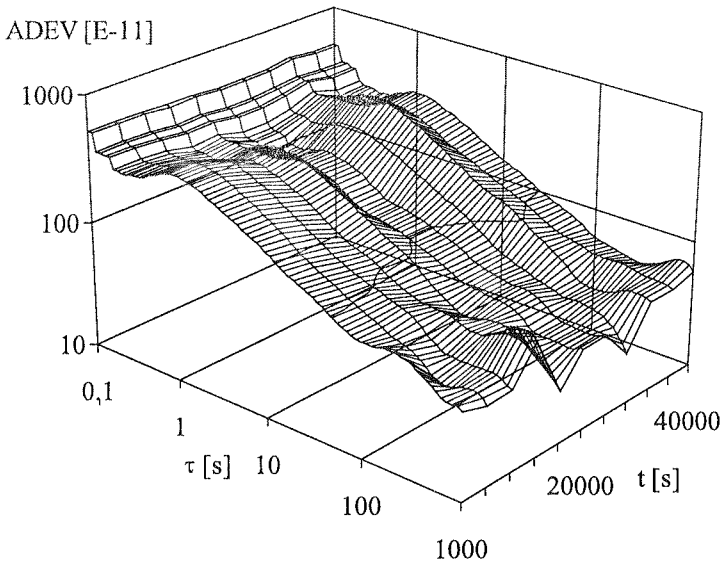


Fig. 3. Example plot of dynamic Allan deviation

segments created within the whole data series $T_s$, the time shift between the initial points of the data segments $t_s$, and the range of observation intervals ($\tau_{min} - \tau_{max}$).

The relation between the whole data series length, the segments' lengths and the time shift $t_s$ determines the number of the segments and the arrangement of the segments (overlapping or non-overlapping). We must also take into consideration the relation between $T_s$ and the maximum observation interval $\tau_{max}$. According to the telecommunication standards and recommendations, the length of the data sequence used for ADEV or TDEV calculation must be 12 to 15 times longer than the maximum observation interval $\tau_{max}$ [1, 2, 3]. The minimum observation interval $\tau_{min}$ is determined by the sampling interval $\tau_0$ : $\tau_{min}$ must be three times longer than $\tau_0$. In practice, the value of the parameter's estimate can be calculated when the length of the data series (in this situation: segment's length) is two times longer than $\tau_{max}$ for ADEV and three times longer for TDEV. Unfortunately, in this case we obtain poor quality of the parameter's estimate.

It may happen that the length of data segment $T_s$, does not fulfill the telecom recommendations, i.e. $T_s$ is shorter than twelve times $\tau_{max}$. In such situation we have two options. The first option is to calculate the parameter's value for each segment for the assumed range of observation intervals (including $\tau_{max}$), but realizing rather poor quality of the estimate for longer observation intervals (of course, $T_s$ has to be two or three times longer than $\tau_{max}$). The second option is to shorten the maximum observation interval $\tau_{max}$ to the value of $T_s/12$ (in accordance with the recommendations) and to calculate the parameter's value for a smaller range of observation intervals [5].

## 3. IDENTIFICATION OF CHANGES USING DYNAMIC ADEV AND DYNAMIC TDEV

In order to demonstrate the applicability of the dynamic approach to the characterization of synchronization signals, the computations of dynamic ADEV and dynamic TDEV for different time error sequences were performed. The common Allan deviation and time deviation were also computed for better comparison of the results obtained. The data sequences used for computation contain the time error samples taken with sampling interval $\tau_0 = 1/30$ s during the time T of 20000 s.

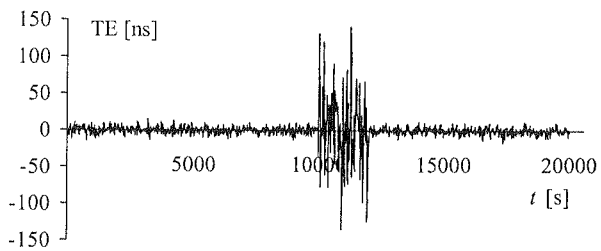


Fig. 4. White phase noise sequence changing its level (sequence A)

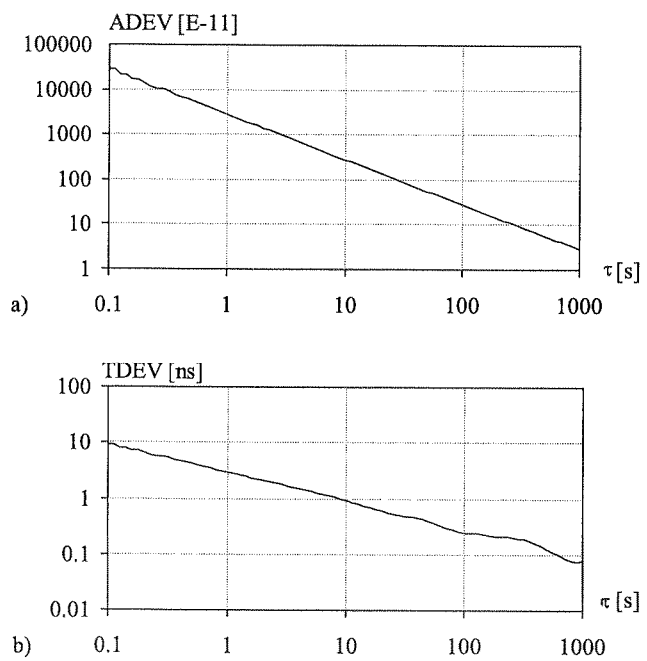


Fig. 5. Allan deviation ADEV (a) and time deviation TDEV (b) for the time error sequence A

The first sequence (denoted as A – Fig. 4) represents the samples of white phase noise, which changes its level for the period of 2000 s after the half of the sequence. The common ADEV and TDEV computed for the observation intervals from 0.1 s to 1000 s are presented in Fig. 5. The slopes of these parameters are typical for the white phase noise and do not indicate the change of the noise level in the middle of the sequence.

The dynamic ADEV and dynamic TDEV for sequence A are presented in Fig. 6. These parameters were computed for 11 overlapping segments with length of $T_s$ = 4000 s and segment's shift $t_s$ = 1500 s. The change of the noise level is well recognized with the use of both parameters.

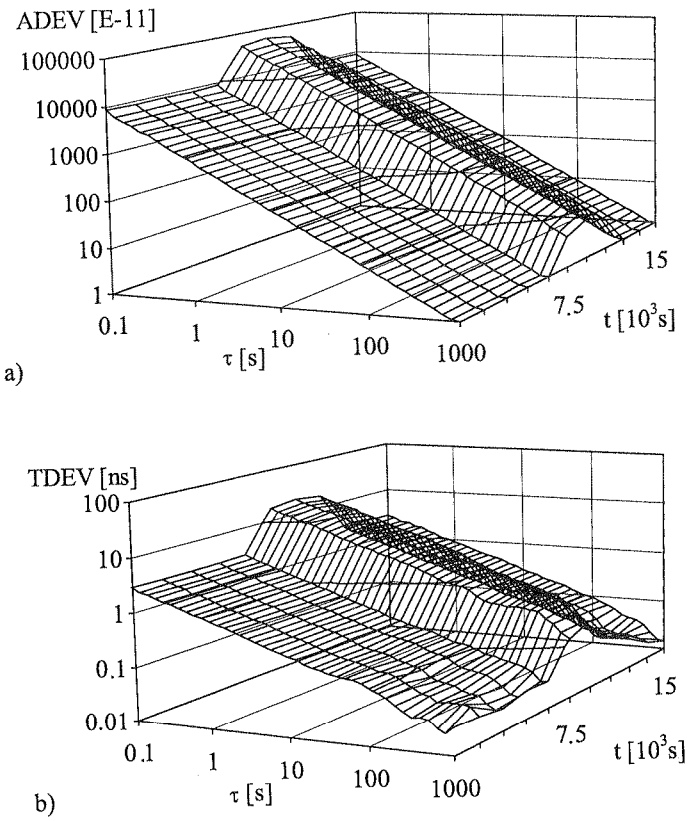


Fig. 6. Dynamic ADEV (a) and dynamic TDEV (b) for the time error sequence A

The next data sequence, (denoted as B – Fig. 7) represents the white phase noise WPM which changes its type to the white frequency noise WFM for the period of 2000 s after the half of the sequence. The Allan deviation ADEV and the time deviation TDEV, computed for this sequence, are presented in Fig. 8. It is hard to recognize the presence of the white frequency noise in the analyzed data sequence from the ADEV

plot. The change of the TDEV slope in the third and fourth decades of the plot indicates only the presence of the white phase noise and the white frequency noise.

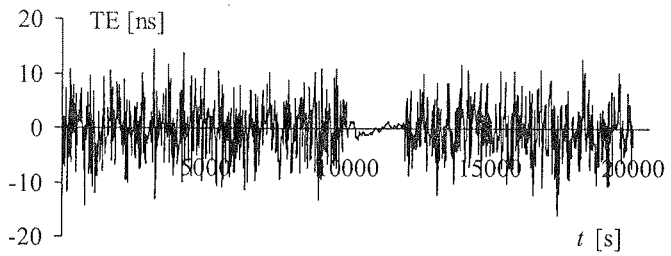


Fig. 7. White phase noise sequence with the white frequency noise inserted (sequence B)

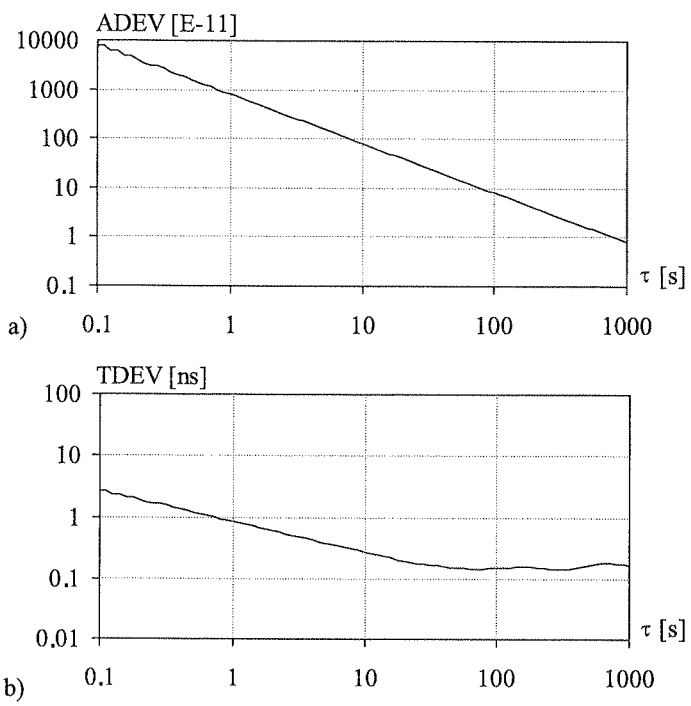


Fig. 8. Allan deviation ADEV (a) and time deviation TDEV (b) for the time error sequence B

The form of the WFM presence in the time error sequences B presented in Fig. 7 can be concluded from the plots of the dynamic ADEV and the dynamic TDEV, presented in Fig. 9. These parameters were computed similarly as for the previous time error sequence. However, the shape of the dynamic TDEV recognizes the presence of the WFM noise much better than the shape of the dynamic ADEV.

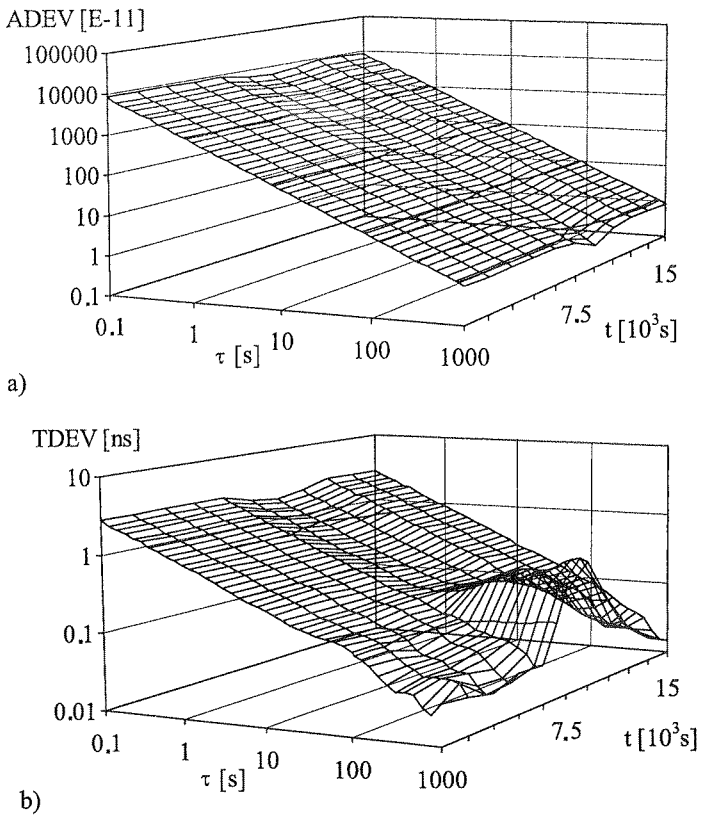


Fig. 9. Dynamic ADEV (a) and dynamic TDEV (b) for the time error sequence B

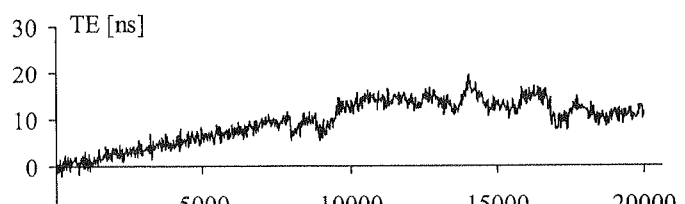


Fig. 10. Time error sequence C combining some kinds of phase behavior

The ti
the noise
indicative.
culating th
Next calcul
"suspected"
the type of
not so easy
C, and pres
white frequ

Fig. 11. A

The sha
ted for the
behavior. T
length, com
noise startin

The time error sequences A and B were generated artificially and the changes of the noise level and type were intentionally exaggerated so that they could be more indicative. It is obvious that we can deduct the presence of these changes before calculating the parameters if we make an initial review of the whole time error sequence. Next calculating the common ADEV or TDEV for the whole data sequence and for the "suspected" data segment, we can characterize the time error sequence and conclude the type of the inserted change. The time error sequence C, presented in Fig. 10, is not so easy to evaluate. The slope of time deviation TDEV, computed for the sequence C, and presented in Fig. 11, indicates the presence of the white phase noise and the white frequency noise.

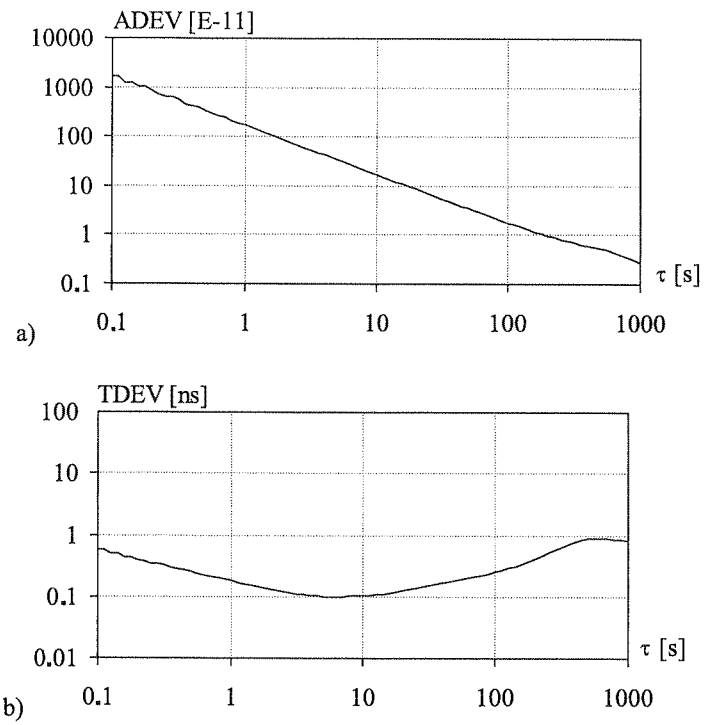


Fig. 11. Allan deviation ADEV (a) and time deviation TDEV (b) for the time error sequence C

The shapes of the dynamic Allan deviation and the dynamic time deviation, computed for the time error sequence C (Fig. 12), enable the final evaluation of the signal's behavior. The sequence C represents the white phase noise on the whole sequence length, combining with the linear phase drift at the beginning and the white frequency noise starting from about 7500 s.

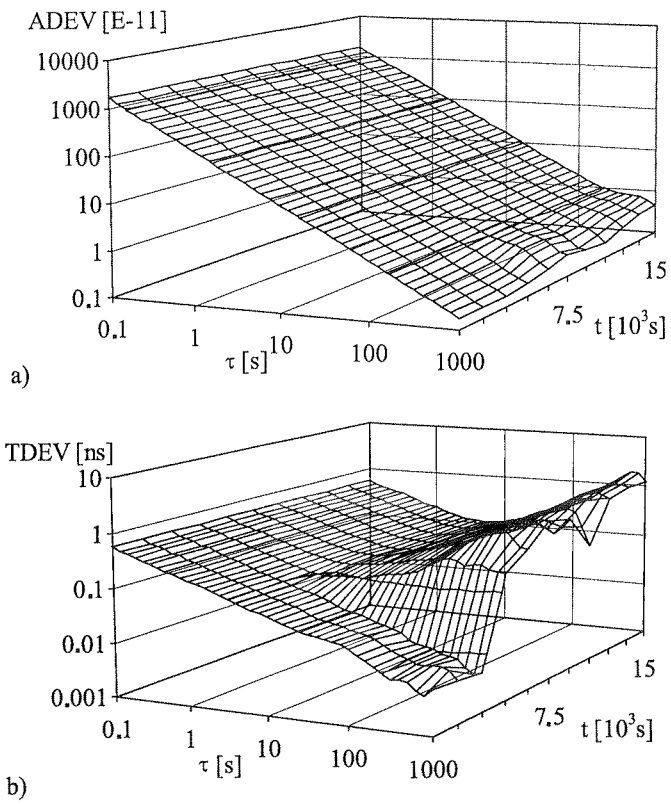


Fig. 12. Dynamic ADEV (a) and dynamic TDEV (b) for the time error sequence C

## 4. COMPUTATION OF DADEV AND DTDEV FOR OVERLAPPING AND NON-OVERLAPPING DATA SEGMENTS

The dynamic parameters of synchronization signals can be computed for non-overlapping and overlapping data segments. The arrangement of the segments influences the form of the presented result, and may affect the final conclusions of the performed calculations. Four procedures of DADEV and DTDEV computation, using different arrangement of the data segments, were analyzed in the paper [6]. The calculations were performed for the time error sequences taken with sampling interval $\tau_0 = 1/30$ s during the time T of 20000 s. The first procedure (proc. I) was used in the calculation presented in Section 3 of this paper. The data sequence was divided into 11 overlapping data segments with the length of 4000 s and segment's shift of 1500 s. The length of the data segment for the second procedure (proc. II) is 10000 s (half of the length of the data series), and the segment's shift is 1000 s. The calculations using the third and fourth procedures were performed for non-overlapping data segments. The data sequence was divided into five non-overlapping segments with the length of 4000 s

for procedure III. The range of observation intervals was from 0.1 s to 1000 s, so the relation between $T_s$ and $\tau_{max}$ fulfills only the practical requirement. For procedure IV there were more non-overlapping segments (20) than for procedure III, with shorter length (1000 s). Therefore the range of observation intervals was smaller, but the relation between $T_s$ and $\tau_{max}$ was better. As result, more curves on the 3D-graph for the shorter range of $\tau$ but with better quality of the estimate were obtained. The quantities determining these four procedures are presented in Table 1 [6].

Table 1

Details of computation procedures

| procedure | overlapping segments | observation intervals | segment's length | segment's shift | number of segments |
|---|---|---|---|---|---|
| | | $\tau_{min} - \tau_{max}$ | $T_s$ [s] | $t_s$ [s] | |
| I | yes | 0.1–1000 | 4000 | 1500 | 11 |
| II | yes | 0.1–1000 | 10000 | 1000 | 11 |
| III | no | 0.1–1000 | 4000 | 4000 | 5 |
| IV | no | 0.1–100 | 1000 | 1000 | 20 |

The results of common ADEV and TDEV computations, as well as DADEV and DTDEV computations, using procedure I for the sequences A and B, are presented in Section 3 of the paper. The results of DADEV and DTDEV computation using procedures II, III, and IV for the sequence A are presented in Fig. 13–15. The plots of DADEV and DTDEV computed using procedures II, III, and IV for the sequence B are presented in Fig. 16–18 [6].

The best illustration of the changes was obtained using procedure IV (non-overlapping short segments). The number of curves obtained using procedure III (Fig. 14 and 17) is too small to indicate the instant of the change and to show its dynamic feature. The number of curves in the case of procedure IV better expresses the dynamic character of the parameters. The short length of the segments allows the changes to be identified in the analyzed signal, but limits the range of observation intervals $\tau$ – the maximum observation interval $\tau_{max}$ must be shorter.

In the case of procedures which use the overlapping data segments for computation, better results were obtained by means of procedure I. The segments in procedure II are too long. The shapes in Fig. 13 and 16 illustrate some change, but it is not possible to fix its initial and final instant. All segments, excluding the first one, cover the period of magnified or changed noise, which affects the computation results.

The shapes of dynamic TDEV (especially for procedure IV, Fig. 18) better indicate the presence of WFM noise. In the case of DADEV, only the result obtained by means of procedure IV (Fig. 18) indicates the presence of the period of changed noise.

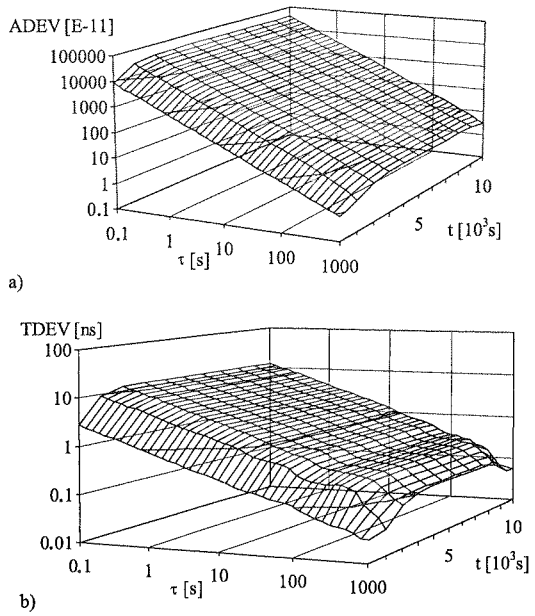


Fig. 13. DADEV (a) and DTDEV (b) for time error sequence A obtained by means of procedure II

Fig. 15. DA

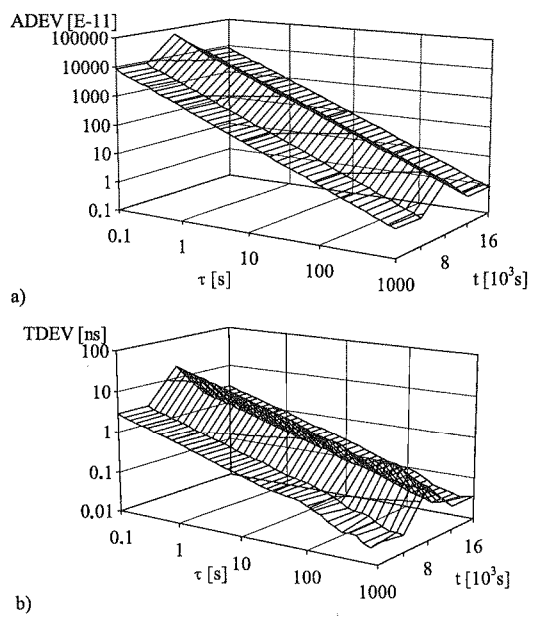


Fig. 14. DADEV (a) and DTDEV (b) for time error sequence A obtained by means of procedure III

Fig. 16. DA

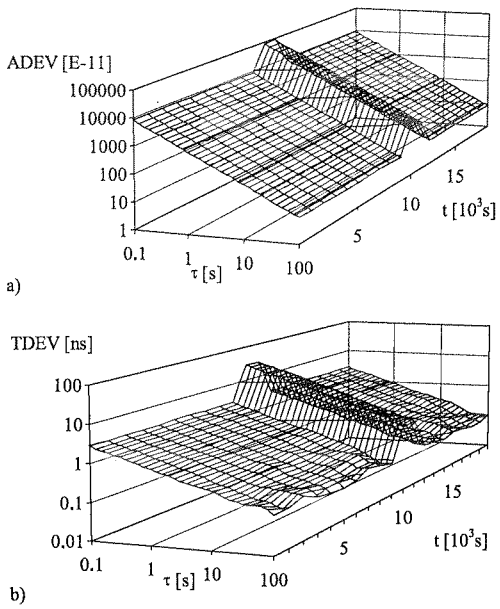


procedure II

Fig. 15. DADEV (a) and DTDEV (b) for time error sequence A obtained by means of procedure IV

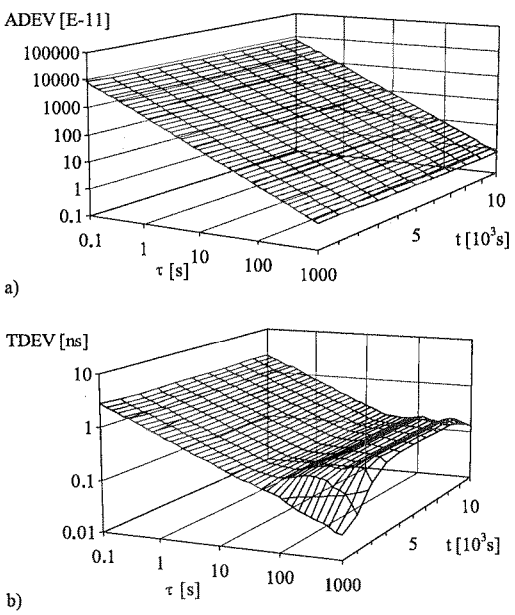


procedure III

Fig. 16. DADEV (a) and DTDEV (b) for time error sequence B obtained by means of procedure II

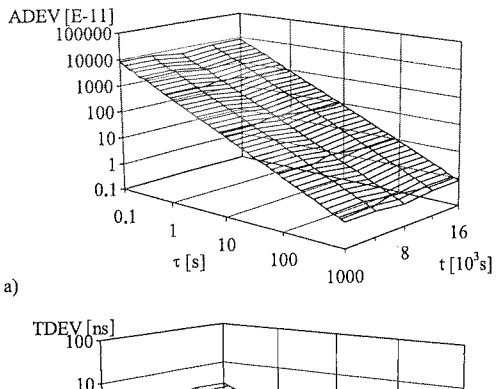


Fig. 17. DADEV (a) and DTDEV (b) for time error sequence B obtained by means of procedure III

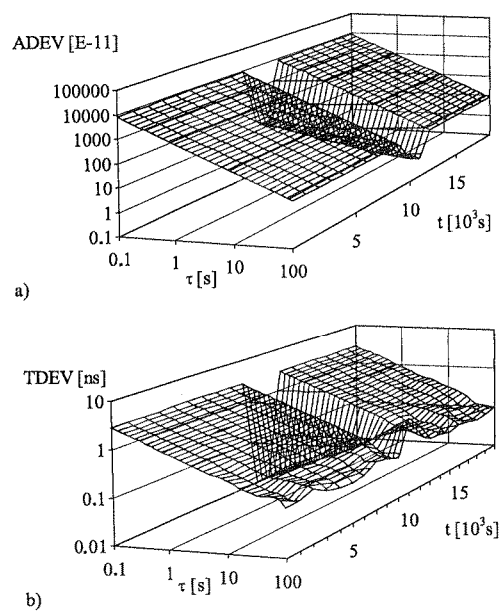


Fig. 18. DADEV (a) and DTDEV (b) for time error sequence B obtained by means of procedure IV

The general suggestions, presented in [6], for computation procedures of the dynamic parameters are the following. If we want to obtain good dynamic character of the results using non-overlapping segments (as in the case of procedure IV), the length of segments must be rather short ($T_s$ <<T) and therefore $\tau_{max}$ is rather short. In order to perform the analysis for longer observation intervals, we must use the overlapping data segments with extended length. A number of segments greater than 10 is suggested, in order to obtain "dynamic" character of the expected result. The segments should be very short in comparison with the length of the whole data sequence in the case of non-overlapping segments (e.g. $T_s$ <0.1 T). The segment's length in the case of overlapping segments cannot exceed the quarter of the data sequence's length [6].

## 5. TIME EFFECTIVE METHODS FOR COMPUTATING THE DYNAMIC PARAMETERS

The number of time error samples necessary for the reliable estimation (when the recommendations are fulfilled) and the complication of the estimator formulae (1 and 2) result in a rather long computing time of the estimates. The problem of time-consuming computation becomes even more serious in the case of the dynamic ADEV and dynamic TDEV, if the calculations are performed independently for each data segment. Some procedures, intended to make the computation process time effective were proposed in [5].

s of procedure III

The first procedure consists in the initial creation of new data sequences before the parameter's calculation for current observation interval $\tau = n\tau_0$ (i.e. current $n$). New sequences contain the squares of second differences in the case of ADEV and of third differences in the case of TDEV. Then the calculation of the parameter for the current observation interval for each data segment is performed. As result, only the operation of summing (using previously computed squares of appropriate differences) is performed. In this situation the order of computation is changed. The calculation of the parameter's value for the current $n$ for each data segment is performed first. Then the data preprocessing as well as the parameter's value computation for the next observation interval are carried out.

The second procedure uses the data reduction methods presented in [7, 8]. The calculations of the parameter for the observation interval greater than some threshold (e.g. 10 s or 100 s) are performed using decimated data (in the case of ADEV calculation) or averaged data (in the case of TDEV calculation). Small error (about 5%) may appear as the result of data reduction [7, 8].

Both methods presented above may be combined. In the first step the data reduction using decimation (for ADEV) or averaging (for TDEV) is performed. Then a new sequence containing the squares of appropriate differences is created using previously reduced data.

ıs of procedure IV

These methods were analyzed in [5]. The data preprocessing using initial computation of the squares of differences enables shorter parameter calculation time only in

the case of overlapping data segments. In the second case, for non-overlapping data segments this type of preprocessing is not time effective. Application of data reduction methods brings good results in both cases – overlapping and non-overlapping data segments. General suggestions were the following:

- calculation with square preprocessing and data reduction in the case of overlapping data segments;
- independent calculation (without square preprocessing) and data reduction in the case of non-overlapping data segments.

## 6. CONCLUSIONS

The dynamic Allan deviation and the dynamic time deviation are very useful tools for evaluation of the synchronization signals in the telecommunication network. The dynamic approach to ADEV and TDEV calculation allows the variations of the phase noise affecting the analyzed signal to be recognized. Particular lengths and quantities – the length of data segment, the segment's shift and the range of observation intervals – should be chosen carefully before the calculation process in order to obtain useful results of calculation. The data preprocessing procedures – square preprocessing, averaging or decimation – may be very helpful for the time effective computation process of dynamic parameters.

## 7. REFERENCES

1. ANSI T1.101-1999, Synchronization interface standard.
2. ETSI EN 300 462, Generic requirements for synchronization networks (1998).
3. ITU-T Rec. G.810, Considerations on timing and synchronization issues (08/96).
4. L. Galleani, P. Tavella: *The characterization of clock behavior with the dynamic Allan variance*, Proceedings of the 2003 IEEE International Frequency Control Symposium and 17th European Frequency and Time Forum, Tampa (USA), 5-8 May 2003, pp. 239-244.
5. A. Dobrogowski, M. Kasznia: *Time effective methods of calculation of dynamic parameters of synchronization signal*, Proceedings of the 18th European Frequency and Time Forum, Guildford (UK), 5-7 April 2004.
6. A. Dobrogowski, M. Kasznia: *Dynamic parameters of synchronization signals for non-overlapping and overlapping data segments*, Proceedings of the 19th European Frequency and Time Forum, pp. 509-514, Besancon (France), 21-24 March 2005.
7. A. Dobrogowski, M. Kasznia: *Modification of the raw data set for time efficient ADEV and TDEV assessment*, Proceedings of the 14th European Frequency and Time Forum, pp. 338-342, Torino (Italy), 14-16 March 2000.
8. A. Dobrogowski, M. Kasznia: *Impact of time error data preprocessing for TDEV assessment*, Proceedings of the 15th European Frequency and Time Forum, pp. 463-467, Neuchatel (Switzerland), 6-8 March 2001.

ELECTRONICS AND TELECOMMUNICATIONS QUARTERLY, 2007, 53, no 1, pp. 23–38

# On line routing of guaranteed bandwidth with restoration

IRENEUSZ OLSZEWSKI

*Wydział Telekomunikacji i Elektrotechniki*
*Uniwersytet Technologiczno-Przyrodniczy*
*Al. Prof. S. Kaliskiego 7*
*85-796 Bydgoszcz*
*e-mail: Ireneusz.Olszewski@utp.edu.pl*

*Otrzymano 2005.12.27*
*Autoryzowano 2006.05.10*

In this paper the problem of finding a pair of link (node) disjoint active Label Switched Path (LSP) and backup LSP in Multi Protocol Label Switching (MPLS) networks is considered. It was assumed that capacity on the links of the backup Label Switched Paths can be shared. We focus on online algorithms for routing of guaranteed bandwidth of active LSPs and backup LSPs under partial information model in order to optimize the total amount of bandwidth consumed in the MPLS network. We consider only the case of protection against single link (node) failure.

In this paper the comparison of two known routing algorithms was carried out. The first of them is based on Integer Linear Programming [3, 4]. The second one is based on active-path-first heuristics [8]. In order to avoid the trap-problem the concept of Conflicting Link Set is used. Moreover, new algorithm based on active-path-first heuristics was proposed too. In this paper special attention has been paid to bandwidth consumed in the network, number of rejected connection set-up requests and running time of considered algorithms. The obtained results have proved that the proposed algorithm is comparable to the other algorithms but it has shorter running time then the existing ones.

*Keywords:* Protection, Routing, Bandwidth Sharing, Multi Protocol Label Switching (MPLS)

## 1. INTRODUCTION

A network can be designed considering only initial factors, but load and traffic characteristics are changing with time. Network resources also can vary due to new resources requests or topology changes (e.g., node or link failure). One of the most important parts of designing a quality of service (QoS) is reliability of the network [5]. Multi-Protocol Label Switching provides a protection mechanisms against failures.

MPLS fault protection mechanisms use Backup Label Switched Path establishment. Both 1+1 and 1:1 protection mechanisms are possible. In the case 1+1 the capacity on the backup LSPs cannot be shared. Depending on the recovery scope, the Label Switched Path (LSP) is either switched at the ingress node and egress node (path protection) or locally at the nodes adjacent to the link failure (link protection). A protection scheme where a recovery LSP is pre-established for each link is called MPLS Fast Reroute [2, 5]. Another method of setting up alternative Label Switched Path is Reverse Backup Path. In this method a recovery LSP is set-up from the node of the failure link in reverse direction to the source node of the working LSP and along a node-disjoint backup path to the destination node [2], [5]. Haskin has proposed pre-establishing reverse backup path by the same node of the working path [5, 6]. Another recovery scheme in the MPLS network is the MPLS restoration scheme. In this case, the recovery LSP are established on demand after link (node) failure detection. Similar to protection scheme the recovery can be done locally or globally [1, 7].

In this paper the problem of finding a pair of link (node) disjoint paths (active LSP and backup LSP) is considered. We consider the case of protection against single link (node) failure in the network. It should be noticed, that if some active LSPs are link-disjoint then their backup LSPs can share backup bandwidth on the same link of the network [2]. The amount of sharing bandwidth that can be achieved on the links of the the backup paths is a function of the information available to the routing algorithm [2, 4]. There are three cases of link-usage information model to the routing algorithms: none, complete and partial information. In the first model (none information) only the residual bandwidth on each link is available for the routing algorithm. In the second model (complete information) the routing algorithm knows the routes for active path and backup path for all requests currently in progress. The complete information model permits the best sharing of bandwidth [2, 4, 7], but it is not always useful, as the amount of information needed for this model is very huge. In the third model (partial information) the routing algorithm knows total bandwidth used by active paths and the total bandwidth used by backup paths on each link. Instead of the residual bandwidth as in the first model, this additional information can be obtained from traffic engineering extensions to routing protocols [4]. In this paper we have assumed partial link-usage information model to the routing algorithms. Online routing algorithm computes active LSP and backup LSP under partial information model in order to optimize the total amount of bandwidth consumed in the network. If available bandwidth is not sufficient for active and backup LSP then the request is rejected.

The rest of the paper is organized as follows. In the second part the problem formulation has been given. In the third part of the paper the analyzed algorithms have been presented. In the fourth part of the paper the results obtained have been shown. In the final part the conclusions have been drawn.

## 2. PROBLEM DEFINITION

In this paper it was assumed, that all connection set-up requests are not known a priori. Hence, only on-line (or dynamic) routing algorithm, that computes active LSP and backup LSP, can be considered. In this paper it was assumed, that all LSP set-up requests with random bandwidth arrive one-by-one.

Let $G(N, E, C)$ be the network, where $N$ is the set of nodes (routers) and $E$ is the set of unidirectional links (arcs). $C$ is $m$-vector of the bandwidth of the links. Let $n$ denote the number of nodes and $m$ the number of links in the network. Moreover, let current request is for $b$ units of bandwidth between nodes $s$ and $d$. In order to set-up this request, let cost of using link $(i, j)$ on the active path is $a_{ij}$ and cost of using link $(i, j)$ on the backup path is $c_{ij}$. These costs will be evaluated later.

The problem of finding two link disjoint paths between a given pair of nodes $s$ and $d$ in the network with the minimal total cost can be stated as follows [3]:

$$Min\left(\sum_{(i,j)\in E} a_{i,j}\, x_{i,j} + \sum_{(i,j)\in E} c_{i,j}\, y_{i,j}\right) \tag{1}$$

$$\sum_j x_{i,j} - \sum_j x_{j,i} = 0 \qquad i \neq s, d \tag{2}$$

$$\sum_j x_{s,j} - \sum_j x_{j,s} = 1 \tag{3}$$

$$\sum_j x_{d,j} - \sum_j x_{j,d} = -1 \tag{4}$$

$$\sum_j y_{i,j} - \sum_j y_{j,i} = 0 \qquad i \neq s, d \tag{5}$$

$$\sum_j y_{s,j} - \sum_j y_{j,s} = 1 \tag{6}$$

$$\sum_j y_{d,j} - \sum_j y_{j,d} = -1 \tag{7}$$

$$x_{ij} + y_{ij} \leqslant 1 \qquad \forall (i, j) \in E \tag{8}$$

$$x_{ij}, y_{ij} \in \{0, 1\} \tag{9}$$

The vector $x$ represents the flow on the active path and the vector $y$ represents the flow on the backup path. When $x_{ij}$ is set to 1 then link $(i, j)$ is used on the active path and when $y_{ij}$ is set to 1 then link $(i, j)$ is used on the backup path. Equation (8) assures that link $(i, j)$ can not be used on the active and backup path. In the case of shared

backup bandwidth the cost of using backup bandwidth $c_{ij}$ on the link $(i, j)$ is a fraction of the cost of using active bandwidth $a_{ij}$ on this link $(0 \leqslant c_{ij} \leqslant a_{ij})$.The problem of finding two link disjoint paths between nodes $s$ and $d$, were $c_{ij} \leqslant a_{ij}$, is NP-complete [8]. This problem so-called Minimum Sum problem with Ordered Dual cost (MSOD) is the main objective of the paper. A more general version of this problem, where relationship between costs $a_{ij}$ and $c_{ij}$ on each link $(i, j)$ is arbitrary, is NP-complete too [3, 8].

Let DISJOINT PATH () be the procedure which solves the problem of finding two link disjoint paths between nodes $s$ and $d$ in dual link cost network. This procedure returns active LSP and backup LSP and their total weight denoted by $OPT$. The weight of active path is given as the sum of $a_{ij}$ for all links on this paths and the weight of the backup path is given as the sum of $c_{ij}$ for all links on this paths. Now we will evaluate the cost $a_{ij}$ of using link $(i, j)$ on the active path and cost $c_{ij}$ of using link $(i, j)$ on the backup path.

Let $F_{ij}$ represent the total amount of bandwidth reserved by active path on link $(i, j)$, and let $G_{ij}$ represent the total amount of bandwidth reserved by backup path on the same link $(i, j)$. Moreover, let $R_{ij}$ represent the residual bandwidth of link $(i, j)$. For each link the following is true:

$$C_{i,j} = F_{i,j} + G_{i,j} + R_{i,j} \tag{10}$$

Let $A_{ij}$ be the set of active LSPs that use link $(i, j)$ and $B_{ij}$ be the set of backup LSPs that use link $(i, j)$. Since it is assumed robustness under single link failure, it is possible to share bandwidth of some link on backup paths among demands whose active paths do not use the same links. Let $\theta_{i,j}^{u,v}$ represent the cost of using link $(u, v)$ on the backup path if the link $(i, j)$ is used on the active path. To compute the quantity $\theta_{i,j}^{u,v}$ we first define the set $\phi_{i,j}^{u,v} = \mathrm{A}_{i,j} \cap \mathrm{B}_{u,v}$. This is the set of demands that use link $(i, j)$ on the active path and use link $(u, v)$ on the backup path. Let the sum of all demands $b_k$ in the set $\phi_{i,j}^{u,v}$ be equal $\delta_{i,j}^{u,v} = \sum_{k \in \phi_{i,j}^{u,v}} b_k$. The quantity $\delta_{i,j}^{u,v}$ is the amount of bandwidth needed on the link $(u, v)$ in order to backup the active LSPs currently using link $(i, j)$. Recall, that the current request is for $b$ units of bandwidth between nodes $s$ and $d$. Moreover, the total bandwidth of $\delta_{i,j}^{u,v} + b$ units is needed on link $(u, v)$, if the current request with bandwidth of $b$ units uses link $(i, j)$ on the active path and uses link $(u, v)$ on the backup path. So, if $\delta_{i,j}^{u,v} + b \leqslant G_{u,v}$, then no additional reservation is needed on the link $(u, v)$ (cost of the current backup request on this link is set to 0), but if $\delta_{i,j}^{u,v} + b > G_{u,v}$, then $\delta_{i,j}^{u,v} + b - G_{u,v}$ units of additional bandwidth is needed on the link $(u, v)$. If this additional bandwidth is not available from residual bandwidth on link $(u, v)$ then the cost $\theta_{i,j}^{u,v}$ is set to infinity. Now, the cost $\theta_{i,j}^{u,v}$ can be written as follows [3, 4]:

$$\theta_{i,j}^{u,v} = \begin{cases} 0 & \delta_{i,j}^{u,v} + b \leqslant G_{u,v} \text{ and } (i,j) \neq (u,v) \\ \delta_{i,j}^{u,v} + b - G_{u,v} & \delta_{i,j}^{u,v} + b > G_{u,v} \text{ and } R_{u,v} \geqslant \delta_{i,j}^{u,v} + b - G_{u,v} \\ & \text{and } (i,j) \neq (u,v) \\ \infty & \text{Otherwise} \end{cases} \tag{11}$$

In the case of complete information model the cost $\theta_{i,j}^{u,v}$ can be used as the function of $\delta_{i,j}^{u,v}$ and then the routing problem can be formulated as integer linear programming problem [3]. In order to use the cost $\theta_{i,j}^{u,v}$ in the case of partial information model the range of changes $\delta_{i,j}^{u,v}$, without knowing the set of active paths $A_{ij}$ and the set of the backup paths $B_{ij}$, has to be evaluated. It has been noticed that:

$$\delta_{i,j}^{u,v} \leqslant F_{ij} \qquad \forall(i,j) \qquad \forall(u,v) \tag{12}$$

Hence the cost $\theta_{i,j}^{u,v}$ can be written as follows:

$$\theta_{i,j}^{u,v} = \begin{cases} 0 & F_{ij} + b \leqslant G_{u,v} \text{ and } (i,j) \neq (u,v) \\ F_{ij} + b - G_{u,v} & F_{ij} + b > G_{u,v} \text{ and } R_{u,v} \geqslant F_{ij} + b - G_{u,v} \\ & \text{and } (i,j) \neq (u,v) \\ \infty & \text{Otherwise} \end{cases} \tag{13}$$

If active path $AP$ has been chosen, then value of total active bandwidth $F_{ij}$ can be evaluated as [3]: $M = \max\limits_{(i,j)\in AP} F_{ij}$. For known value of $M$ the cost of used link $(u,v)$ on the backup path $c_{u,v}$ can be determined as:

$$c_{uv} = \begin{cases} 0 & M + b \leqslant G_{u,v} \\ M + b - G_{u,v} & M + b > G_{u,v} \text{ and } R_{u,v} \geqslant M + b - G_{u,v} \\ \infty & \text{Otherwise} \end{cases} \tag{14}$$

It should be noticed, that the amount of share bandwidth on the backup path influences the choice of active path, so the active path cannot be chosen independently on backup path [3]. Since value of $F_{ij}$ is unknown (the active path is not found) then value of $F_{ij}$ should be incremented from $M = 0$ to $M = \overline{M}$; where: $\overline{M} = \max\limits_{(i,j)\in E} F_{ij}$. For each value of $M$ cost of using link $(i,j)$ on the active path $a_{ij}$ and cost of using link $(i,j)$ on the backup path $c_{ij}$ can be calculated and then active path and backup path can be found (by DISJOINT PATH ()). Below we refer algorithm for solving routing problem under partial information model [3, 4]. Variable $BEST$ is the "cheapest" total cost of active and backup paths.

Algorithm 1:

STEP1: Let $M = 0$. If $BEST = \infty$ then

STEP2: If $M > \overline{M}$ then exit else compute the cost $a_{ij}$ for using each link $(i, j)$ on the active path as:

$$a_{i,j} = \begin{cases} b & \text{if } F_{i,j} \leqslant M \\ \infty & \text{Otherwise} \end{cases} \tag{15}$$

Also compute $c_{ij}$, the cost to use each link $(i, j)$ on the backup paths as:

$$c_{i,j} = \begin{cases} 0 & \text{if } M + b \leqslant G_{i,j} \\ M + b - G_{i,j} & M + b > G_{i,j} \text{ and } R_{i,j} \geqslant M + b - G_{i,j} \\ \infty & \text{Otherwise} \end{cases} \tag{16}$$

STEP 3: Solve DISJOINT PATH (). If the optimal solution to this problem is $OPT$ and the value of $OPT < BEST$ then set $BEST = OPT$. Increment $M$ and return to STEP 2.

In order to speed up this algorithm, instead of iterating $M$ from $0$ to $\overline{M}$, it is enough to do computations for $M = F_{ij}$ for links $(i, j)$ [3]. If different links have the same $F_{ij}$ values it is enough to do experiment only once for these links.

## 3. ANALYZED ALGORITHMS

One class of algorithms solving Minimum Sum problem with Ordered Dual cost is based on Integer Linear Programming problem (ILP) [3]. This problem can be solved using branch-and-bound method or packet optimization (CPLEX) but we need a fast algorithm to do on-line routing for large network.

### 3.1. A HEURISTIC ALGORITHMS BASED ON ILP AND ACTIVE-PATH-FIRST

In [3] the problem of finding a pair of link disjoint paths with minimum total cost (MSOD) is defined as Integral Linear Programming problem. The dual-based algorithm solving primal problem and dual problem to this primal problem is developed. A feasible solution to the dual problem is a lower bound for optimal solution to the primal problem and a feasible solution to the primal problem is an upper bound for optimal solution. The algorithm DISJOINT PATH 1(), which solves the MSOD problem, generates lower and upper bounds by obtaining feasible solution to the primal and dual using a dual-based heuristics. This process terminates if lower bound is greater or equal to upper bound or these bounds remain unchanged in 10 iterations. The upper bound is the solution to the MSOD problem. A drawback of DISJOINT PATH 1() is that it involves solving many of the shortest path problems for each iteration. The number of iterations in the worst case is bounded by number of links in the network (see Algorithm 1).

Another class of algorithms for the MSDO problem is Active Path First (AFP). In the algorithms, based on AFP, active path is found first using Dijkstra algorithm and then backup path is found after removing links belonging to the active paths [8]. The main problem of these heuristics is that since the active path is found, these algorithms may not be able to find link disjoint backup path, even though a pair of disjoint paths exist when another active path is used first [8]. This problem is called trap-problem.

The COnflicting Link Exclusion (COLE) heuristics for Min-Min problem is proposed in [8]. In this problem the objective is to minimize the length of the shorter one of the two paths. The idea of COLE is based on defining Conflicting Link Set for a given active path and then using this set to split the primal problem into a sub-problems of finding a pair active path and backup path. The Conflicting Link Set is a such subset of minimum number links on the active path that using all these links (on this active path) makes impossible finding a link disjoint backup path. Fig.1. illustrates the example of Conflicting Link Set $T = \{e_1, e_2\}$ [8]. For active path *s-1-2-3-4-5-6-7-d*, containing links $e_1$ and $e_2$, there is no link-disjoint backup path. Let Conflicting Link Set be split into two disjoint subset: inclusion set $I$ and exclusion set $O$. Let $P(I, O)$ be the sub-problem of primary problem of finding a pair active path and backup path. The active path is the shortest one among all possible active paths that must use the links in inclusion set $I$, but must not use the links in exclusion set $O$. The original problem of finding two link disjoint paths with the shortest total weight can be represented by $P(\varnothing, \varnothing)$. For example in fig. 1. the original problem $P(\varnothing, \varnothing)$ can be split into two sub-problems: $P(\{e_1\}, \varnothing)$ and $P(\varnothing, \{e_1\})$ and next the $P(\{e_1\}, \varnothing)$ can be split into two sub-problems $P(\{e_1\}, \{e_2\})$ and $P(\{e_1, e_2\}, \varnothing)$. The sub-problem $P(\{e_1, e_2\}, \varnothing)$ does not have to be considered as there is no solution for this sub-problem [8]. The algorithm based on Conflicting Link Set tries to find the best solution to each sub-problem and select the better one.

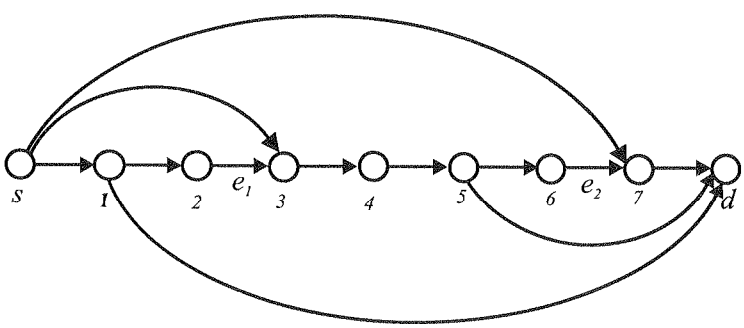


Fig. 1. Example of Conflicting Link Set

The main algorithm DISJOINT PATH 2() is based on active-path-first heuristics. If the trap problem occurs then the COLE heuristics is used. For given active path the Conflicting Link Set is calculated and the original problem is split into sub-problems $P(I, O)$ as described above. A drawback of COLE is that the number of sub-problems

$P(I, O)$ for a given primary active path for which there is no link-disjoint backup path can be very large. Each sub-problem $P(I, O)$ involves solving two shortest path problems. Moreover, max-flow procedure with complexity function $O(n^3)$ must be used to find Conflicting Link Set for a given active path for which there is no backup path.

### 3.2. PROPOSED ALGORITHM

After introducing two different approaches to find path pair in the network we give a new approach to this problem. Algorithm solving this problem is called DISJOINT PATH 3(). Similarly to algorithm DISJOINT PATH 2() first the shortest active path is found. Then, after removing all links belonging to this active path the algorithm tries to find link-disjoint backup path. If such backup path exists, the algorithm terminates with two shortest paths in term of total bandwidth consumed. If link disjoint backup path for this active path cannot be found then the algorithm tries to escape from the trap as follows: it tries to find any backup path with cost $c_{ij}$ on link $(i, j)$. If no backup path can be found then the algorithm terminates and there is no active and backup path pair between nodes $s$ and $d$. If any backup path exists for the active path then let link $(i, j) \in \varphi_{s,d}$, where $\varphi_{s,d}$ is set of common links $(i, j)$ belonging to the active path $(AP)$ and the backup path $(BP)$ between pair of nodes $s$ and $d$. Now, we define the cost of bypassing link $(i, j)$ by node $k_1$ denoted by $\kappa^a_{i,j}(k_1)$ on the active path and cost of bypassing link $(i, j)$ by node $k_2$ denoted by $\kappa^b_{i,j}(k_2)$ on the backup path. These costs are defined as follows:

$$\begin{aligned} \kappa^a_{i,j}(k_1) &= \min_{\substack{k_1 \notin BP \\ k_1 \neq i,j}} (a_{i,k_1} + a_{k_1,j} - a_{i,j}) \\ \kappa^b_{i,j}(k_2) &= \min_{\substack{k_2 \notin AP \\ k_2 \neq i,j}} (c_{i,k_2} + c_{k_2,j} - c_{i,j}) \end{aligned} \tag{17}$$

where $k_1$ ($k_2$) is the node for which the function $\kappa^a_{i,j}(k_1)$ ($\kappa^b_{i,j}(k_2)$) reaches minimum. If $\kappa^a_{i,j}(k_1) \leqslant \kappa^b_{i,j}(k_2)$ for given link $(i, j) \in \varphi_{s,d}$ then the node $k_1$ is inserted between node $i$ and node $j$ on active path (The active path: $s - \ldots - i - j - \ldots - d$ is changed on: $s - \ldots - i - k_1 - j - \ldots - d$). Fig. 2 shows the active path (dotted line): *s-3-4-d* and the backup path (dashed line): *s-1-2-4-d*. The active path has been found first. Let the weights $c_{4,k_2}$ and $c_{k_2,d}$ are infinity for backup path. There is no link-disjoint backup path for this active path. In this case, there is only one link $(4, d) \in \varphi_{s,d}$. The set $\varphi_{s,d}$ allows to escape from the trap problem on the link $(4,d)$. The value $\kappa^a_{4,d}(k_1)$ is finite ($\kappa^a_{4,d}(k_1) = a_{4,k_1} + a_{k_1,d} - a_{4,d}$) but $\kappa^b_{4,d}$ is infinite ($c_{4,k_2} = \infty, c_{k_2,d} = \infty$). Since $\kappa^a_{4,d}(k_1) < \kappa^b_{4,d}(k_2)$ then it is sufficient to insert node $k_1$ between node $4$ and node $d$ on the active path to avoid the trap problem. To optimize the total consumed bandwidth on both paths the link-disjoint backup path is found (again using Dijkstra's algorithm) after removing links along to the new active path. If $|\varphi_{s,d}| > 1$, where $|.|$ denotes the cardinality of the set, we can obtain a new active paths and a new backup path. For

example, let $\varphi_{s,d} = \{(i,j),(j,l)\}$. If $\kappa^a_{i,j}(k_1) < \kappa^b_{i,j}(k_2)$ and $\kappa^a_{j,l}(k_1) > \kappa^b_{j,l}(k_2)$ we will obtain the active path $AP$: $s - ... - i - k_1 - j - l - ... - d$ and the backup path $BP$: $s - ... - i - j - k_2 - l - ... - d$. In this case we need to find a backup path for the active path $AP$ after removing links along the active path and then repeat the same process first by eliminating link along the backup path $BP$ and then determining the active path.

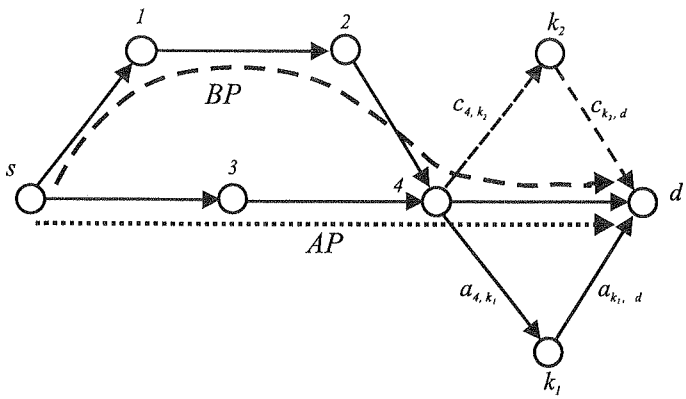


Fig. 2. Illustration of active path ($AP$) and link joint backup path ($BP$)

Now we will give algorithm for solving the problem of finding two link disjoint paths between nodes $s$ and $d$. Let the active path be denoted by $AP$ and the backup path be denoted by $BP$. The idea of DISJOINT PATH 3() algorithm is given below:

DISJOINT PATH 3() algorithm;
STEP1: Find the active path $AP$; Remove all links along $AP$; Find the shortest backup path $BP$; If $BP$ exist then $OPT$:= total cost of the active path and the backup path and exit else go to STEP2;
STEP2: Find $BP$ not link disjoint to $AP$; If $BP$ does not exist then write "There is no disjoint paths" and exit else compute $\kappa^a_{i,j}(k_1), \kappa^b_{i,j}(k_2)$ for each link $(i,j) \in \varphi_{s,d}$. If $\kappa^a_{i,j}(k_1) \leqslant \kappa^b_{i,j}(k_2)$ then insert the node $k_1$ between node $i$ and $j$ on the active path $AP$ ($AP$: $s - ... - i - k_1 - j - ... - d$) else insert node $k_2$ between node $i$ and node $j$ on the backup path $BP$ ($BP$: $s - ... - i - k_2 - j - ... - d$). If $\kappa^a_{i,j}(k_1) = \inf, \kappa^b_{i,j}(k_2) = \inf$ then there is no active path and backup path (The request is rejected);
STEP 3: Remove all links along the active paths $AP$ and find the shortest backup path. Compute the total cost of those Active Path $AP$ and backup path. Repeat the same process first by removing links along the backup path $BP$ and then find the shortest active path. Compute total cost for each path pairs. Choose the path pairs (active path and backup path) with the "cheapest" cost. $OPT$:= the "cheapest" cost.

To compute the shortest path (active or backup) between pair of nodes $s$ and $d$ the Dijkstra's algorithm with complexity function equal $O(n^2)$ is being used. The

complexity of computing function of DISJOINT PATH 3() for choosing link-disjoint active path and backup path for given $M$ (in Algorithm 1) as follows: In the first step complexity of removing all links along to a path is $O(n)$ and computing cost of path pair is $O(n)$. So, complexity function of the first step is $O(n^2+n^2+n+n) \approx O(n^2)$. The complexity of the second step is computed for the worst case, where cardinality of the set $\varphi_{s,d}$ is $n-1$. The complexity of computing $\kappa^a_{i,j}(k_1), \kappa^b_{i,j}(k_2)$ for all links $(i,j) \in \varphi_{s,d}$ is $O((n-1)(n-2)) \approx O(n^2)$. The complexity of the third step is $O(2(n+n^2+n)) \approx O(n^2)$. The complexity of DISJOINT PATH 3() can be written as $O(n^2+n^2+n^2)) \approx O(n^2)$.

### 3.3. NODE DISJOINT PATH

Problem of finding node disjoint path can be shown as the problem of finding link disjoint path [3]. There is enough to split each node into two nodes (sub-nodes) with directed link between them. One of them is the ingress node where all incoming links terminate and the other is the egress node where all the outgoing links terminate. The failure of direct link between any two sub-nodes is equivalent to the node failure.

## 4. PERFORMANCE EVALUATION

### 4.1. USED TOPOLOGIES AND STREAM OF REQUEST

In our study we use three different network topologies. The first network (case 1) contains 15 nodes (routers) and 56 unidirectional links. The 44 of them have the capacity of 60 units and the rest have the capacity of 240 units. The second network (case 2) contains 20 nodes and 82 unidirectional links. The 58 of them have the capacity of 60 units and the rest have the capacity of 240 units. The third network (case 3) contains 30 nodes and 128 unidirectional links. The 102 of them have the capacity of 60 units and the rest have the capacity of 240 units. Requests arrive randomly one at the time. The source and the destination for the demands are picked at random for each case. If there is no capacity for the active path or the backup path then the request is rejected. In the first case 100 requests uniformly distributed between 1 and 10 units arrive into the network for each routing algorithm. In the second case 140 requests uniformly distributed between 3 and 8 units arrive into the network for each routing algorithm. In the third case 200 requests uniformly distributed between 3 and 8 units arrive into the network for each routing algorithm. In our study in each case we performed ten experiments with different stream of requests. In each experiment all routing algorithms, presented in section 3, are run for the same stream of requests. Fig. 3 shows the topology structure of the network [3, 4] used for the first case. The thin links have the capacity of 60 units and the thick links have the capacity of 240 units (the same capacity in each direction).

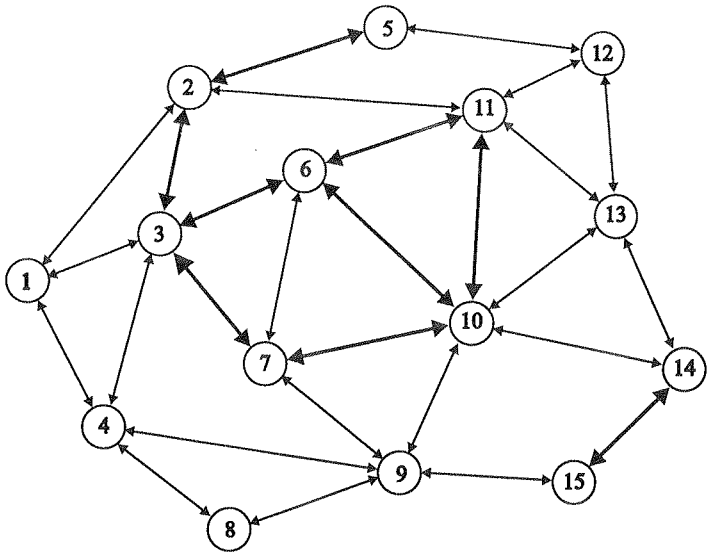


Fig. 3. Topology structure of considered network

### 4.2. EXPERIMENTAL RESULTS

In our study it was observed that Disjoint Path 2() algorithm can get a loop. This loop arises as follows. For given active path $AP_1$, for which there is no link-disjoint backup path $BP$, a Conflicting Link Set is found. Let this set be $T_1 = \{e_1\}$. The original problem $P(\varnothing, \varnothing)$ can be split into two sub-problems: $P(\{e_1\}, \varnothing)$ and $P(\varnothing, \{e_1\})$. The sub-problem $P(\{e_1\}, \varnothing)$ does not have to be considered because there is no solution. For a given sub-problem $P(\varnothing, \{e_1\})$ next active path $AP_2$ is found. The new $AP_2$ found still does not have link-disjoint backup path $BP$. In this case, a new conflicting link set is found. Let this new set be $T_2 = \{e_2\}$. For a given sub-problem $P(\varnothing, \{e_2\})$ a new active path is found (The sub-problem $P(\{e_2\}, \varnothing)$ is omitted). If this new active path is $AP_1$ then the loop arises. An example for the third case: $AP_1$ (14-13-10-7-9-8-21-22-29) $\rightarrow$ $P(0, \{9-8\})$ $\rightarrow$ $AP_2$ (14-13-10-7-9-17-21-22-29) $\rightarrow$ $P(0, \{9-17\})$ $\rightarrow$ $AP_1$ (14-13-10-7-9-8-21-22-29). In order to avoid this problem both $e_1$, $e_2$ links can be blocked and then $AP_3$ can be computed. This approach eliminates some number of sub-problems $P(I, O)$ but it makes that running time is shorter.

Figure 4 shows total amount of bandwidth consumed by the requests (for both active path and backup path) for the case 1 after 100 requests. In Table 1 the total bandwidth consumed obtained for cases 2 and 3 has been shown. These results prove that total amount of consumed bandwidth obtained after usage of Disjoint Path 2 and proposed Disjoint Path 3 is smaller then after usage of Disjoint Path 1. This is because Active Path First based heuristics can achieve near optimal solution [8].

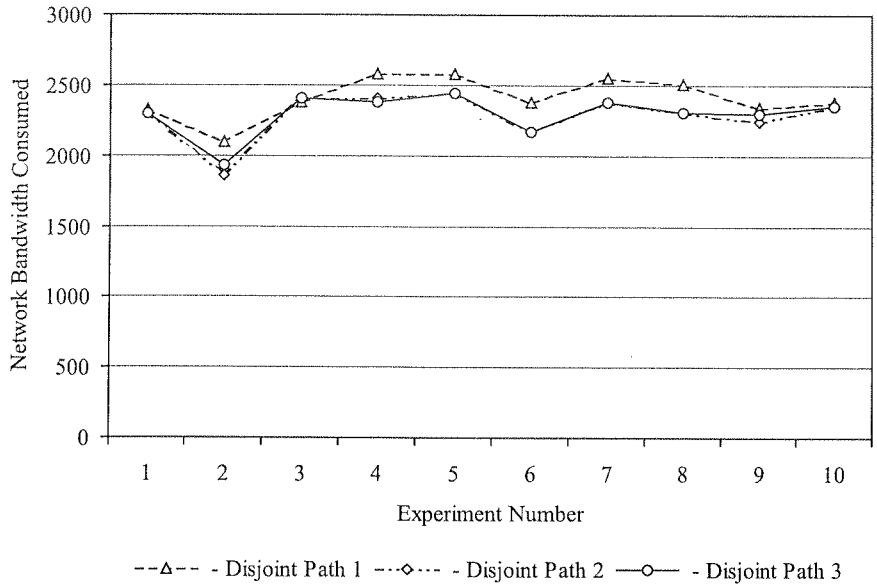


Fig. 4. Total network bandwidth consumed for 10 experiments

Table 1

Total consumed bandwidth for the case 2 and 3 (10 experiments)

| Case 2 (20 nodes, 82 links) | | | | | | | | | | |
|---|---|---|---|---|---|---|---|---|---|---|
| Experiment | 1 | 2 | 3 | 4 | 5 | 6 | 7 | 8 | 9 | 10 |
| Disjoint Path 1 | 2 507 | 2 246 | 2 244 | 2 285 | 2 466 | 2 618 | 2 331 | 2 434 | 2 305 | 2 482 |
| Disjoint Path 2 | 2 140 | 2 200 | 2 071 | 2 207 | 2 369 | 2 424 | 2 281 | 2 172 | 2 311 | 2 286 |
| Disjoint Path 3 | 2 222 | 2 232 | 2 071 | 2 342 | 2 369 | 2 459 | 2 281 | 2 172 | 2 311 | 2 286 |
| Case 3 (30 nodes, 128 links) | | | | | | | | | | |
| Disjoint Path 1 | 5 946 | 6 447 | 5 859 | 5 856 | 5 736 | 6 105 | 5 887 | 6 080 | 6 149 | 5 778 |
| Disjoint Path 2 | 5 734 | 5 883 | 5 576 | 5 601 | 5 872 | 5 943 | 5 548 | 5 671 | 5 681 | 6 093 |
| Disjoint Path 3 | 5 643 | 6 002 | 5 295 | 5 601 | 5 942 | 5 902 | 5 608 | 5 689 | 5 665 | 6 082 |

Fig. 5 shows the number of rejected requests for the first case. In appendix (Table 2) the same results for case 2 (20 nodes, 82 links) and case 3 (30 nodes, 128 links) have been shown. For assumed values of bandwidth of requests the number of requests rejected by proposed algorithm (Disjoint Path 3 ()) is much smaller then the number of requests rejected by Disjoint Path 1 (average 167% in the case 1; 88% in the case 2 and 52% in the case 3) and a little smaller then the number of requests rejected by Disjoint Path 2 (average 6% in the case 1; 4% in the case 2 and 3% in the case 3).

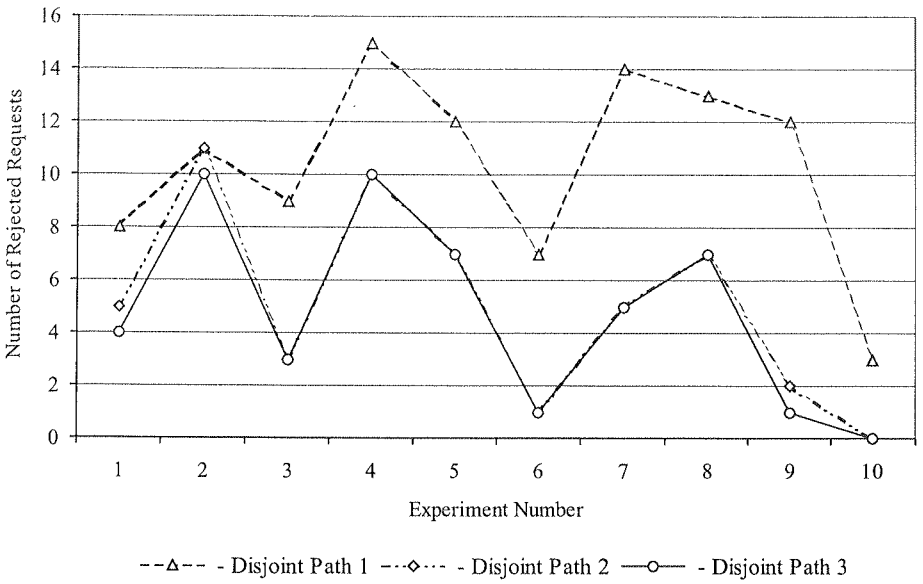


Fig. 5. Number of rejected requests for the case 1 (10 experiments)

Table 2

Number of rejected requests for the case 2 and 3 (10 experiments)

| Case 2 (20 nodes, 82 links) | | | | | | | | | | |
|---|---|---|---|---|---|---|---|---|---|---|
| Experiment | 1 | 2 | 3 | 4 | 5 | 6 | 7 | 8 | 9 | 10 |
| Disjoint Path 1 | 8 | 12 | 7 | 10 | 8 | 9 | 7 | 8 | 12 | 15 |
| Disjoint Path 2 | 5 | 7 | 7 | 6 | 4 | 7 | 4 | 3 | 3 | 7 |
| Disjoint Path 3 | 4 | 6 | 7 | 6 | 4 | 7 | 4 | 3 | 3 | 7 |
| Case 3 (30 nodes, 128 links) | | | | | | | | | | |
| Disjoint Path 1 | 37 | 36 | 31 | 28 | 41 | 44 | 37 | 37 | 39 | 40 |
| Disjoint Path 2 | 30 | 28 | 24 | 22 | 22 | 29 | 23 | 24 | 22 | 27 |
| Disjoint Path 3 | 28 | 26 | 23 | 22 | 24 | 25 | 23 | 23 | 22 | 27 |

Fig. 6. shows the running time of algorithms for all requests in the case 1. The same results for case 2 and case 3 are shown in Table 3. Obtained results prove that the proposed algorithm has the shorter running time than Disjoint Path 1 and Disjoin Path 2 for all cases. In the case 1 this algorithm is average 63% faster than Disjoint Path 1 and 49% than Disjoint Path 2. In the case 2 Disjoint Path 3 is average 67% faster than Disjoint Path 1 and 46% than Disjoint Path 2. In the last case this algorithm

is average 84% faster than Disjoint Path 1 and 150% than Disjoint Path 2. It should be noticed, that the running time is critical for each on-line routing algorithm.

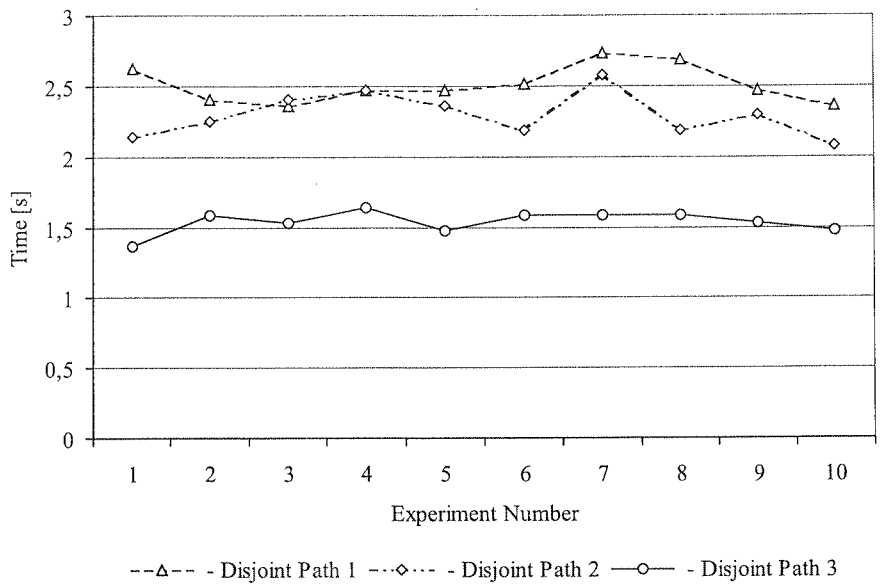


Fig. 6. The running time of algorithms for case 1 (10 experiments)

Table 3

The running time of algorithms (in [s]) for case 2 and case 3 (10 experiments)

| Case 2 (20 nodes, 82 links) | | | | | | | | | | |
|---|---|---|---|---|---|---|---|---|---|---|
| Experiment | 1 | 2 | 3 | 4 | 5 | 6 | 7 | 8 | 9 | 10 |
| Disjoint Path 1 | 2.41 | 2.74 | 2.19 | 2.36 | 2.25 | 2.63 | 2.25 | 2.25 | 2.3 | 2.47 |
| Disjoint Path 2 | 2.19 | 2.08 | 1.92 | 1.97 | 2.08 | 2.47 | 2.14 | 1.97 | 1.81 | 2.25 |
| Disjoint Path 3 | 1.48 | 1.42 | 1.42 | 1.37 | 1.42 | 1.48 | 1.42 | 1.42 | 1.37 | 1.48 |
| Case 3 (30 nodes, 128 links) | | | | | | | | | | |
| Disjoint Path 1 | 20.1 | 22.18 | 19 | 21.69 | 20.54 | 21.8 | 20.26 | 19.99 | 21.75 | 19.33 |
| Disjoint Path 2 | 24.93 | 27.95 | 21.69 | 25.97 | 26.58 | 37.07 | 23.61 | 31.19 | 33.22 | 28.34 |
| Disjoint Path 3 | 9.99 | 11.69 | 10.49 | 10.38 | 11.36 | 12.46 | 10.38 | 11.64 | 12.68 | 10.82 |

Fig. 7 shows efficiency of Disjoint Path 2 (DP2) and Disjoint Path 3 (DP3) algorithms for case 1. This efficiency of Disjoint Path 3 is defined as quotient number of removed trap problem (in step 3 of this algorithm) divided by the number of calls of step 2 (there is no link disjoint backup path in step 1 of this algorithm). Similarly

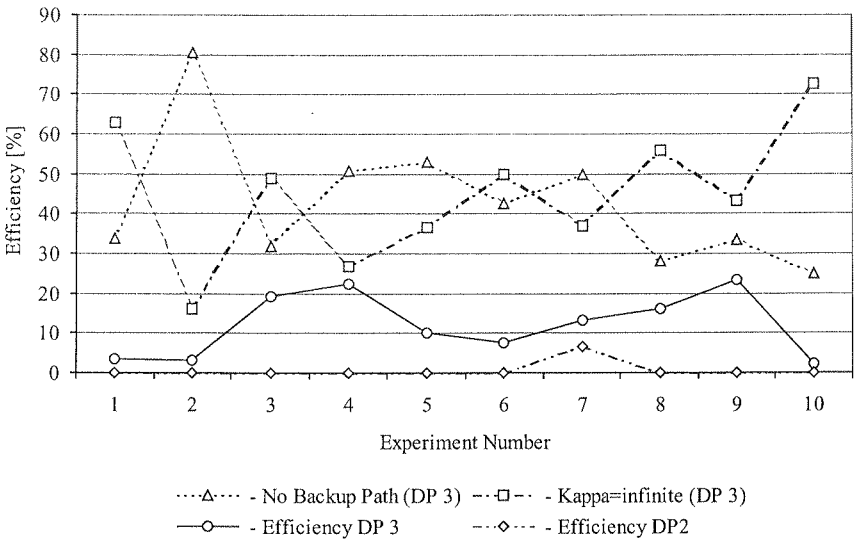


Fig. 7. Efficiency analyzed algorithms for case I

Table 4

Efficiency of analyzed algorithms (in [%]) for case 2 and 3

| Case 2 (20 nodes, 82 links) | | | | | | | | | | |
|---|---|---|---|---|---|---|---|---|---|---|
| Experiment | 1 | 2 | 3 | 4 | 5 | 6 | 7 | 8 | 9 | 10 |
| No BP (DP3) | 42.9 | 48.3 | 43.8 | 69.0 | 50.0 | 37.6 | 55.4 | 72.0 | 34.8 | 73.7 |
| Kappa=inf (DP3) | 51.4 | 34.5 | 56.3 | 28.6 | 45.5 | 48.4 | 28.6 | 24.0 | 39.1 | 5.3 |
| Efficiency DP3 | 5.7 | 17.2 | 0.0 | 2.4 | 4.5 | 14.0 | 16.1 | 4.0 | 26.1 | 21.1 |
| Efficiency DP2 | 0.0 | 0.0 | 0.0 | 0.0 | 2.3 | 0.0 | 0.0 | 0.0 | 0.0 | 0.0 |
| Case 3 (30 nodes, 128 links) | | | | | | | | | | |
| No BP (DP3) | 43.1 | 53.1 | 31.3 | 50.3 | 39.7 | 57.0 | 56.9 | 38.0 | 26.8 | 41.7 |
| Kappa=inf (DP3) | 51.4 | 43.7 | 61.7 | 46.2 | 55.2 | 29.4 | 38.8 | 53.6 | 65.0 | 51.6 |
| Efficiency DP3 | 5.5 | 3.1 | 7.0 | 3.5 | 5.2 | 13.6 | 4.2 | 8.4 | 8.2 | 6.7 |
| Efficiency DP2 | 0.7 | 0.6 | 1.1 | 0.6 | 0.0 | 0.0 | 0.0 | 1.0 | 0.0 | 1.6 |

this efficiency is defined in Disjoint Path 2. Moreover, fig 7 shows quotient of number of cases when there is not backup path without disjoint constraint divided by number of calls of step 2 in Disjoint Path 3 (No Backup Path (DP3) in fig.7) and quotient of number of cases where $\kappa^a_{i,j} = \inf$ and $\kappa^b_{i,j} = \inf$ at least for one link $(i, j) \in \varphi_{s,d}$ divided by number of calls of step 2 (Kappa=infinite (DP 3) in fig.7). It should be noticed, that if $\kappa^a_{i,j} = \inf$ and $\kappa^b_{i,j} = \inf$ at least for one link $(i, j) \in \varphi_{s,d}$ then there is no link-disjoint

backup path found by Disjoint Path 3 to given active path between pair of nodes $s$ and $d$. The same results are shown in table 4 for case 2 and case 3. The obtained results prove that average efficiency of Disjoint Path 3 is 12.1% in case 1, 11.1% in case 2 and 6.5% in case 3, and it is higher than efficiency of Disjoint Path 2.

## 5. CONCLUSIONS

In this paper the problem of finding a pair of link (node) disjoint active path and backup path in online setting is considered. It was assumed that the capacity on the backup paths can be shared. We focus on online algorithms for routing of guaranteed bandwidth of active and backup paths under partial information model. It was assumed that the main objective of the routing algorithm is to optimize the total amount of bandwidth consumed on active paths and on backup paths for every request in the network. We assumed that the routing algorithm know the total bandwidth used by active paths and total bandwidth used by backup paths on each link of the network.

In this paper the comparison of two known routing algorithms has been carried out. The first algorithm is based on Integer Linear Programming. The second algorithm is based on concept of Conflicting Link Set. Moreover, the new algorithm based on the cost of bypassing links $(i, j)$, which cause trap problem was proposed. In this paper the special attention has been paid to bandwidth consumed in the network, number of rejected requests and the running time of considered algorithms. The obtained results proved that proposed algorithm performs very well in comparison to the other algorithms and it has faster running time than the existing algorithms. The proposed algorithm should be improved for local scheme restoration.

## 6. REFERENCES

1. A. Autenrieth, A. Kirstädter: *Engineering End-to-End IP Resilience Using Resilience-Differentiated QoS*, IEEE Communications Magazine, January 2002.
2. E. Calle, T. Jové, J.L. Marzo, A. Urra: *A Protection Performance Components in MPLS network*. Computer Communications Journal, Vol. 27, Issue 12, pp. 1220-1228, July 2004.
3. M. Kodialam, T.V. Lakshman: *Dynamic Routing of Bandwidth Tunnels with Restoration*, IEEE INFOCOM 2000 Mar. 2000, pp. 902-911.
4. M. Kodialam, T.V. Lakshman: *Restorable Dynamic QoS Routing*, IEEE Communications Magazine, June 2002.
5. J.L. Marzo, E. Calle: *QoS Online Routing and MPLS Multilevel Protection: A Survey*, IEEE Communications Magazine, October 2003.
6. J.L. Marzo, E. Calle, C. Scoglio, T. Anjali: *Adding QoS Protection in Order to Enhance MPLS QoS Routing*, Proc. ICC,03, Anchorage, AK, May 2003.
7. S. Norden, M.M. Buddhikot, M. Waldvogel, S. Suri: *Routing Bandwidth-Guaranteed Paths with Restoration in Label-Switched Networks*, Computer Networks, October 2004, 46(2): 197-218.
8. D. Xu, Y. Chen, Y. Xiong, Ch. Qiao, X. He: *On Finding Disjoint in Single and Dual Link Cost Networks*, IEEE INFOCOM 2004.

# Analysis of properties of the multiwavelength source with an acousto-optic frequency shifter

ANDRZEJ DOBROGOWSKI, JAN LAMPERSKI, PIOTR STĘPCZAK

*Katedra Systemów Telekomunikacyjnych i Optoelektroniki, Politechnika Poznańska*
*ul. Piotrowo 3A, 60-965 Poznań*
*E-mail: dobrog@et.put.poznan.pl, jlamper@et.put.poznan.pl,*
*pstepcz@et.put.poznan.pl*

*Otrzymano 2006.03.02*
*Autoryzowano 2006.05.17*

The article presents the simulation of a ring configuration system which generates a multiwavelength signal (comb of carriers), together with its basic components: a single laser, an optical splitter, an acousto-optic frequency shifter (AOFS) and an optical amplifier (OA). Optical filters are used to shape the spectrum of the generated multiwavelength signal in the system. Combs with a number of carriers ranging from 20 to 60 were accomplished, with an optical carrier to noise ratio (OCNR) higher than 30dB.

*Keywords:* multiwavelength source, optical frequency comb, acousto-optic frequency shifter

## 1. INTRODUCTION

One of the trends in the development of Dense Wavelength Division Multiplexing (DWDM) systems is increasing the number of optical channels, with simultaneous decreasing the interchannel spacing [1]. Together with increasing density, there is also a rise in significance of stability of the optical carriers forming multiwavelength sources. The optical fiber ring configuration systems with the comb filter are considered a promising group of comb multiwavelength sources. In the optical loop of such systems, either an optical fiber Raman amplifier, or erbium doped fiber amplifier (EDFA) is applied. The Raman ring laser with 9 channels with 100-GHz spacing and 19 channels with 50-GHz spacing has been obtained with the uniformity of about 5 and 8 dB, respectively [2]. In the case of using Raman amplifier, length of the optical loop (which is several kilometers long) and high level of power of the optical pomp required (higher than 1W) are disadvantageous. The main EDFA drawback is a large room

temperature homogenous linewidth (11 nm), which makes it impossible to generate a uniform optical comb with small channel spacing [3]. The homogenous linewidth can be decreased to 0.8nm at liquid nitrogen temperature [4]. The multiwave operation of laser at room temperature was also obtained by using the frequency shifter [5] in the optical loop, in order to prevent a steady state oscillation with a dominant frequency. Nevertheless, the interchannel spaces obtained were not smaller than 0.8 nm (100GHz).

Another solution is a ring configuration with a source laser coupled into the optical loop which consists of an acousto-optic frequency shifter (AOFS) and an optical amplifier. The AOFS determines frequency comb intervals [6]. The beam of the source laser is introduced to the optical loop by the optical splitter. The experimental results of generating a comb with several carriers and stable intervals of 110MHz were demonstrated [6]. It was shown that the number of carriers in the comb increased together with the decreasing level of the optical loop losses. However, the power of the successive carriers was falling and it was impossible to obtain carriers with equal power level, because of a limited compensation of the optical loop losses. The carriers generated in the combs were characterized by very stable frequency spacing, which results from the system concept. In this paper the simulation experiment of generating optical carrier combs using a frequency-translating optical loop is described. The uniformity and OCNR of carriers in the combs are investigated.

## 2. ANALYZED SYSTEM

A block diagram of the ring multiwavelength generator is presented in Fig. 1. The source laser (LD) output is coupled into the optical frequency shifting loop. AOFS operating at 3.125 GHz has two outputs: non-shifting ($out_0$) and shifting ($out_1$). The shifted output AOFS beam is amplified and combined with the source laser beam by optical coupler (OC) and again directed to the frequency shifter input.

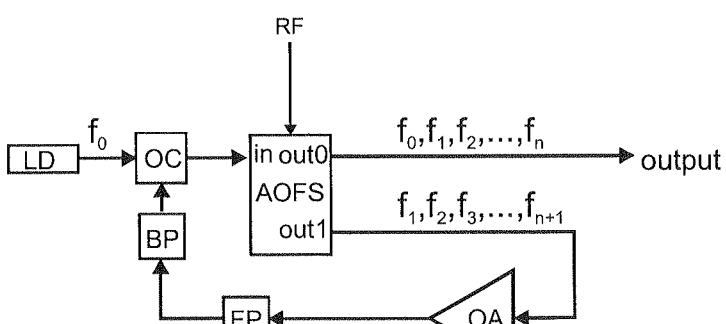


Fig. 1. Block diagram of the ring multiwavelength source: LD – Laser Diode, AOFS – Acousto Optic Frequency Shifter, OA – Optical Amplifier, RF – Radio Frequency signal, OC – Optical Coupler, BP – Band-pass Filter, FP – Fabry-Perot Filter

The repetition of the process leads to generating a frequency grid and a multiwavelength beam at the AOFS non-shifting output. The interchannel spacing is determined by RF frequency which controls AOFS. The optical amplifier (OA) compensates loop losses. The band-pass (BP) filter determines the number of generated carriers. The Fabry-Perot (FP) filter limits the interchannel noise power.

The system operation was simulated by using mathematical models of optical elements. An optical coupler, an AOFS and fusion splices were described using the power transfer coefficients. In case of AOFS, the transfer of the optical beam from an input to an adequate output was described with the following coefficients:

$$T_{in-out_0} = T_{AOFS} \cdot (1 - \eta)$$
$$T_{in-out_1} = T_{AOFS} \cdot \eta \tag{1}$$

where $T_{AOFS}$ is the optical power transmission coefficient, $\eta$ is the diffraction efficiency of AOFS.

Spectral transmittance of the BP filter has a trapezoidal form in the logarithmic scale. The slopes of the filter characteristic were fit according to the specification of the Chameleon filter offered by Micron Optics Inc [7]. The filter attenuation in the stop-band was equal to 80dB, and in the pass-band totaled 0.5dB.

The FP filter is described with transmittance function [8]:

$$T_{FP}(f) = \frac{A}{1 + \frac{4AR}{(1-R)^2} \sin^2\left(\pi \frac{f - f_O}{FSR}\right)} \tag{2}$$

where $A$ is the internal loss of cavity, $R$ is the mirror reflectance, $FSR$ (Free Spectral Range) is the frequency mode spacing.

The source laser (LD) power density spectrum was modeled with the Lorenz function [9]:

$$\rho(f) = \frac{2 \cdot P_O}{\pi \cdot \Delta f_{FWHM} \left[1 + \left(\frac{f - f_O}{\Delta f_{FWHM}}\right)^2\right]} \tag{3}$$

where $P_O$ is the optical power of laser beam, $\Delta f_{FWHM}$ is 3dB linewidth, and $f_O$ is the central lasing frequency.

The optical amplifier was modeled basing on spectral characteristics of the gain and of the noise figure, according to the HighWave Optical Technologies technical specification [10]. Therefore, that simple model based on measurement characteristics retained the properties of an actual amplifier.

Just for the sake of comparison, a system in "multiple cascade" configuration, having module structure schematically shown in Fig. 2, was also investigated. Each frequency shifter module (FSM) consists of EDFA amplifier as well as BP and FP filters connected to the AOFS shifting output. BP and FP filters at the output of the

amplifier were used to limit the amplifier wideband noise. In this system the number of modules determines a number of the carriers generated.

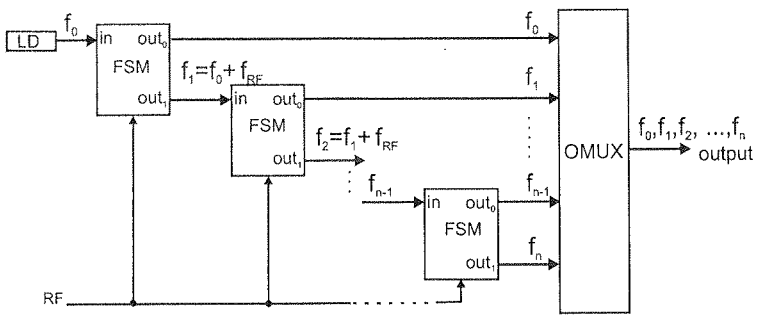


Fig. 2. The cascade configuration of a multiwavelength source: FSM – Frequency Shift Module consisting of AOFS, EDFA, BP and FP filter, OMUX – Optical Multiplexer, LD – Laser Diode

## 3. NUMERICAL RESULTS

Numerical algorithms for the comb generator simulation were carried out in the Matlab environment. The simulations were performed for a system with BP filter in the optical loop and a system with BP and FP filters. Both the optical carrier noise ratio (OCNR) in a channel and the non-uniformity of the comb of carriers, understood as a difference between the highest and the lowest value of an envelope of a power density spectrum of carriers, were determined.

Table 1

Selected results of simulation

| Filter | Number of carriers | Nonuniformity | OCNR |
|---|---|---|---|
| BP | 20 | 0.83 dBm | 21.1 dB |
| | 28 | 3.71 dBm | 18.2 dB |
| | 40 | 10.72 dBm | 13.8 dB |
| | 60 | 16.63 dBm | 7.5 dB |
| BP + FP | 20 | 0.09 dBm | 37.4 dB |
| | 28 | 0.18 dBm | 36.3 dB |
| | 40 | 2.41 dBm | 33.7 dB |
| | 60 | 6.92 dBm | 29.9 dB |

The calculations were carried out for the combs with 20 to 60 carriers. The LD power was constant, its linewidth was equal to 60 MHz. The BP filter width was matched to an assumed number of carriers. The FP filter limited the noise in interchannel

intervals. In the systems generating 20 to 27 carriers, an optical loop attenuator with attenuation ranging from 0.7dB to 0.01dB was used. The attenuator allowed to obtain the non-uniformity values of comb carriers below 1dBm. For 28 carriers and more, the system operates without an attenuator. Selected results are given in Table 1. The table is divided into two parts, reflecting the system with BP filter alone and with both BP and FP filters. The best results (Tab.1) were obtained after combining BP and FP filters. An increase in the number of carriers in the comb caused a drop of the amplifier gain and, consequently, a decrease of spectral power density, as well as a rise of non-uniformity.

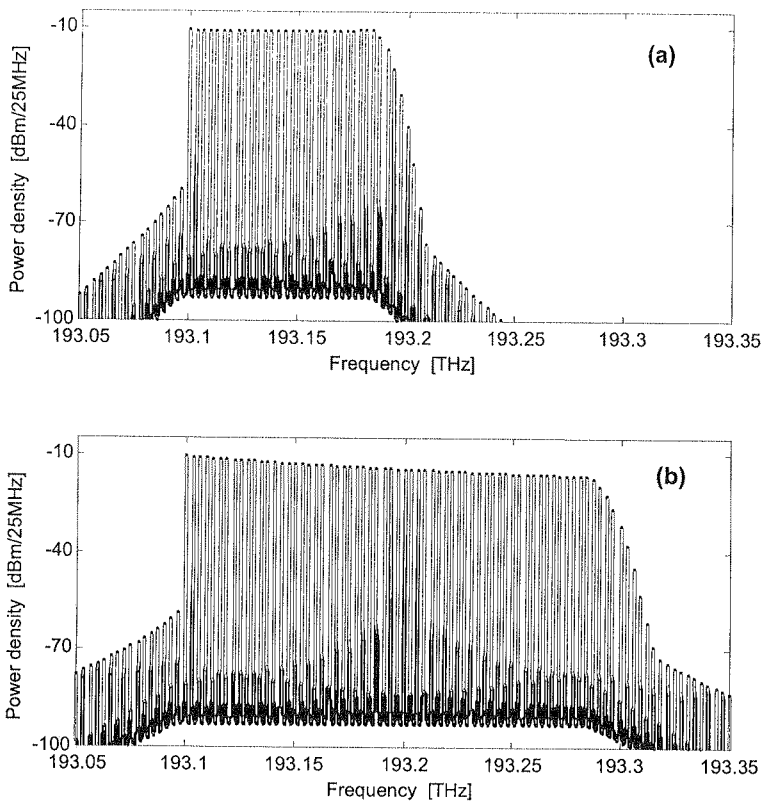


Fig. 3. Power density spectrum of a comb with a) 28 and b) 60 carriers generated in a ring system with BP and FP filters

In Fig. 3, the power density spectrum of the comb with 28 and 60 carriers is presented. For the comb with 28 carriers the non-uniformity reaches the value of 0.18dBm, and in case of 60 carriers the non-uniformity is equal to 6.9dBm. In the considered system, the optical amplifier is a main source of the noise. The noise and the signal powers influence the gain and the noise figure of the amplifier. A multiple beam circulation mechanism of carrier generation results in the accumulation of noise. As the noise power increases when generating successive carriers, the gain of the amplifier drops

and can be insufficient for the compensation of the optical loop losses. An FP filter, with a width at half maximum FWHM of 100 MHz, limits the interchannel noise and, also, narrows the spectral bandwidth of the successive carriers. In Fig. 4, the power density spectrum of the first and the last carrier for a 28-carrier comb is presented. The linewidth of the 28th carrier is less than this of the first carrier by 35 MHz and by 108 MHz at the 3 dB and 20 dB levels respectively. Limiting the spectrum width of the carriers causes a decrease of their power. This effect, together with the noise buildup during circulation, results in the lowest OCNR of the last comb carrier. In case of the combs with 20, 28, 40 and 60 carriers, the OCNR equals 37.4 dB, 36.3 dB, 33.7 dB and 29.9 dB, respectively.

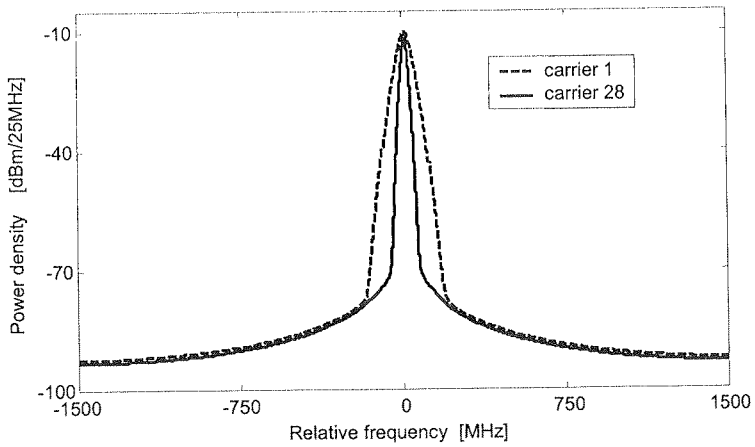


Fig. 4. Zoom on the power density spectrum of a) first and b) last carriers of the 28 optical frequency comb

The power of noise in generated multiwave signals increases significantly after removing the FP filter from the optical loop of the system. Fig. 5 compares OCNR values for systems with a BP filter alone and with BP and FP filters in the optical loop. Removing the FP filter causes a significant decrease of OCNR. For 60 carriers, the OCNR of the last one decreases to 7.5 dB.

In the "multiple cascade" configuration system a comb with 334 carriers and with non-uniformity equal to 5.2 dBm was obtained (the number of 334 carriers resulted from the accepted EDFA model). The OCNR of the last carrier in the comb was equal to 36.3 dB. Abandoning FP filter also causes a decrease of the OCNR of the last carrier to the value of 21.2 dB. For the time being, the economical factor is responsible for the lack of applications of any "multiple cascade" configuration system.

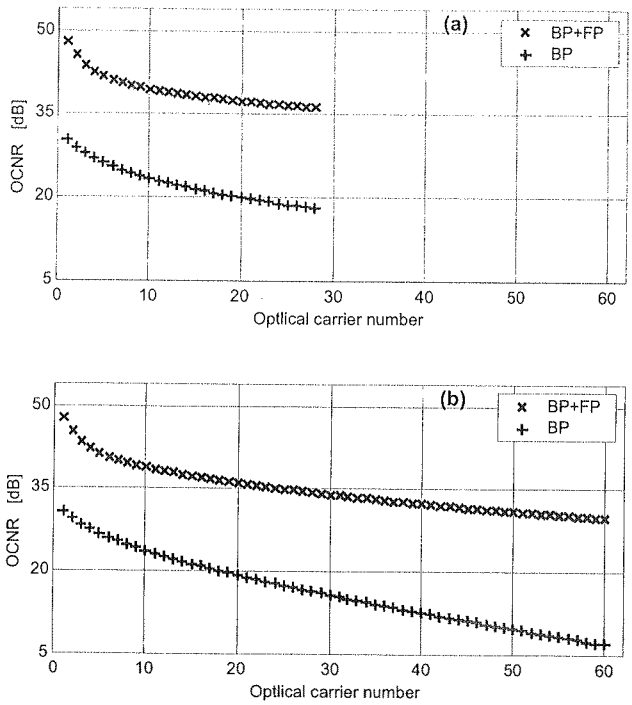


Fig. 5. OCNR values for a) 28, b) 60 carrier combs generated in systems with BP filter (+) and BP+FP filter (x) in the optical loop

## 4. CONCLUSION

A multifrequency ring generator has been investigated. The spectra of the carrier power comb densities were calculated. The results of the simulation show that it is possible to obtain combs featuring parameters suitable for practical applications, among others in a very dense WDM. For example, the comb containing 28 optical carriers with the interchannel spacing equaling 3.125 GHz and with both the uniform power density spectrum and OCNR higher than 36 dB has been obtained. To achieve the carrier combs with such parameters, it is necessary to apply a BP filter, which strongly limits noise beyond the carriers band and a FP filter restricting the noise at interchannel intervals. Additionally, the effect of noise accumulation is limited.

## 5. ACKNOWLEDGMENTS

This work was supported by Ministry of Science and Higher Education (formerly State Committee for Scientific Research) under project no. 3 T11d 014 27.

## 6. REFERENCES


1. J. Hecht: *Speeding up transmission rates with slower signals.* Laser Focus World, November 2002, pp. 91-96.
2. J.H. Lee, W.T. Han, U.C. Peak, Y. Chung: *Multiwavelength Raman fiber-ring laser based on tunable cascaded long-period fiber grating.* Photonics Technology Letters, 2003, vol. 15, no. 3, pp. 383-385.
3. H.L. An, X.Z. Lin, E.Y.B. Pun, H.D. Liu: *Multi-wavelength operation of an erbium-doped fiber ring laser using a dual-pass Mach-Zehnder comb filter.* Optics Communications 169, 1999, pp. 159-165.
4. S. Yamashita, K. Hotate: *Multiwavelength erbium-doped fiber laser using intracavity etalon and cooled by liquid nitrogen.* Electronics Letters, 1996, vol. 32, no. 14, pp. 1298-1299.
5. A. Bellamere, M. Karasek, M. Rochette, S. LaRochelle, M. Tetu: *Room temperature multifrequency erbium-doped fiber laser anchored on the ITU frequency grid.* Journal of Lightwave Technology, June 2000, vol. 18, no. 6, pp. 825-831.
6. P. Coppin, T.G. Hodgkinson: *Novel optical frequency comb synthesis using optical feedback.* Electronics Letters, 1990, vol. 26, no. 1, pp. 28-30.
7. Data catalogue Micron Optics Inc, *Chameleon Thin Film Tunable Filter*, www.micronoptics.com
8. N. Grote, H. Venghaus: *Fiber Optic Communication Devices. Springer-Verlag*, Berlin Heidelberg 2001, p. 268.
9. G.P. Agrawal: *Fiber-Optic Communication System.* John Wiley & Sons, Inc. 1997, p. 121.
10. Data catalogue HighWave Optical Technologies, www.highwave-tech.com

ELECTRONICS AND TELECOMMUNICATIONS QUARTERLY, 2007, 53, no 1, pp. 47–62

# Characterization of Weibull fading channels

KRYSTYNA MARIA NOGA[1], GEORGE K. KARAGIANNIDIS[2]

[1]*Department of Ship Automation,*
*Gdynia Maritime University, Poland,*
*jagat@am.gdynia.pl*
[2]*Electrical & Computer Engineering Department,*
*Aristotle University of Thessaloniki, Greece,*
*geokarag@auth.gr*

*Otrzymano 2006.04.20*
*Autoryzowano 2006.06.30*

This paper presents important statistical properties of the two-parameter Weibull distribution, as a suitable model to describe wireless transmission in fading channels. Exact closed form expressions are presented for the univariate probability density functions (PDF), cumulative density functions (CDF), the moments of envelope, amount of fading (AF) and the moment generating function (MGF) associated with the output signal-to-noise ratio (SNR). We also presented the multivariate Weibull distribution.

*Keywords:* multipath fading channel, Weibull distribution, correlated Weibull fading

## 1. INTRODUCTION

Radio wave propagation through wireless channels is a complicated phenomenon. Wireless channels often include multiple-path propagation, in which the signal has more than one path from the transmitter to the receiver. Such multipath can be caused by atmospheric refraction or reflection, and by reflection from the ground or from objects such as buildings. The reflected path can interfere with the direct path in a phenomenon called fading. Precise mathematical and quantitative description of the fading channel is too complex. However, several models have been proposed to characterize the radio channel. Generally, these models can be classified into two major classes: statistical models and deterministic propagations models [1]. Statistical models follow statistical impulse response modelling of the multipath fading channel, based on experimental

data measurements, while the propagation models utilize the electromagnetic wave propagation theory to characterize the radio propagation [1].

In Polish literature the Weibull distribution is rather seldom used for description of the wireless channel. Only in the A. Jakubiak et al. papers [2, 3, 4], one can find examples using Weibull distribution for description and modeling of the passive disturbances in radar systems. Besides the Weibull distribution is only mentioned in papers [5] as one of three non – Gaussian models of disturbances which one used in practice, i. e. except log-normal distribution and $K$-distribution. In paper [5] also is presented another distribution which is used for description of the disturbances, i. e. Suzuki distribution. Additionally in A. Jakubiak et al. papers [4, 6, 7] the methods of generation of samples of signal with Weibull distribution are presented.

In this paper we present important statistical properties of the Weibull distribution, as a suitable model to describe wireless transmission in fading channels. The paper is organized as follows: in Section 2 is described the Weibull fading channel, i.e. the probability density functions (PDF), cumulative density functions (CDF), the moments of envelope, amount of fading (AF) and the moment generating function (MGF) associated with the output signal-to-noise ratio (SNR), are presented. In Section 2 examples of generating Weibull distributed random variables are also presented. Exact closed form expressions are studied for the univariate and the multivariate probability density functions in Section 3. While in Section 4, useful concluding remarks are provided.

## 2. THE WEIBULL FADING CHANNEL

We consider a digital receiver operating in a flat fading environment, with the received signal given by

$$y(t) = r(t)\, x(t) \cos\left[2\pi f t + \theta(t)\right] + n(t) \tag{1}$$

where $f$ is the carrier frequency, $x(t)$ is the transmitted signal, $\theta(t)$ is the random phase uniformly distributed over the range $[0, 2\pi)$, $r(t)$ is the fading envelope, $n(t)$ is additive white Gaussian noise (AWGN) with zero mean and one-side spectral density $N_0$. We assume that the noise is independent of the fading. The fading environment have been extensively explored in the literature. When there is no line-of-sight (LOS) direct path, the fading envelope of the received signal follows the Rayleigh probability density function (PDF) [8, 9, 10, 11]. When there is a LOS path from the transmitter, the received signal is the sum of a scattered and direct component. Then the envelope of this signal is a Rice random variable [8, 9, 10, 11]. The Rice distribution is also known as Nakagami-$n$ distribution. Rice fading is observed in the microcellular urban, suburban land mobile and picocellular indoor environments. It is also describes the dominant path of satellite and ship to ship radio links [8]. When the orthogonal components of fading signal have normal distributions with different variances and zero average values, then the receiver operates in a Hoyt fading environment [8, 10, 11]. The

Hoyt (also called as Nakagami-$q$) distribution is normally observed on satellite links subject to strong ionospheric scintillation [8]. Another common distribution used to characterize the envelope in radio channel is the Nakagami-$m$ (Nakagami) distribution. The land-mobile, indoor-mobile multipath propagation and scintillating ionospheric radio links are frequently described by this distribution [10]. Both the Rayleigh distribution, the Rice and Hoyt are special cases of Nakagami-$m$ distribution. In last year Nakagami distribution has been widely adopted for multipath modelling in wireless communications [8, 10].

Another distribution used to model the fading envelope is the Weibull distribution. It is an empirical distribution, which was introduced by Walodi Weibull at The Royal Institute of Technology of Sweden in 1939 for estimating machinery lifetime and became widely known in 1951 [12]. Nowadays, the Weibull distribution is used in several fields of science. For example, it is a very popular statistical model in reliability engineering and failure data analysis [13, 14]. It is also used in some other applications, such as weather forecasting and data fitting of all kinds, while it is widely applied in radar systems to model the dispersion of the received signals level produced by some types of clutters [15]. Concerning wireless communications, the Weibull distribution seems to exhibit good fit to experimental fading channel measurements, for both indoor [16, 17, 18, 19] and outdoor [20, 21, 22, 23] environments, with a reasonable physical justification to be given in [24]. However, only very recently the topic of digital communications over Weibull fading channels has begun to receive some interest [25, 26, 27, 28, 29, 30].

### 2.1. STATISTICAL PROPERTIES OF THE WEIBULL DISTRIBUTION

When the receiver operates in a Weibull fading environment, the envelope is obtained as non-linear function of the modulus of multipath components, at what the non-linearity is expressed in terms of a parameter $\alpha > 0$. In such channel the randomly variable (RV) $R$ which represented envelope we can write as

$$R = (X^2 + Y^2)^{1/\alpha} \tag{2}$$

where $X$ and $Y$ are independent zero mean Gaussian random variables with identical variances $\sigma_x^2 = \sigma_y^2 = \sigma^2$, they represented the orthogonal components of fading signal. The probability density function of the envelope is given by [31]

$$p_r(r) = \frac{\alpha r^{\alpha-1}}{r_0} \exp\left(-\frac{r^\alpha}{r_0}\right); \qquad r \geqslant 0, \quad \alpha \geqslant 0 \tag{3}$$

where $\alpha$ is a shape parameter, $r_0 = E\{r^\alpha\}$ and $E\{\}$ denotes statistical averaging. In the special case when $\alpha = 2$ the equation (3) describes the Rayleigh distribution and for $\alpha = 1$ becomes an exponential distribution [32].

Because $r_0 = \left[E\left\{r^2\right\}/\Gamma(1+2/\alpha)\right]^{\alpha/2} = [\Omega/\Gamma(1+2/\alpha)]^{\alpha/2}$, where $\Omega = E\left\{r^2\right\}$, and $\Gamma(m)$ is gamma function [33]

$$\Gamma(m) = \int_0^\infty x^{m-1}\exp(-x)dx \tag{4}$$

expression (3) we can write in another adequate form [8, 16]

$$p_r(r) = \alpha\left(\frac{\Gamma\left(1+\frac{2}{\alpha}\right)}{\Omega}\right)^{\alpha/2} r^{\alpha-1}\exp\left[-\left(\frac{r^2}{\Omega}\Gamma\left(1+\frac{2}{\alpha}\right)\right)^{\alpha/2}\right] r \geqslant 0 \tag{5}$$

From the formula (2) it can be seen that

$$R^\alpha = S^2 \tag{6}$$

where $S$ is the Rayleigh envelope. For normalized envelope $Z = R/\sqrt[\alpha]{r_0}$ the PDF of $Z$ we can write as

$$p_z(z) = \alpha z^{\alpha-1}\exp(-z^\alpha); \quad z \geqslant 0 \tag{7}$$

The PDF of Weibull envelope is shown in figure 1 for various parameters.

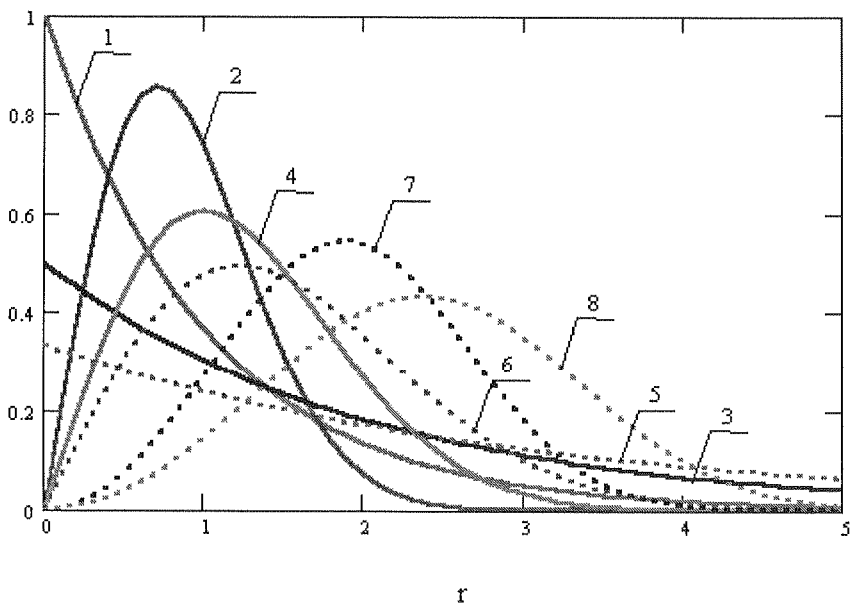


Fig. 1. The Weibull probability density function
1. $\alpha = 1$, $r_0 = 1$; 2. $\alpha = 2$, $r_0 = 1$; 3. $\alpha = 1$, $r_0 = 2$; 4. $\alpha = 2$, $r_0 = 2$;
5. $\alpha = 1$, $r_0 = 3$; 6. $\alpha = 2$, $r_0 = 3$; 7. $\alpha = 3$, $r_0 = 10$; 8. $\alpha = 3$, $r_0 = 20$

Cumulative distribution function (CDF) for the Weibull channel is given by [34, 35]

$$F_R(r) = \int_0^r p_r(r)\,dr = 1 - \exp\left(-\frac{r^\alpha}{r_0}\right) = 1 - \exp\left(-\left(\frac{r^2}{\Omega}\Gamma\left(1+\frac{2}{\alpha}\right)\right)^{\alpha/2}\right); r \geqslant 0 \quad (8)$$

Simultaneously, for normalized envelope we obtain

$$F_Z(z) = 1 - \exp(-z^\alpha);\ z \geqslant 0 \quad (9)$$

Cumulative distribution function for the Weibull envelope is shown in figure 2.

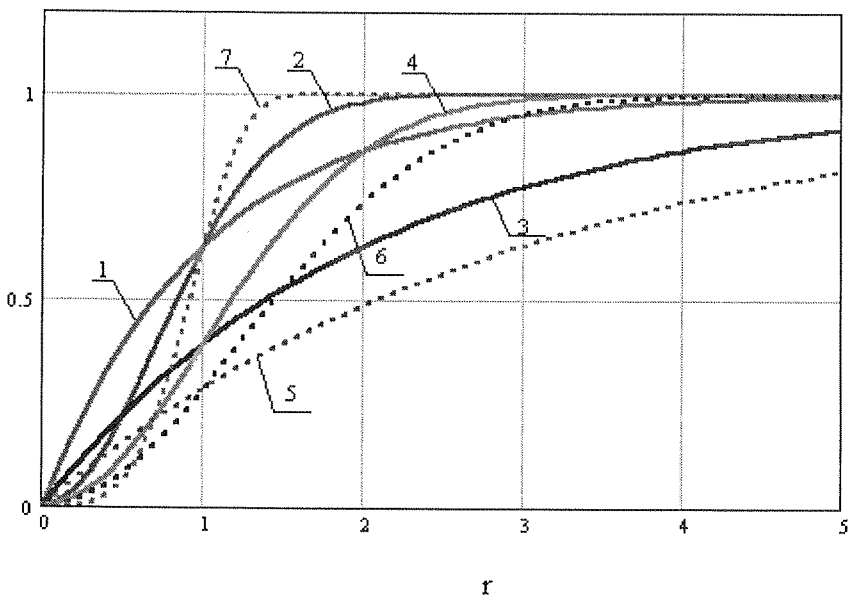


Fig. 2. Weibull CDF
1. $\alpha = 1$, $r_0 = 1$; 2. $\alpha = 2$, $r_0 = 1$; 3. $\alpha = 1$, $r_0 = 2$; 4. $\alpha = 2$, $r_0 = 2$;
5. $\alpha = 1$, $r_0 = 3$; 6. $\alpha = 2$, $r_0 = 3$; 7. $\alpha = 4$, $r_0 = 1$

The $k$-th moment of fading envelope in Weibull channel with parameter $\alpha$ is given by

$$E\left\{r^k\right\} = r_0^{\frac{k}{\alpha}}\Gamma\left(1+\frac{k}{\alpha}\right) = \left[\frac{\Omega}{\Gamma\left(1+\frac{2}{\alpha}\right)}\right]^{\frac{k}{2}}\Gamma\left(1+\frac{k}{\alpha}\right) \quad (10)$$

Then the mean value and variance for Weibull fading envelope are properly equal

$$E\{r\} = \sqrt[\alpha]{r_0}\Gamma\left(1+\frac{1}{\alpha}\right) = \left[\frac{\Omega}{\Gamma\left(1+\frac{2}{\alpha}\right)}\right]^{\frac{1}{2}}\Gamma\left(1+\frac{1}{\alpha}\right) \quad (11)$$

$$\operatorname{var}\{r\} = r_o^{\frac{2}{\alpha}}\left[\Gamma\left(1+\frac{2}{\alpha}\right) - \Gamma^2\left(1+\frac{1}{\alpha}\right)\right] = \Omega\left[1 - \frac{\Gamma^2\left(1+\frac{1}{\alpha}\right)}{\Gamma\left(1+\frac{2}{\alpha}\right)}\right] \tag{12}$$

Of course for normalized envelope $Z$ we obtain

$$E\left\{z^k\right\} = \Gamma\left(1+\frac{k}{\alpha}\right) \tag{13}$$

The best known performance measure of digital communication system is signal-to-noise ratio (SNR) given by

$$\rho = \frac{r^2 E_b}{2N_0} \tag{14}$$

where $E_b$ is energy per bit. Next we assumed, without loss of generality, that $E_b$ is normalized to 1. In Weibull channel SNR is distributed according to [8]

$$p_\rho(\rho) = \frac{\alpha}{2}\left(\frac{\Gamma\left(1+\frac{2}{\alpha}\right)}{\overline{\rho}}\right)^{\alpha/2} \rho^{\frac{\alpha}{2}-1} \exp\left[-\left(\frac{\rho}{\overline{\rho}}\Gamma\left(1+\frac{2}{\alpha}\right)\right)^{\alpha/2}\right]; \rho \geqslant 0 \tag{15}$$

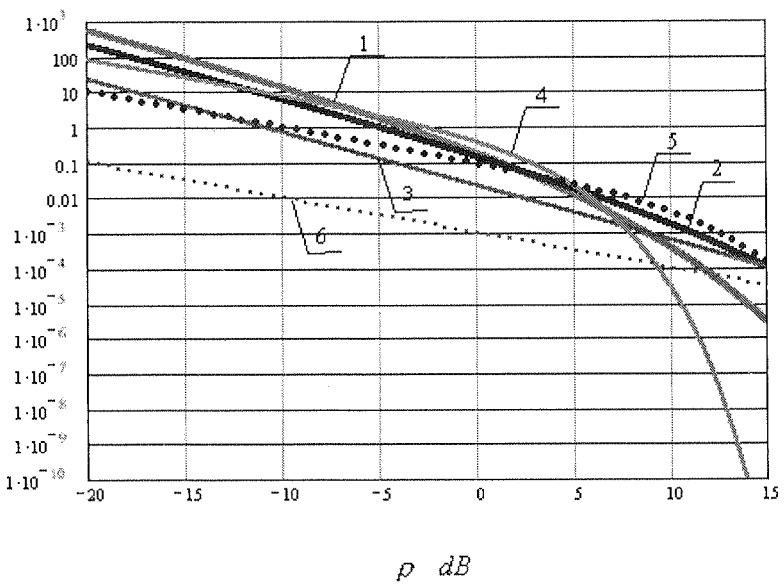


Fig. 3. The probability density function of SNR
1. $\alpha = 1$, $\overline{\rho} = 1$ dB; 2. $\alpha = 1$, $\overline{\rho} = 10$ dB; 3. $\alpha = 1$, $\overline{\rho} = 30$ dB;
4. $\alpha = 2$, $\overline{\rho} = 1$ dB; 5. $\alpha = 2$, $\overline{\rho} = 10$ dB; 6. $\alpha = 2$, $\overline{\rho} = 30$ dB

where $\overline{\rho} = E\{\rho\}$ is the expected SNR. We must note that $\rho$ is also a Weibull random variable. The probability density function of the SNR is shown in figure 3 for various parameters.

The corresponding CDF for SNR is

$$F_\rho(\rho) = 1 - \exp\left[-\left(\frac{\rho}{\overline{\rho}}\Gamma\left(1+\frac{2}{\alpha}\right)\right)^{\alpha/2}\right];\quad \rho \geqslant 0 \tag{16}$$

The moment generating function (MGF) associated with $\rho$ can be expressed as [32]

$$M_\rho(s) = \int_0^\infty \exp(s\rho)p_\rho(\rho)\,d\rho = \frac{\alpha}{2}\left(\frac{\Gamma\left(1+\frac{4}{\alpha}\right)}{\overline{\rho}}\right)^{\alpha/4}(2\pi)^{(2-\alpha)/4}\sqrt{\frac{2}{\alpha}}\left(\frac{-2s}{\alpha}\right)^{-\alpha/2}\times$$
$$\times\, G_{1,\alpha/2}^{\alpha/2,1}\left[\left(\frac{\Gamma\left(1+\frac{4}{\alpha}\right)}{\overline{\rho}}\right)^{-\alpha/4}\left(\frac{-2s}{\alpha}\right)^{c/2}\middle|\begin{matrix}1\\ 1,1+2/\alpha,\ldots,(\alpha-2)/\alpha\end{matrix}\right] \tag{17}$$

where $G_{1,\alpha}^{\alpha,1}(\,)$ is the Meijer's $G$ – function [33], see also Appendix.

Another important characteristics of fading channel is the amount of fading (AF). It is associated with the fading PDF and is defined as the ratio of variance to the square mean

$$AF = \frac{\operatorname{var}\{r^2\}}{[E\{r^2\}]^2} = \frac{E\left\{\left(r^2-\Omega\right)^2\right\}}{\Omega^2} = \frac{E\{r^4\}-\Omega^2}{\Omega^2} = \frac{E\{\rho^2\}-[E\{\rho\}]^2}{[E\{\rho\}]^2} = \frac{E\{\rho^2\}-(\overline{\rho})^2}{(\overline{\rho})^2} \tag{18}$$

We see that AF depends only on the first moments of amplitude fading or SNR. AF is considered as a unified measure for the severity of fading [8]. The amount of fading for the Weibull channel is given by

$$AF = \frac{\Gamma\left(1+\frac{4}{\alpha}\right)}{\Gamma^2\left(1+\frac{2}{\alpha}\right)} - 1 \tag{19}$$

This parameter varies between 0 and $\infty$.

### 2.2. GENERATING OF WEIBULL DISTRIBUTED RANDOM VARIABLES

Let $U$ is a random variable of the uniform distribution in the interval (0, 1]. Then the random variable

$$W = [-r_0 \ln(1-U)]^{1/\alpha} = [-\ln(1-U)]^{1/\alpha} \left[\frac{\Omega}{\Gamma\left(1+\frac{2}{\alpha}\right)}\right]^{1/2} \tag{20}$$

has a Weibull distribution with parameters $\alpha$ and $\Omega = E\{r^2\}$. It results from the form of the cumulative distribution function, which is given by equation (8). Weibull envelope obtained from formula (20) is presented on figure 4.

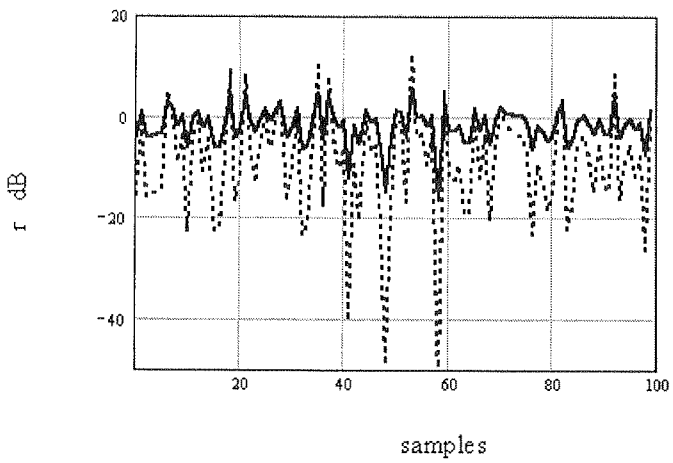


Fig. 4. Weibull envelope (100 samples), $\Omega = 1$, $\alpha = 1$ – dot line, $\alpha = 3$ – solid line

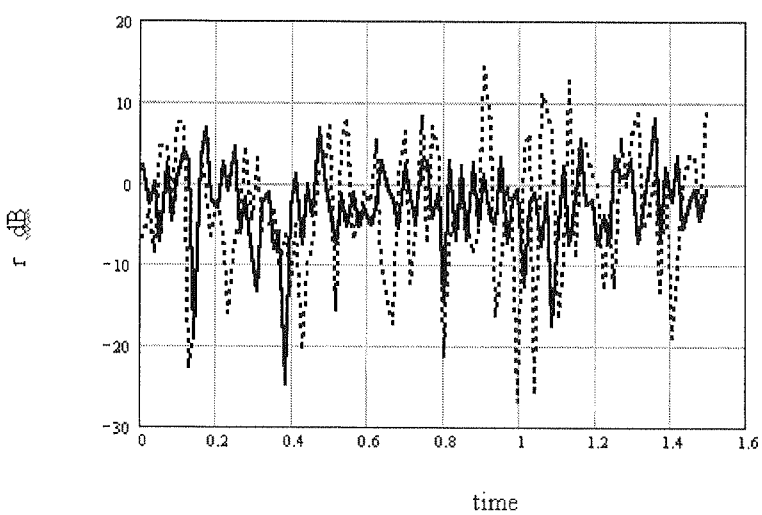


Fig. 5. Weibull envelope waveform generated with standard Mathcad function for 100 samples, $r_0 = 1$, $\alpha = 1$ – dot line, $\alpha = 2$ – solid line

Another method of generating Weibull waveform is based on using standard Mathcad function *rweibull*$(m, \alpha)$, which returns a vector of $m$ random numbers having the Weibull distribution with parameter $\alpha$. That results are presented on figure 5.

We can also generate Weibull fading envelope using Gaussian RV and expression (2). The results are presented in figure 6, at what we assume that mean value of the Gaussian RV equal zero and the standard deviation $\sigma = 1$.

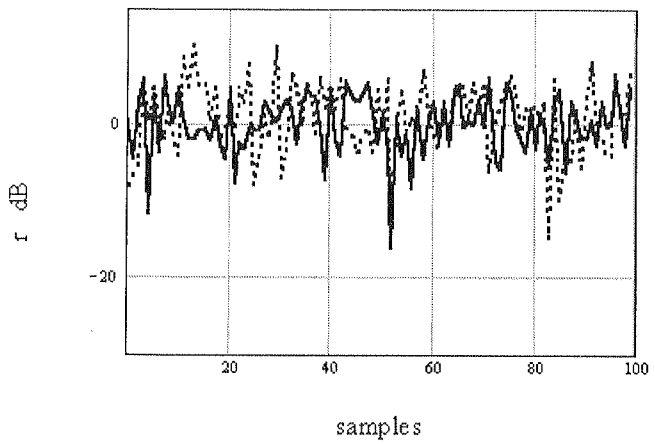


Fig. 6. Weibull envelope waveform generated with Gaussian RV for 100 samples, $\sigma^2 = 1$, $\alpha = 2$ – dot line, $\alpha = 3$ – solid line

Other methods for modeling and simulating the Weibull envelope are presented in the Gang Li et al. papers [36, 37] and in the Farina et al. paper [38]. The authors using Weibull model for presenting the clutter amplitude in modern radar systems, such as high resolution radars, and radars operating at low grazing angles. Also W.J. Szajnowski [39] discussed other method for generating the Weibull signals with a desired correlation matrix and specified parameters. The method presented here uses a nonlinear transformation of random Gaussian vectors with correlated components.

## 3. THE GAUSSIAN-BASED MULTIVARIATE WEIBULL DISTRIBUTION

Multivariate statistics is a useful mathematical tool for modelling and analyzing realistic wireless channels with correlated fading. Such fading channels are usually met in digital contemporary communications systems employed with diversity receivers with not sufficiently separated antennae where space or polarization diversity is applied (e.g. handheld mobile terminals and indoor base-stations). In these applications, the correlation among the channels results in a degradation of the diversity gain obtained [8, 40]. Reviewing the open technical literature, there are several papers applying multivariate statistics for fading channel modelling with most of them concerning the Rayleigh and Nakagami-*m* distributions. In an early work, Nakagami has defined the

$m$-bivariate probability density function [10], while many years later, an infinite series representation for the bivariate Rayleigh and Nakagami-$m$ cumulative distribution functions have been presented by Tan and Beaulieu [41]. In a later work [42], Simon and Alouini have proposed an alternative CDF expression for the bivariate Rayleigh distribution, being in the form of a single integral with finite limits and an integrand composed of elementary functions. Recently, Karagiannidis et al. [43] have introduced the multivariate Nakagami-$m$ PDF with exponential correlation and identically distributed (i.d.) fading statistics. An infinite series approach for its corresponding CDF and a bound of the error resulting from the truncation of the infinite series have been also included. By approximating the correlation matrix with a Green's matrix, the same authors have generalized [7] to the arbitrarily correlated Nakagami-$m$ distribution [44]. Additionally, Mallik [45] has presented useful analytical PDF and CDF expressions for the multivariate Rayleigh distribution with exponential and constant correlation matrix which agree with those in [43] for the special case where the Nakagami-$m$ reduces to the Rayleigh distribution.

In order to analyze the performance of diversity receivers operating over more realistic correlated fading channels, multivariate Weibull statistical analysis must be utilized. Several classes of multivariate Weibull distributions have been proposed in [46, 47, 48, 49, 50, 51], but only very recently a published work dealt with the class of multivariate Weibull distribution, generated from correlated Gaussian processes [52].

### 3.1. THE BIVARIATE WEIBULL DISTRIBUTION

Starting from the bivariate Rayleigh distribution, we introduce the bivariate Weibull fading model derived from not necessarily identical distributed Gaussian random variables as [52]. The bivariate PDF of the correlated Rayleigh random variables $S_1$ and $S_2$, the CDF and the $(n + m)$ th order joint moment of $S_1$ and $S_2$ are expressed respectively as [8, 10, 43, 45]

$$p_{s_1,s_2}(s_1, s_2) = \frac{4 s_1 s_2}{\Omega_1 \Omega_2 (1-\gamma)} \exp\left[-\frac{1}{1-\gamma}\left(\frac{s_1^2}{\Omega_1} + \frac{s_2^2}{\Omega_2}\right)\right] I_0\left(\frac{2\sqrt{\gamma}\, r_1^2\, r_2^2}{(1-\gamma)\sqrt{\Omega_1 \Omega_2}}\right) \tag{21}$$

$$\begin{aligned} F_{s_1,s_2}(s_1, s_2) = {} & 1 - \exp\left(\frac{s_1^2}{\Omega_1}\right) Q_1\left(\sqrt{\frac{2}{1-\gamma}}\frac{s_2}{\sqrt{\Omega_2}}, \sqrt{\frac{2\gamma}{1-\gamma}}\frac{s_1}{\sqrt{\Omega_1}}\right) + \\ & - \exp\left(\frac{s_2^2}{\Omega_2}\right)\left[1 - Q_1\left(\sqrt{\frac{2\gamma}{1-\gamma}}\frac{r_2}{\sqrt{\Omega_2}}, \sqrt{\frac{2}{1-\gamma}}\frac{s_1}{\sqrt{\Omega_1}}\right)\right] \end{aligned} \tag{22}$$

and

$$E\left\{S_1^n, S_2^m\right\} = (1-\gamma)^{\frac{n+m+2}{2}}\,\Omega_1^{\frac{n}{2}}\Omega_2^{\frac{m}{2}}\,\Gamma\left(\frac{2+n}{2}\right)\Gamma\left(\frac{2+m}{2}\right){}_2F_1\left(\frac{2+n}{2}, \frac{2+m}{2}; 1; \gamma\right) \tag{23}$$

where $\Omega_i = E\left\{S_i^2\right\}$ for $i = 1, 2$, $I_0(\alpha)$ is a modified Bessel function of the first kind and zero order [33]

$$I_o(\alpha) = \frac{1}{2\pi}\int_0^{2\pi} \exp(\alpha\cos\phi)\, d\phi \;=\; \sum_{k=0}^{\infty}\frac{(\alpha/2)^{2k}}{(k!)^2} \tag{24}$$

$Q_1(\alpha,\beta)$ is the first order Marcum's function [8, 33]

$$Q_1(\alpha,\beta) = \int x\exp(-\frac{x^2+\alpha^2}{2})I_0(\alpha x)\, dx \tag{25}$$

${}_2F_1(a, \cdot b; x; y)$ is the Gauss hypergeometric function [33]

$${}_2F_1(a, \cdot b; x; y) = \frac{\Gamma(x)}{\Gamma(x-b)\Gamma(b)}\int t^{b-1}(1-t)^{x-b-1}(1-ty)^{-a}\, dt \tag{26}$$

and $\gamma$ is the power correlation coefficient between $S_1^2$ and $S_2^2$, which is defined as [8]

$$\gamma = \frac{\operatorname{cov}\left\{S_1^2, S_2^2\right\}}{\sqrt{\operatorname{var}\left\{S_1^2\right\}\operatorname{var}\left\{S_2^2\right\}}};\quad 0 \leqslant \gamma < 1 \tag{27}$$

By using (2), (6) and (21) the joint PDF of the Weibull distributed random variable $R_1$ and $R_2$ can be expressed as [52]

$$\begin{aligned} p_{r_1,r_2}(r_1,r_2) &= |J|\, p_{s_1,s_2}(s_1,s_2) = \\ &= \frac{\alpha_1\alpha_2\, r_1^{\alpha_1-1}\, r_2^{\alpha_2-1}}{r_{01}\, r_{02}\,(1-\gamma)}\exp\left[-\frac{1}{1-\gamma}\left(\frac{r_1^{\alpha_1}}{r_{01}}+\frac{r_2^{\alpha_2}}{r_{02}}\right)\right] I_0\left(\frac{2\sqrt{\gamma}\, r_1^{\alpha_1/2}\, r_2^{\alpha_2/2}}{(1-\gamma)\sqrt{r_{01}\, r_{02}}}\right) \end{aligned} \tag{28}$$

where $|J|$ is the Jakobian of the transformation and $r_{oi} = E\left\{r_i^{\alpha_i}\right\}$.

The $(n+m)$ th order joint moment of Weibull random variable $R_1$ and $R_2$ can be written as [52]

$$\begin{aligned} E\left\{R_1^n, R_2^m\right\} &= E\left\{S_1^{2n/\alpha_1}, S_2^{2m/\alpha_2}\right\} = \\ &= (1-\gamma)^{1+n/\alpha_1+m/\alpha_2}\, r_{01}^{n/\alpha_1}\, r_{02}^{m/\alpha_2}\,\Gamma\left(1+\frac{n}{\alpha_1}\right)\Gamma\left(1+\frac{m}{\alpha_2}\right){}_2F_1\left(1+\frac{n}{\alpha_1}, 1+\frac{m}{\alpha_2}; 1; \gamma\right) \end{aligned} \tag{29}$$

The joint CDF of $R_1$ and $R_2$ we can obtained as

$$F_{R_1,R_2}(r_1,r_2) = F_{S_1,S_2}\left(s_1^{2/\alpha_1}, s_2^{2/\alpha_2}\right) \tag{30}$$

Power correlation coefficient between $R_1^2$ and $R_2^2$ can be expressed as [52]

$$\varsigma = \frac{\operatorname{cov}\left\{R_1^2, R_2^2\right\}}{\sqrt{\operatorname{var}\left\{R_1^2\right\}\operatorname{var}\left\{R_2^2\right\}}} = \frac{(1-\gamma)^{1+2/\alpha_1+2/\alpha_2}\,{}_2F_1\left(1+\frac{2}{\alpha_1}, 1+\frac{2}{\alpha_2}; 1; \gamma\right) - 1}{\sqrt{\frac{\Gamma\left(1+\frac{4}{\alpha_1}\right)}{\Gamma^2\left(1+\frac{2}{\alpha_1}\right)} - 1}\sqrt{\frac{\Gamma\left(1+\frac{4}{\alpha_2}\right)}{\Gamma^2\left(1+\frac{2}{\alpha_2}\right)} - 1}}; 0 \leqslant \zeta < 1 \tag{31}$$

### 3.2. THE MULTIVARIATE WEIBULL DISTRIBUTION WITH EXPONENTIAL CORRELATION

Several fading correlation models have been proposed and used for the performance analysis of various wireless systems, corresponding to specific modulation, detection and diversity combining schemes. One of the most frequently used models is the exponential correlation one, which has been firstly addressed by Aalo in [40]. This models corresponds to the scenario of multichannel reception from equispaced diversity antennae, in which the correlation among the pairs of combined signals decays as the spacing between the antennae increases [8].

The multivariate PDF of the identical distributed Rayleigh random variable $S_i$ for $i = 1, 2, ..., L$, with exponential correlation is given by [45]

$$p_S(s) = \left(\frac{2}{\Omega}\right)^L \frac{\prod_{i=1}^{L} s_i}{(1-\gamma)^{L-1}} \exp\left\{\frac{-1}{(1-\gamma)\Omega}\left[s_1^2 + s_L^2 + (1-\gamma)\sum_{i=2}^{L-1} s_i^2\right]\right\} \prod_{i=1}^{L-1} I_0\left[\frac{2\sqrt{\gamma}}{(1-\gamma)\Omega} s_i s_{i+1}\right] \tag{32}$$

where $\Omega = E\left(s_i^2\right)$ for $i = 1, 2, ..., L$, $L$ is the number of correlated RV's, $\vec{s} = (s_1, s_2, ..., s_L)$ and $\vec{S} = (S_1, S_2, ..., S_L)$, $\gamma$ is the Gaussian power correlation coefficient between two successive RV's (e.g. between $S_i^2$ and $S_{i+1}^2$ while in general, the correlation coefficient between $S_i^2$ and $S_j^2$ is given by $\gamma_{i,j} = \gamma_{j,i} = \gamma^{|i-j|}$ when $i \neq j$, and $\gamma_{i,j} = 1$, when $i = j$ with $i, j = 1, 2, ..., L$.

By applying the transformation given by (2) in (32) and by using the standard method for the transformation of RV's described in [53], the joint PDF of the Weibull RVs $R_i$ for $i = 1, 2, ..., L$ can be obtained in closed-form as

$$p_R(r) = \frac{\prod_{i=1}^{L} \alpha_i r_i^{\alpha_i - 1}}{r_0^L (1-\gamma)^{L-1}} \exp\left\{ \frac{-1}{(1-\gamma) r_0} \left[ r_1^{\alpha_1} + r_L^{\alpha_L} + (1+\gamma) \sum_{i=2}^{L-1} r_i^{\alpha_i} \right] \right\} \times \times \prod_{i=1}^{L-1} I_0 \left[ \frac{2\sqrt{\gamma}}{(1-\gamma) r_0} r_i^{\alpha_i/2} r_{i+1}^{\alpha_{i+1}/2} \right] \tag{33}$$

where $r_0 = r_{0i} = E\left\{R_i^{\alpha_i}\right\}$, $\vec{R} = (R_1, R_2, ..., R_L)$ and marginal PDF is given by (3) for $i = 1, 2, ..., L$.

## 4. CONCLUDING REMARKS

We have presented important statistical properties of the two parameters Weibull distribution, which can be efficiently used to study the performance of mobile communications systems, operating over fading channels. More specifically, the univariate Webull distribution was presented, with exact closed-form expressions for the PDF, CDF and the moments of the envelope. We also have presented the multivariate Webull distribution.

In Poland, bibliography on Weibull fading is not very wide. Most of the information can be found in foreign papers, especially in conference publications and journals. In spite of huge development of Internet, not all publications are accessible, for many researches interested in transmission over fading channel. The access to some publications is possible after login to suitable bases. So, the presented paper is the synthetic attempt of complex description the Weibull fading channel.

The presented theoretical results will be applied to analyze the performance in digital transmisson over Weibull fading channels. We will do it in next paper.

## 5. REFERENCES


1. S.B. Rassol: *Analysis of random access methods over fading channel for finite buffer systems*, Master Thesis f Science, Department of Electrical Engineering, King Fahd University, Saudi Arabia, January 2005.
2. A. Jakubiak: *Radiolokacyjne zakłócenia bierne – ich powstawanie i właściwości*, Przegląd Telekomunikacyjny i Wiadomości Telekomunikacyjne, Nr 4, 2001, ss. 258-264, in Polish.
3. A. Jakubiak, W. Czarnecki: *Zastosowanie symulacji komputerowej w analizie i klasyfikacji radiolokacyjnych zakłóceń biernych typu clutter*, Przegląd Telekomunikacyjny i Wiadomości Telekomunikacyjne, Nr 3, 2000, in Polish.
4. A. Jakubiak: *Metody klasyfikacji radiolokacyjnych zakłóceń biernych*, Prace Naukowe Elektronika, No 126, Oficyna Wydawnicza Politechniki Warszawskiej, Warszawa 2000.
5. A. Jakubiak: *Wykrywanie sygnału użytecznego na tle zakłóceń Suzuki*, XI Krajowe Sympozjum Nauk Radiowych, Poznań, 2005, in Polish.

6. A. Jakubiak, M. Muczko, A. Zieliński: *Wybrane metody modelowania komputerowego zakłóceń biernych*, Przegląd Telekomunikacyjny i Wiadomości Telekomunikacyjne, Nr 4, 2000, in Polish.
7. A. Jakubiak: *Metody i algorytmy symulacji radiolokacyjnych zakłóceń biernych*, Kwartalnik Elektroniki i Telekomunikacji, 2000, Vol. 46, Nr 2, ss. 237-253, in Polish.
8. M.K. Simon, M.S. Alouini: *Digital communication over fading channels, a unified approach to performance analysis*, John Wiley & Sons, New York, 2005, 2nd edition.
9. A. Wojnar: *Teoria sygnałów*, WNT, Warszawa 1988, in Polish.
10. M. Nakagami: *The -distribution – A general formula of intensity distribution of rapid fading*, in Statistical Methods in Radio Wave Propagation, Oxford, U.K., Pergamon, 1960, pp. 3-36.
11. K. Noga: *Zaawansowane modele probabilistyczne sygnałów w kanałach z zanikami*, Kwartalnik Elektroniki i Telekomunikacji, 2000, Vol. 46, Nr 1, ss. 47-62, in Polish.
12. W. Weibull: *A statistical distribution function of wide applicability*, Journal of Applied Mechanics, No. 27, 1951.
13. R. Ramakumar: *Reliability Engineering – Fundamentals and Applications*, Englewood Cliffs, NJ: Prentice-Hall, 1993.
14. R.B. Abernethy: *The New Weibull Handbook*, 4th ed. New York, Barringer & Assoc., 2000.
15. M. Sekine, Y.H. Mao: *Weibull Radar Clutter*. London, U.K., IEE, 1990.
16. H. Hashemi: *The indoor radio propagation channel*, Proceedings of the IEEE, Vol. 81, No. 7, July 1993, pp. 943-968.
17. B. Babich, G. Lombardi: *Statistical analysis and characterization of the indoor propagation channel*, IEEE Transactions on Communications, Vol. 48, No. 3, March 2000, pp. 455-464.
18. R. Kattenbach, T. Englert: *Investigation of short term statistical distributions for path amplitudes and phases in indoor environment*, Proc. IEEE Vehicular Technology Conference, Ottawa, ON, Canada, May 1998, pp. 2114-2118.
19. R. Ganesh, K. Pahlavan: *On the modeling of fading multipath indoor radio channels*, in Proc. IEEE Global Telecommunications Conference, Vol. 3, Dallas, TX, November 1989, pp. 1346-1350.
20. N.S. Adawi et al.: *Coverage prediction for mobile radio systems operating in the 800/900 MHz frequency range*, IEEE Transactions on Vehicular Technology, Vol. 37, No. 1, February 1988, pp. 3-72.
21. N.H. Shepherd: *Radio wave loss deviation and shadow loss at 900 MHz*, IEEE Transactions on Vehicular Technology, Vol. VT-26, 1977, pp. 309-313.
22. M.A. Taneda, J. Takada, K. Araki: *A new approach to fading: Weibull model*, Proceedings IEEE International Symposium Personal, Indoor, Mobile Radio Communications, Osaka, Japan, September 1999, pp. 711-715.
23. A. Healy, C.H. Bianchi, K. Sivaprasad: *Wideband outdoor channel sounding at 2.4 GHz*, Proceedings IEEE Antennas Propagation for Wirelles Communications, Waltham, MA, November 2000, pp. 95-98.
24. M.D. Yacoub: *The $\alpha-\mu$ distribution: A general fading distribution*, Proceedings IEEE International Symposium Personal, Indoor, Mobile Radio Communications, Lisbon, Portugal, September 2002, pp. 629-633.
25. M.-S. Alouini, M.K. Simon: *Performance of generalized selection combining overWeibull fading channels*, Proceedings IEEE Vehicular Technology Conference, Vol. 3, Atlantic City, NJ, October 2001, pp. 1735-1739.
26. N.C. Sagias, D.A. Zogas, G.K. Karagiannidis, G.S. Tombras: *Performance analysis of switched diversity receivers in Weibull fading*, Electronics Letters, Vol. 39, No. 20, October 2003, pp. 1472-1474.
27. N.C. Sagias, G.K. Karagiannidis, G.S. Tombras: *Error rate analysis of switched diversity receivers in Weibull fading*, Electronics Letters, Vol. 40, No. 11, May 2004, pp. 681-682.

28. N.C. Sagias, G.K. Karagiannidis, D.A. Zogas, P.T. Mathiopoulos, G.S. Tombras: *Performance analysis of dual selection diversity in correlated Weibull fading channels*, IEEE Transactions on Communications, Vol. 52, No. 7, July 2004, pp. 1063-1067.
29. N.C. Sagias, P.T. Mathiopoulos, G.S. Tombras: *Selection diversity receivers in Weibull fading. Outage probability and average signal-to-noise ratio*, Electronics. Letters., Vol. 39, No. 25, December 2003, pp. 1859-1860.
30. J. Cheng, C. Tellambura, N.C. Beaulieu: *Performance of digital linear modulations on Weibull slow-fading channels*, IEEE Transactions on Communications, Vol. 52, No. 8, August 2004, pp. 1265-1268.
31. M.D. Yacoub, D.B. Costa, U.S. Dias, G. Fraidenraich: *Join statistics for two correlated Weibull variates*, IEEE Antennas and Wireless Propagation Letters, Vol. 4, 2005, pp. 129-132.
32. J. Cheng, C. Tellambura, N.C. Beaulieu: *Performance analysis of digital modulations on Weibull fading channels*, Proceedings IEEE Vehicular Technology Conference (VTC Fall'03), Orlando, October 2003, pp. 236-240.
33. S. Gradstein, M. Ryzhik: *Tables of Integrals, Sums, Series and Products*, London, UK., Academic, 1964.
34. http://en.wikipedia.org/wiki/Weibull_distribution
35. http://www.weibull.com
36. G. Li, K.B. Yu: *A method for simulation of coherent Weibull clutter*, Proceedings of the Twentieth Southeastern Symposium on System Theory, 1988, pp. 691-695.
37. G. Li, K.B. Yu: *Modelling and simulation of coherent Weibull clutter*, IEE, Radar and Signal Proceedings, February 1989, pp. 2-12.
38. A. Farina, A. Russo, F. Scannapieco: *Radar detection in coherent Weibull*, IEEE Transactions on Acoustics, Speech and Signal Processing, Vol. ASSP-35, No. 6, June 1987, pp. 893-895.
39. W.J. Szajnowski: *The generation of correlated Weibull clutter for signal detection problem*, IEEE Transactions on Aerospace & Electronics Systems, Vol. AES-13, No. 5, 1977, pp. 536-540.
40. V.A. Aalo: *Performance of maximal-ratio diversity systems in a correlated Nakagami-fading environment*, IEEE Transactions on Communications, Vol. 43, No. 8, August 1995, pp. 2360-2369.
41. C.C. Tan, N.C. Beaulieu: *Infinite series representations of the bivariate Rayleigh and Nakagami-m distributions*, IEEE Transactions on Communications, Vol. 45, No. 10, pp. 1159-1161, October 1997.
42. M.K. Simon, M.-S. Alouini: *A simple integral representation of the bivariate Rayleigh distribution*, IEEE Communications Letters, Vol. 2, No. 5, pp. 128-130, May 1998.
43. G.K. Karagiannidis, D.A. Zogas, S.A. Kotsopoulos: *On the multivariate Nakagami-m distribution with exponential correlation*, IEEE Transactions on Communications Vol. 51, No. 8, pp. 1240-1244, August 2003.
44. G.K. Karagiannidis, D.A. Zogas, S.A. Kotsopoulos: *An efficient approach to multivariate Nakagami- distribution using Green's matrix approximation*, IEEE Transactions Wireless Communications, Vol. 2, No. 5, pp. 883-889, September 2003.
45. R.K. Mallik: *On multivariate Rayleigh and exponentials distributions*, IEEE Transactions on Information Theory, Vol. 49, No. 6, pp. 1499-1515, June 2003.
46. I. Olkin, Y.L. Tong: *Positive dependence of a class of multivariate exponential distributions*, SIAM Journal on Control and Optimization, Vol. 32, pp. 965-974, 1994.
47. L. Lee: *Multivariate distributions having Weibull properties*, Journal of Multivariate Analysis, Vol. 9, pp. 267-277, 1979.
48. P. Hougaard: *A class of multivariate failure time distributions*, Biometrika, Vol. 73, pp. 671-678, 1986.
49. M. Crowder: *A multivariate distribution with Weibull connections*, Journal of Royal Statistics Society, Vol. 51, pp. 93-107, 1989.
50. P. Hougaard: *Analysis of Multivariate Survival Data*, Berlin, Germany: Springer-Verlag, 2000.

51. S. Kotz, N. Balakrishnan, N.L. Johnson: *Continuous Multivariate Distributions*, Vol. 1, Models and Applications, New York: Wiley, 2000.
52. N.C. Sagias, G.K. Karagiannidis: *Gaussian Class Multivariate Weibull Distributions: Theory and Applications in Fading Channels*, IEEE Transactions on Information Theory, Vol. 51, No. 10, pp. 3608-3619, October 2005.
53. A. Papoulis: *Probability, Random Variables and Stochastic Processes*, 3-rd edition, New York, McGraw-Hill, 2001.
54. R.K. Mallik, M.Z. Win: *Analysis of hybrid selection/maximal-ratio combining in correlated Nakagami fading*, IEEE Transactions on Communications, Vol. 50, No. 8, pp. 1372-1383, August 2002.
55. http://mathworld.wolfram.com/MeijerG-Function.html

## APPENDIX

The Meijer's $G$ – function is a general function which reduces to simpler special functions. That function is definied by [33, 55]

$$G_{p,q}^{m,n}\left(x\left|\begin{matrix}a_1,\ldots,a_p\\ b_1,\ldots,b_q\end{matrix}\right.\right)\equiv\frac{1}{2\pi i}\int_{\gamma_l}\frac{\prod_{j=1}^{m}\Gamma\left(b_j-s\right)\prod_{j=1}^{n}\Gamma\left(1-a_j+s\right)}{\prod_{j=n+1}^{p}\Gamma\left(a_j-s\right)\prod_{j=m+1}^{q}\Gamma\left(1-b_j+s\right)}x^s\,ds \tag{A1}$$

The Meijer's $G$ – function is implemented in Mathematica as MeijerG( ). Special cases of Meijer – $G$ function include [55]

$$G_{2,2}^{1,2}\left(x\left|\begin{matrix}1,\ 1\\ 1,\ 0\end{matrix}\right.\right)=\ln\left(x+1\right) \tag{A2}$$

$$G_{2,2}^{1,2}\left(x\left|\begin{matrix}1,\ 1\\ 1,\ 1\end{matrix}\right.\right)=\frac{x}{x+1} \tag{A3}$$

$$G_{0,2}^{1,0}\left(\frac{x}{2}\left|\begin{matrix}-\\ 0,\ 0.5\end{matrix}\right.\right)=\frac{\cos\left(\sqrt{2x}\right)}{\sqrt{\pi}} \tag{A4}$$

$$G_{1,0}^{0,1}\left(x\,|1-\alpha\right)=x^{-\alpha}\exp\left(-\frac{1}{x}\right) \tag{A5}$$

# Efficient variable partitioning method for functional decomposition

MARIUSZ RAWSKI

*Warsaw University of Technology*
*Institute of Telecommunications Poland*
*rawski@tele.pw.edu.pl*

*Otrzymano 2006.09.04*
*Autoryzowano 2006.11.23*

In recent years the functional decomposition has found an application in many fields of modern engineering and science, such as combinational and sequential logic synthesis for VLSI systems, pattern analysis, knowledge discovery, machine learning, decision systems, data bases, data mining etc. However, its practical usefulness for very complex systems has been limited by the lack of an efficient method for selecting the appropriate input variable partitioning. This is an NP-hard problem and thus heuristic methods have to be used to efficiently and effectively search for optimal or near-optimal solutions.

In this paper, a heuristic method for the input variable partitioning is discussed. The method is based on an application of evolutionary algorithms, what allows exploring the possible solution space of problem while keeping the high-quality solutions in this reduced space. The experimental results show that the proposed heuristic method is able to construct an optimal or near optimal solution very efficiently even for large systems. It is much faster than the systematic method while delivering results of comparable quality.

*Keywords:* logic synthesis, functional decomposition, evolutionary algorithms

## 1. INTRODUCTION

Nowadays, by taking advantage of the opportunities provided by modern microelectronic technology, we are able to build very complex digital circuits and systems at relatively low cost in a single chip. However, the opportunities created by advances in microelectronics cannot be fully exploited because of weaknesses of the traditional logic design methods. Current methodologies and productivity improvements are failing to keep pace with the rapid and ongoing increase in complexity and technology improvements. According to International Technology Roadmap for Semiconductors

(1997) annual growth rate in complexity of digital devices is equal to 58% while annual growth rate in productivity is only 21%.

The traditional logic synthesis methods do not take hard structural constraints into consideration. In principle, they relate only to some very special cases of possible implementation structures involving certain minimal, functionally complete systems of logic gates (e.g. AND+OR+NOT, AND+EXOR, MUX). They require post synthesis technology mapping for other implementation structures. If the actual synthesis target strongly differs from these minimal systems, e.g. if it involves a lot of complex gates, look-up table FPGAs or (C)PLDs, no technology mapping can guarantee a good result because the initial synthesis is performed without a close relation to the actual target. The influence of advanced logic synthesis procedures on the quality of hardware implementation of signal and information processing systems is especially important in case of applications targeted to FPGA structures based on look-up tables (LUT).

Field Programmable Gate Array (FPGA) devices are an array of programmable logic cells interconnected by a matrix of wires and programmable switches. Each cell performs a simple logic function defined by a designer's program. An FPGA has a large number (to over 330,000) of these cells available to use as building blocks in complex digital circuits. The ability to manipulate the logic at the gate level means that designer can construct a custom processor to efficiently implement the desired function.

There are several approaches to FPGA-based logic synthesis. The most common approach relies on breaking the synthesis process down into two phases: a technology independent phase and a technology mapping phase. The first of these two attempts to generate an optimal abstract representation of the logic circuit. For the combinational logic, the abstract representation is a Boolean Network – i.e. a directed acyclic graph $G(V,E)$ structure where each node $v \in V$ represents an arbitrarily complex single-output logic function. The second phase then maps the design onto cells of a user-specified target library, and performs technology dependent optimizations taking the given constraints into account.

For FPGAs the constraints are specific because their structures differ from the structures of the standard ASIC technologies. Look-up table based architecture is a prevalent type among many FPGA architectures. LUT-based FPGAs consist of an array of LUTs, each of which can implement any Boolean function with up to $k$ (typically 4 or 5) inputs. A Boolean network can be directly realized by a one-to-one mapping between nodes and LUTs if every node in the network is feasible i.e. has up to $k$ input variables.

Therefore, there has recently been much research in the field of the functional decomposition of combinational circuits and sequential machines [2, 3, 7, 9, 12, 17, 22]. Some of the most promising recent approaches in pattern analysis, knowledge discovery, machine learning, decision systems, data bases, data mining etc. are also based on general functional decomposition [4, 12, 21, 26].

Functional decomposition consists of breaking down a complex system of discrete functions or relations [16] into a network of smaller and relatively independent co-operating sub-systems, in such a way that the original system's behavior is preserved, some constraints are satisfied and some objectives are optimized. The motivation for using functional decomposition in system analysis and design is to reduce the complexity of the problem under consideration through the divide-and-conquer paradigm and to find an appropriate network of coherent sub-systems: a system is decomposed into a set of smaller subsystems, such that each of these is easier to analyze, understand or synthesize. Although functional decomposition gives very good results in the logic synthesis of digital circuits, machine learning, decision systems and other fields [2, 4, 18, 21, 25, 26], its practical usefulness for very complex systems is limited by the lack of an efficient method for the construction of high quality sub-systems.

In the functional decomposition process the following three factors play an extremely important role: an appropriate input variable partitioning, decision which (multi-valued) function will be computed by a certain subsystem and encoding of the subsystem's function with binary output variables.

Since the Ashenhurst-Curtis decomposition have been proposed, the research has been focused in forming new decomposition techniques [15]. The researchers have developed many types of decompositions, but they are still based on Ashenhurst's ideas. Since many of these decomposition techniques were designed for a specific type of problem, they have become obsolete, either by the advent of new technologies or new algorithms. Thus, there have been very few attempts to reduce the complexity of Ashenhurst-Curtis' input variable partition problem.

There are two types of algorithms solving this problem. The algorithms finding decompositions without using any search heuristics. The basic idea of these algorithms is to limit the search to some input variable partitions. This is done by using different functional methods to choose which partitions will be evaluated. These methods select partitions through Reed-Muller expansions, Fourier transforms, binary difference equations, and technology-based mappings [10], [15], [23], [24].

The second type of algorithms utilize different heuristic methods. In [18] the input variable partitioning method based on information relationship measures was presented, which produced optimal or sub-optimal results for factions of considerable size.

In recent years the use of the genetic algorithms has received widespread attention [5], [14]. This approach has been used to find approximate solutions to NP-complete optimization problems [8]. However, to the best author's knowledge, there have been few successful applications of genetic algorithms in the area of decomposition based logic synthesis.

In the paper a method of input variable partitioning based on evolutionary algorithm is discussed. A number of the resulting sub-function's values is used here as a criterion for testing individual solutions and assigning fitness, since the strong correlation of the number of the sub-function's values with the decomposition's quality has been showed in [19]. Application of the evolutionary algorithms for construction

of the input variable partition allows reducing the search space to a manageable size while keeping the high-quality solutions in the reduced space.

After an introduction to functional decomposition and evolutionary algorithms, the new heuristic input partitioning method is presented. Subsequently some experimental results are discussed, which are reached with a prototype tool that implements the method. The experimental results demonstrate that the proposed method is able to construct optimal or near optimal decompositions efficiently, even for large systems. It is much faster than the systematic method while delivering results of a comparable quality.

## 2. BASIC THEORY

### 2.1. REPRESENTATION AND ANALYSIS OF BOOLEAN FUNCTIONS WITH BLANKETS

Here only some information that is necessary for an understanding of this paper is reviewed. More detailed description of functional decomposition based on partition calculus can be found in [1].

A Boolean function can be specified using the concept of cubes (input terms, patterns) representing some specific sub-sets of minterms. In a minterm, each input variable position has a well-specified value. In a cube, positions of some input variables can remain unspecified and they represent "any value" or "don't care" (–). A **cube** may be interpreted as a $p$-dimensional subspace of the $n$-dimensional Boolean space or as a product of $n$-$p$ variables in Boolean algebra ($p$ denotes the number of components that are '–').

For pairs of cubes and for a certain input subset $B$, we define the **compatibility relation** COM as follows: each two cubes $S$ and $T$ are compatible (i.e. $S, T \in \mathrm{COM}(B)$) if and only if $x(S) \sim x(T)$ for every $x \subseteq B$. The compatibility relation $\sim$ on {0, –, 1) is defined as follows [1]: $0 \sim 0$, $- \sim -$, $1 \sim 1$, $0 \sim -$, $1 \sim -$, $- \sim 0$, $- \sim 1$, but the pairs (1, 0) and (0, 1) are not related by $\sim$. The compatibility relation on cubes is reflexive and symmetric, but not necessarily transitive. In general, it generates a "partition" with non-disjoint blocks on the set of cubes representing a certain Boolean function $F$. The cubes contained in a block of the "partition" are all compatible with each other.

"Partitions" with non-disjoint blocks are referred to as rough partitions (r-partitions) [12], [17], blankets [1] or set systems [7]. The concept of blanket is a simple extension of ordinary partition and typical operations on blankets are strictly analogous to those used in the ordinary partition algebra.

A **blanket** on a set $S$ is such a collection of (not necessary disjoint) distinct subsets $B_i$ of $S$, called blocks, that

$$\bigcup_i B_i = S$$

**Example 1** (Blanket-based representation of Boolean functions).

Table 1

Example function

| | $x_1$ | $x_2$ | $x_3$ | $x_4$ | $y_1$ | $y_2$ |
|---|---|---|---|---|---|---|
| 1 | 0 | 0 | – | – | 1 | 1 |
| 2 | 1 | 0 | – | 0 | 1 | 0 |
| 3 | – | 0 | 0 | – | 1 | – |
| 4 | – | – | 1 | 1 | 0 | – |
| 5 | – | 1 | 1 | 0 | 0 | 0 |
| 6 | – | 1 | – | 1 | – | 1 |
| 7 | 0 | – | 0 | 1 | 1 | – |

For function $F$ from Table 1, the blankets induced by particular input and output variables and by the two-output function on the set of function $F$'s input patterns (cubes) are as follows:

$$\beta_{x1} = \{\overline{1, 3, 4, 5, 6, 7}; \overline{2, 3, 4, 5, 6}\},$$
$$\beta_{x2} = \{\overline{1, 2, 3, 4, 7}; \overline{4, 5, 6, 7}\},$$
$$\beta_{x3} = \{\overline{1, 2, 3, 6, 7}; \overline{1, 2, 4, 5, 6}\},$$
$$\beta_{x4} = \{\overline{1, 2, 3, 5}; \overline{3, 4, 6, 7}\},$$
$$\beta_{y1} = \{\overline{1, 2, 3, 6, 7}; \overline{4, 5, 6}\},$$
$$\beta_{y2} = \{\overline{1, 3, 4, 6, 7}; \overline{2, 3, 4, 5, 7}\},$$
$$\beta_{y1y2} = \beta_{y1} \cdot \beta_{y2} = \{\overline{1, 3, 6, 7}; \overline{2, 3, 7}; \overline{4, 5}; \overline{4, 6}\}.$$

The product of two blankets $\beta_1$ and $\beta_2$ is defined as follows:

$\beta_1 \cdot \beta_2 = \{B_i \cap B_j | B_i \in \beta_1 \text{ and } B_j \in \beta_2\}$,

For two blankets we write $\beta_1 \leq \beta_2$ if and only if for each $B_i$ in $\beta_1$ there exists a $B_j$ in $\beta_2$ such that $B_i \subseteq B_j$. The relation $\leq$ is reflexive and transitive.

For example:

$\beta_{x1x2} = \beta_{x1} \cdot \beta_{x2} = \{\overline{1, 3, 4, 7}; \overline{4, 5, 6, 7}; \overline{2, 3, 4}; \overline{4, 5, 6}\}$,

$\beta_{x1x2} \leqslant \beta_{x1}$.

Information on the input patterns of a certain function $F$ is delivered by the function's inputs and used by its outputs with precision to the blocks of the input and output blankets. Knowing the block of a certain blanket, one is able to distinguish the elements of this block from all other elements, but is unable to distinguish between elements of the given block. In this way, information in various points and streams of discrete information systems can be modeled using blankets.

### 2.2. FUNCTIONAL DECOMPOSITION

The set $X$ of function's input variable is partitioned into two subsets: *free variables* $U$ and *bound variables* $V$, such that $U \cup V = X$. Assume that the input variables $x_1, ..., x_n$ have been relabeled in such way that:

$U = \{x_1, ..., x_r\}$ and

$V = \{x_{n-s+1}, ..., x_n\}$.

Consequently, for an $n$-tuple $x$, the first $r$ components are denoted by $x^U$, and the last $s$ components, by $x^V$.

Let $F$ be a Boolean function, with $n > 0$ inputs and $m > 0$ outputs, and let $(U, V)$ be as above. Assume that $F$ is specified by a set $\mathcal{F}$ of the function's cubes. Let $G$ be a function with $s$ inputs and $p$ outputs, and let $H$ be a function with $r + p$ inputs and $m$ outputs. The pair $(G, H)$ represents a serial decomposition of $F$ with respect to $(U, V)$, if for every minterm $b$ relevant to $F$, $G(b^V)$ is defined, $G(b^V) \in \{0, 1\}^p$, and $F(b) = H(b^U, G(b^V))$. $G$ and $H$ are called blocks of the decomposition.

Let $\beta_V$, $\beta_U$, and $\beta_F$ be blankets induced on the function's $F$ input cubes by the input sub-sets $V$ and $U$, and outputs of $F$, respectively.

**Theorem 1.** Existence of the serial decomposition [1].

If there exists a blanket $\beta_G$ on the set of function $F$'s input cubes such that $\beta_V \leq \beta_G$, and $\beta_U \cdot \beta_G \leq \beta_F$, then $F$ has a serial decomposition with respect to $(U, V)$.

Proof of Theorem 1 can be found in [1].

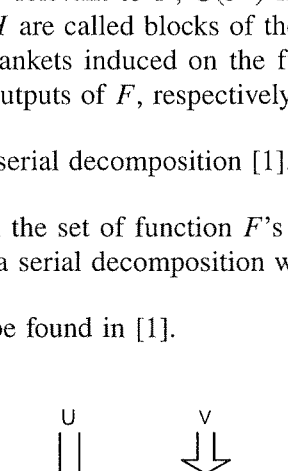


Fig. 1. Schematic represantation of the serial functional decomposition

**Example 2.** For the function from Table 1 specified by a set $\mathcal{F}$ of cubes numbered 1 through 7, consider a serial decomposition with $U = \{x_1\}$ and $V = \{x_2, x_3, x_4\}$.

We find:

$\beta_U = \{\overline{1,3,4,5,6,7}; \overline{2,3,4,5,6}\}$,

$\beta_V = \{\overline{1,2,3}; \overline{3,7}; \overline{1,2}; \overline{4}; \overline{6,7}; \overline{5}; \overline{4,6}\}$,

$\beta_F = \{\overline{4,5}; \overline{4,6}; \overline{2,3,7}; \overline{1,3,6,7}\}$.

It is easily verified that $\beta_G = \{\overline{1,2,3,7}; \overline{5}; \overline{6,7}; \overline{4,6}\}$ satisfies the condition of Theorem 1 (more detailed description of partition calculus can be found in [1]). Thus function $F$ has a serial decomposition with respect to $(U, V)$.

The process of functional decomposition consists of the following steps:

- the selection of an appropriate input support $V$ for block $G$ (input variable partitioning),
- the calculation of the blankets $\beta_U$, $\beta_V$ and $\beta_F$,
- the construction of an appropriate multi-block blanket $\beta_G$ (this corresponds to the construction of the multi-valued function of block $G$),
- the creation of the binary functions $H$ and $G$ by representing the multi-block blanket $\beta_G$ as the product of a number of certain two-block blankets (this is equivalent to encoding the multi-valued function of block $G$ defined by blanket $\beta_G$ with a number of binary output variables).

In a multilevel decomposition, this process is applied to functions $H$ and $G$ repetitively, until each block of the obtained in this way net can be directly mapped in a logic block of a specific implementation structure [10].

The selection of an appropriate input variable partitioning is the main problem in functional decomposition. The choice of sets $U$ and $V$ from set $X$ determines the construction of an appropriate blanket $\beta_G$ which satisfies Theorem 1. The existence of such a blanket $\beta_G$ implies the existence of a serial decomposition. Blankets $\beta_V$, $\beta_G$, $\beta_U \cdot \beta_G$ and $\beta_F$ constitute the basis for the construction of sub-functions $H$ and $G$ in serial decomposition. In other words, knowing $\beta_V$, $\beta_U$ and $\beta_F$, and having $\beta_G$ one can construct particular sub-functions $G$ and $H$.

The input variables of block $G$ and their corresponding blankets and the output blanket $\beta_G$ of block $G$ define together the multi-valued function of block $G$. The structure of $\beta_G$ obviously influences the shape of the sub-functions $G$ and $H$ (Fig. 2). Blanket $\beta_G$ determines the output values of function $G$. Each value of this multi-valued function corresponds to a certain block of the blanket $\beta_G$. Considering the number of values of the multi-valued function of a certain sub-system in decomposition is therefore equivalent to considering the number of blocks in blanket $\beta_G$ of this sub-system. For encoding of $q$ values minimum $\lceil \log_2 q \rceil$ binary variables are required. Thus, if $q$ denotes the number of blocks in $\beta_G$ then the minimum required number of binary outputs from $G$ is equal to $k = \lceil \log_2 q \rceil$.

Since function $H$ is constructed by substituting in the truth table of function $F$ the patterns of values of the primary input variables from set $V$ (bound variables) with the corresponding values of function $G$, it is obvious that the choice of $\beta_G$ influences the sub-function $H$. The outputs of $G$ constitute a part of the input support for block $H$. Thus, the size of block $G$ and the size of block $H$ both grow with the number of blocks in blanket $\beta_G$. The minimum possible number of blocks in $\beta_G$ strongly depends on the input support chosen for block $G$, because $\beta_G$ is computed by merging some blocks of $\beta_V$, this being the blanket induced by the chosen support.

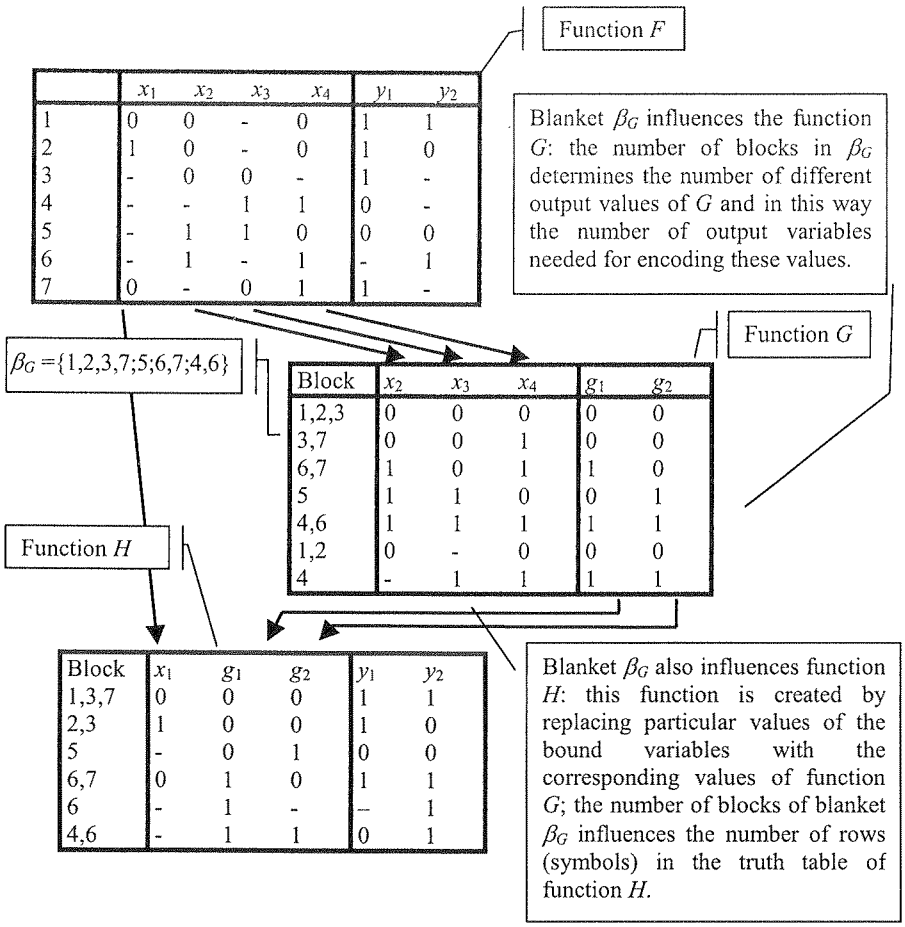


| | $x_1$ | $x_2$ | $x_3$ | $x_4$ | $y_1$ | $y_2$ |
|---|---|---|---|---|---|---|
| 1 | 0 | 0 | - | 0 | 1 | 1 |
| 2 | 1 | 0 | - | 0 | 1 | 0 |
| 3 | - | 0 | 0 | - | 1 | - |
| 4 | - | - | 1 | 1 | 0 | - |
| 5 | - | 1 | 1 | 0 | 0 | 0 |
| 6 | - | 1 | - | 1 | - | 1 |
| 7 | 0 | - | 0 | 1 | 1 | - |

| Block | $x_2$ | $x_3$ | $x_4$ | $g_1$ | $g_2$ |
|---|---|---|---|---|---|
| 1,2,3 | 0 | 0 | 0 | 0 | 0 |
| 3,7 | 0 | 0 | 1 | 0 | 0 |
| 6,7 | 1 | 0 | 1 | 1 | 0 |
| 5 | 1 | 1 | 0 | 0 | 1 |
| 4,6 | 1 | 1 | 1 | 1 | 1 |
| 1,2 | 0 | - | 0 | 0 | 0 |
| 4 | - | 1 | 1 | 1 | 1 |

| Block | $x_1$ | $g_1$ | $g_2$ | $y_1$ | $y_2$ |
|---|---|---|---|---|---|
| 1,3,7 | 0 | 0 | 0 | 1 | 1 |
| 2,3 | 1 | 0 | 0 | 1 | 0 |
| 5 | - | 0 | 1 | 0 | 0 |
| 6,7 | 0 | 1 | 0 | 1 | 1 |
| 6 | - | 1 | - | - | 1 |
| 4,6 | - | 1 | 1 | 0 | 1 |

Fig. 2. Influence of blanket $\beta_G$ on sub-functions $H$ and $G$

Function $H$ is decomposed in the successive steps of the multi-level synthesis process. This is why blanket $\beta_G$ has a direct influence on the next steps of the process. The structure of the blanket $\beta_G$ determines the difficulty of the successive decomposition steps and influences the final result of the synthesis process (characterized by the number of logic blocks and number of logic levels). The number of blocks in blanket $\beta_G$ is the most decisive parameter. Since the strong correlation of the number of blanket $\beta_G$'s blocks with the decomposition's quality has been showed in [19], this number can be used as a criterion for testing individual solutions.

In multi-level logic synthesis methods, the serial decomposition process is applied recursively to functions $H$ and $G$ obtained in the previous synthesis steps until each block of the resulting net can be directly mapped in a single logic block of a specific implementation structure [11, 12]. In the case of look-up table FPGAs, the multi-level

decomposition process ends when each block of the resulting net can be directly mapped into a configurable logic block (CLB) of a specific size (typically the CLB size is from 4 to 6 inputs and 1 or 2 outputs). Although algorithms of multi-level logic synthesis can also use parallel decomposition in order to assist the serial decomposition [10], the final results of the synthesis process strongly depend on the quality of the serial decomposition.

### 2.3. EVOLUTIONARY ALGORITHMS

An evolutionary computing is inspired by Darwin's theory of evolution. In other words, problems are solved by an evolutionary process resulting in the best (fittest) solution (survivor) – the solution is evolved.

'Genetic algorithm' term was introduced by John Holland [6]. In this paper an evolutionary algorithm is used, which is more general term. The evolutionary algorithm is one of heuristics, which not necessarily provides the best possible solution. However, these sub-optimal solutions are considered as acceptable, because in many problems it is not possible to find the best solution in reasonable time. It means that evolutionary algorithms are especially useful for problems with a vast search space and non-polynomial time algorithms solving the given problem.

The evolutionary algorithms need individuals that represent a solution attempt to the problem they are trying to solve. The population needs to be tested to find how well individuals perform, and new individuals are created that are combinations of existing good solutions with some occasional variations. The cycle of testing and creation of new individuals is repeated until a suitable solution is found, all the individuals represent the same solutions, or the search is abandoned [13].

The basic steps of an evolutionary algorithm are presented on Figure 3.

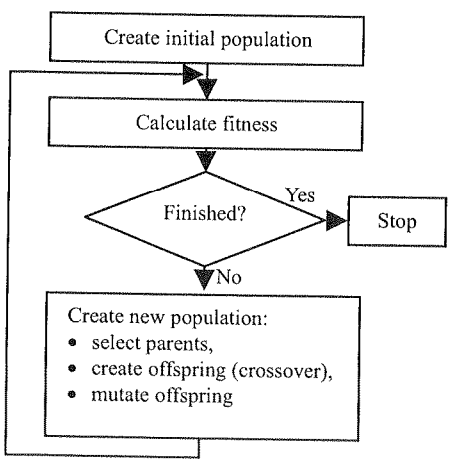


Fig. 3. Schematic representation of the evolutionary algorithm

To construct the algorithm following qualities have to be defined:

- a population of individuals, where each individual represents an encoded form of a possible solution to the problem being solved,
- methods for testing individual solutions and assigning fitness (how good the solution is),
- methods for selecting suitable parents that will be used to produce new individuals (offspring),
- methods for manipulating the encoded forms of individuals, often called "genetic operators"; these operators are used to create new children from parents (for example, "crossover" techniques), and for introducing other variations (such as "mutation") into the population,
- parameters to manipulate the probability and effect of operators.

## 3. EVOLUTIONARY ALGORITHM FOR INPUT VARIABLE PARTITIONING

The input variable partitioning is NP-hard problem. For function $F$ of $n$ input variables and the size $k$ of set $V$ the number of possible solution is described by following formula:

$$l = \binom{n}{k} = \frac{n!}{(n-k)!\,k!}.$$

For large functions the solution space is so huge that heuristic method for solving this problem has to be used.

The analysis of best possible solutions for given Boolean function results in interesting observations. Table 2 presents the best solutions (according to of the number of blanket $\beta_G$'s blocks) of input variable partitioning for *plan* example function from standard benchmark set [27]. This function has 13 inputs and 25 outputs. Each row of table 2 presents the variables belonging to set $U$ (marked by digit '1') and belonging to set $V$ (marked by digit '0'). Best solutions for different sizes of $V$ set are presented, as well as the frequency of appearance of given variable in $V$ set. It can be noticed that some variables often then others appear in bound set for results of best quality. For example variable $x_1$ appears in $V$ set for 16 solutions listed in table 2, while $x_2$ does not belong to $V$ set for any of these solutions. This suggests that for constructing good input variable partitions some variables are more predestined to be included in $V$ and other to be included in $U$ set.

Let us assume that the size of $V$ set is 4. Now, let us create an input variable partitioning in such way that $V$ set consists of variables that according to table 2 are least appropriate to be in bund set: $V = \{x_2, x_3, x_4, x_9\}$ and $U = \{x_1, x_5, x_6, x_7, x_8, x_{10}, x_{11}, x_{12}, x_{13}\}$. As we could expect, the quality of decomposition (according to the number of blanket $\beta_G$'s blocks) is 16 – the worst possible for this size of $V$ set. However let us move "good" variable $x_1$ from set $U$ to set $V$ and "bad" variable $x_2$ from set $V$ to set $U$. The quality of decomposition is now 15, so it has improved. If we now swap variables

$x_3$ and $x_{12}$, the decomposition will have quality 11, so further improvement has been obtained.

Table 2

Best input variable partitions of *plan* example

| $x_1$ | $x_2$ | $x_3$ | $x_4$ | $x_5$ | $x_6$ | $x_7$ | $x_8$ | $x_9$ | $x_{10}$ | $x_{11}$ | $x_{12}$ | $x_{13}$ |
|---|---|---|---|---|---|---|---|---|---|---|---|---|
| $\|U\| = 10, \|V\| = 3, \|\beta_G\| = 5$ | | | | | | | | | | | | |
| **1** | **1** | **1** | 1 | 1 | 1 | **0** | 1 | **1** | 1 | 1 | **0** | **0** |
| **1** | **1** | **1** | 1 | 1 | 1 | **0** | 1 | **1** | 1 | 0 | **1** | **0** |
| **1** | **1** | **1** | 1 | 1 | 1 | **0** | 1 | **1** | 1 | 0 | **0** | **1** |
| **1** | **1** | **1** | 1 | 1 | 0 | **0** | 1 | **1** | 1 | 1 | **0** | **1** |
| **1** | **1** | **1** | 1 | 0 | 1 | **0** | 1 | **1** | 1 | 1 | **0** | **1** |
| **1** | **1** | **1** | 1 | 0 | 0 | **1** | 1 | **1** | 1 | 1 | **0** | **1** |
| **1** | **1** | **1** | 0 | 1 | 1 | **0** | 1 | **1** | 1 | 1 | **1** | **0** |
| **0** | **1** | **1** | 1 | 1 | 1 | **1** | 1 | **1** | 1 | 1 | **0** | **0** |
| **0** | **1** | **1** | 1 | 1 | 1 | **1** | 1 | **1** | 0 | 1 | **1** | **0** |
| **0** | **1** | **1** | 1 | 1 | 1 | **1** | 1 | **1** | 0 | 1 | **0** | **1** |
| **0** | **1** | **1** | 1 | 1 | 1 | **1** | 0 | **1** | 1 | 1 | **1** | **0** |
| **0** | **1** | **1** | 1 | 1 | 1 | **1** | 0 | **1** | 1 | 1 | **0** | **1** |
| **0** | **1** | **1** | 1 | 1 | 1 | **1** | 0 | **1** | 0 | 1 | **1** | **1** |
| **0** | **1** | **1** | 1 | 1 | 1 | **0** | 1 | **1** | 1 | 1 | **1** | **0** |
| **0** | **1** | **1** | 1 | 1 | 1 | **0** | 1 | **1** | 1 | 1 | **0** | **1** |
| **0** | **1** | **1** | 1 | 1 | 0 | **1** | 1 | **1** | 1 | 1 | **0** | **1** |
| **0** | **1** | **1** | 1 | 0 | 1 | **1** | 1 | **1** | 1 | 1 | **0** | **1** |
| **0** | **1** | **1** | 0 | 1 | 1 | **1** | 1 | **1** | 1 | 1 | **1** | **0** |
| $\|U\| = 9, \|V\| = 4, \|\beta_G\| = 7$ | | | | | | | | | | | | |
| **0** | **1** | **1** | 1 | 1 | 1 | **0** | 1 | **1** | 1 | 1 | **0** | **0** |
| $\|U\| = 8, \|V\| = 5, \|\beta_G\| = 11$ | | | | | | | | | | | | |
| **0** | **1** | **1** | 1 | 1 | 1 | **0** | 1 | **1** | 1 | 0 | **0** | **0** |
| **0** | **1** | **1** | 1 | 1 | 1 | **0** | 1 | **1** | 0 | 1 | **0** | **0** |
| **0** | **1** | **1** | 1 | 1 | 1 | **0** | 0 | **1** | 1 | 1 | **0** | **0** |
| $\|U\| = 7, \|V\| = 6, \|\beta_G\| = 17$ | | | | | | | | | | | | |
| **0** | **1** | **1** | 0 | 1 | 1 | **0** | 1 | **1** | 0 | 1 | **0** | **0** |
| Frequency of appearance in $V$ set | | | | | | | | | | | | |
| **16** | **0** | **0** | 3 | 3 | 3 | **13** | 4 | **0** | 5 | 3 | **16** | **13** |

Let us assume that we have two variable partitioning solution ($V_1$, $U_1$) and ($V_2$, $U_2$). We can create another solution by taking part of variables from $V_1$ and part

from $V_2$ and construct $V_3$ (similarly for $U_3$). Taking observation described above into account we can suspect that after such variable exchange it is probable that "good" variables from $V_1$ and $V_2$ will be included in $V_3$. This should improve the quality of new solution in comparison to solution used as "parents". If we preserve improved solutions and eliminate worsen solution we can apply this approach again. Such behavior is characteristic for evolutionary algorithms. This means that evolutionary algorithm may be an efficient way for solving input variable partitioning problem.

The evolutionary algorithm maintains a population of individuals (chromosomes), that represent potential solutions of a given optimization problem. A survival of the fittest individuals is implemented by the selection mechanism. For the next population, as potential solutions, such single organisms are chosen, which adaptation to the environment is the best. The adaptation (quality) of a specific chromosome is evaluated by a fitness function. The chromosomes are evolving through the process of selection, recombination (crossover) and mutation. After a given number of algorithm loops (generations), it is expected that the algorithm has found a satisfactory solution.

In case of input variable partitioning problem the chromosome has to describe individual solution in form of sets $U$ and $V$. In [19] the strong correlation of the number of blanket $\beta_G$'s blocks with the decomposition's quality has been showed. This number can be used to asses the quality (fitness) of given variable partitioning.

The outline of the algorithm solving the input variable partitioning problem is given below.

```
begin
  t := 0
    initialise P^0 (population '0')
    evaluate P^0
    while (not stop condition) do
      begin
        T^t := selection_operator (P^t)
        O^t := crossover_operator (T^t)
      evaluate (O^t)
        if(mutation condition) then
        O^t := mutation_operator (O^t)
          P^(t+1) := O^t
        t := t + 1
      end
end
```

The process is controlled by such algorithm parameters as crossover probability, population size, number of generations, etc. However there is no golden rule how to specify these parameters and it heavily depends on the given problem.

In our approach the algorithm stops after given number of generations. Below some more details of the evolutionary algorithm are discussed.

### 3.1. CHROMOSOME ENCODING

The single chromosome (organism) represents one, possible solution of the input variable partitioning problem. In the method presented in this paper chromosomes are encoded by the integer numbers, each of which represents the number of the input variable assigned to the set $V$ (bound variables) of the decomposition.

**Example 3.**

For 4-input function $F$ from Table 1 a possible solution of the variable partitioning problem can be represented by the set $U = \{x_1\}$ and set $V = \{x_2, x_3, x_3\}$.

The corresponding chromosome encoding is {2 3 4}.

### 3.2. FITNESS FUNCTION

In [19] has been shown that there is a strong correlation of the number of blocks in $\beta_G$ with the decomposition's quality. However the number of blocks in $\beta_G$ strongly depends on the input variable partitioning chosen for the decomposition process. Therefore, the number of blocks in the $\beta_G$ blanket can be used as a good quality measure of the input variable partitioning.

In the presented method the fitness function depends on the number of blocks in $\beta_G$. The less the number of blocks in $\beta_G$, the better fitness of a given chromosome.

For the chromosome from Example 2 the number of blocks in a blanket $\beta_G$ is $k = 4$ (Example 1).

### 3.3. INITIAL POPULATION SELECTION

The initial population $P^0$ is created randomly. Once it is completed, the algorithm checks whether all the inputs (single genes) have been chosen at least once. If some are missing, the additional organism is created with genes which are not included in other organisms of the population.

### 3.4. SELECTION METHOD

The selection method is combination of tournament selection and elitism. Tournament selection chooses randomly two organisms from the population $P^t$, compares them and takes the better one to the $T^t$ population. The number of times such a tournament has to be done to complete whole $T^t$ population depends on the population size. Elitism guarantees that the best organism from $P^t$ is taken to $T^t$ population regardless it was taking part at any tournaments or not.

### 3.5. CROSSOVER (RECOMBINATION)

Crossover operator chooses randomly two organism (called 'parents') and crosses their genetic material (Fig. 4). The crossover probability parameter specifies how often the crossover operator is performed. In proposed method this parameter is set to 0.9. The algorithm checks whether parents have the same genes or not. If so, the crossover operator is not launched and the other potential parents are chosen. If crossover is performed, two new organisms are created (and taken to $O^t$ population). Otherwise parents are taken to $O^t$ population.

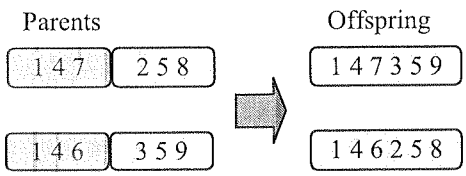


Fig. 4. Schematic representation of the crossover operator

### 3.6. MUTATION

Usually, mutation changes a single gene with very small probability (0.001). However, as experiments proved, in the case of the variable partitioning problem this kind of mutation does not bring any considerable profit for the algorithm performance.

The main problem with the presented algorithm is very fast convergence to the local optimum. Once the algorithm gets to this area, it is very unlikely to find the better solution than this local optimum. To solve this problem, the special kind of mutation was implemented. If the average fitness among the population is very close to the best organism fitness, it is very likely the algorithm got stuck in the local optimum area. Then the special mutation is performed. One gene in each organism is mutated so the mutation probability is very high. As a result, the average fitness degenerates rapidly, but the algorithm gets out of the local optimum area and in many cases the better solution is found.

## 4. EXPERIMENTAL RESULTS

This section compares the heuristic method for input variable partitioning presented in this paper with the method presented in [18] and with the systematic method. The systematic method is based on searching through the whole solution space and choosing an input support that produces blanket $\beta_G$ with minimum possible number of blocks. For these experiments the number of generations in the method based on the evolutionary algorithm was set to 30 and the size of a population was set to 40. The comparisons have been made by applying all methods to several small, medium

and large benchmarks. For the experiments we used a number of functions from the international logic synthesis benchmark set [27].

Table 3

Comparison of the number of blocks in blanket $\beta_G$ obtained by the systematic method, heuristic method from [18] and heuristic method based on evolutionary algorithm for different size of set $V$

| | Size | | | Systematic method | | | | Heuristic based on information relationship measures | | | | Heuristic based on evolutionary algorithm | | | |
|---|---|---|---|---|---|---|---|---|---|---|---|---|---|---|---|
| | inputs | outputs | terms | 3 | 4 | 5 | 6 | 3 | 4 | 5 | 6 | 3 | 4 | 5 | 6 |
| Con1 | 7 | 2 | 20 | 5 | 6 | 6 | 5 | 5 | 7 | 7 | 5 | 5 | 6 | 6 | 5 |
| Donfl | 7 | 6 | 64 | 8 | 14 | 25 | 37 | 8 | 14 | 25 | 37 | 8 | 14 | 25 | 37 |
| z4 | 7 | 4 | 128 | 4 | 6 | 8 | 12 | 4 | 6 | 8 | 12 | 4 | 6 | 8 | 12 |
| Misex1 | 8 | 7 | 18 | 4 | 6 | 7 | 9 | 4 | 6 | 7 | 9 | 4 | 6 | 7 | 9 |
| Root | 8 | 5 | 71 | 5 | 9 | 15 | 17 | 5 | 9 | 15 | 17 | 5 | 9 | 15 | 17 |
| Sqrt | 8 | 4 | 53 | 3 | 4 | 7 | 12 | 3 | 4 | 7 | 12 | 3 | 4 | 7 | 12 |
| Opus | 9 | 10 | 23 | 4 | 6 | 8 | 10 | 4 | 6 | 8 | 10 | 4 | 6 | 8 | 10 |
| 9sym | 9 | 1 | 191 | 4 | 5 | 6 | 7 | 4 | 5 | 6 | 7 | 4 | 5 | 6 | 7 |
| Clip | 9 | 5 | 430 | 6 | 10 | 14 | 18 | 6 | 10 | 14 | 21 | 6 | 10 | 14 | 18 |
| Mark1 | 9 | 20 | 27 | 4 | 6 | 8 | 10 | 4 | 6 | 8 | 10 | 4 | 6 | 8 | 10 |
| Alu2 | 10 | 3 | 391 | 6 | 12 | 24 | 43 | 6 | 12 | 24 | 43 | 6 | 12 | 24 | 43 |
| Sao2 | 10 | 4 | 60 | 4 | 6 | 9 | 11 | 4 | 6 | 9 | 11 | 4 | 6 | 9 | 11 |
| Cse | 11 | 11 | 86 | 3 | 4 | 6 | 9 | 3 | 4 | 6 | 9 | 3 | 4 | 6 | 9 |
| Sse | 11 | 11 | 39 | 4 | 6 | 8 | 11 | 4 | 6 | 8 | 11 | 4 | 6 | 8 | 11 |
| Keyb | 12 | 7 | 147 | 6 | 9 | 13 | 19 | 6 | 9 | 13 | 19 | 6 | 9 | 13 | 19 |
| S1 | 13 | 11 | 110 | 5 | 8 | 13 | 19 | 6 | 8 | 13 | 19 | 5 | 8 | 13 | 19 |
| Plan | 13 | 25 | 115 | 5 | 7 | 11 | 17 | 5 | 7 | 11 | 18 | 5 | 7 | 11 | 17 |
| Styr | 14 | 15 | 140 | 4 | 6 | 9 | 13 | 5 | 7 | 10 | 14 | 4 | 6 | 9 | 13 |
| Ex1 | 14 | 24 | 127 | 4 | 6 | 8 | 11 | 4 | 6 | 8 | 11 | 4 | 6 | 8 | 11 |
| Kirk | 16 | 10 | 304 | 4 | 4 | 5 | 6 | 4 | 5 | 5 | 7 | 4 | 4 | 5 | 6 |
| Duke2_7 | 18 | 1 | 64 | 3 | 4 | 4 | 4 | 4 | 5 | 5 | 5 | 3 | 4 | 4 | 4 |
| Vg2_2 | 25 | 1 | 56 | 3 | 3 | 3 | 3 | 4 | 4 | 4 | 4 | 3 | 3 | 3 | 3 |
| Apex3_3 | 34 | 1 | 208 | 2 | 3 | 4 | 5 | 4 | 4 | 4 | 6 | 2 | 3 | 4 | 5 |
| Seq_2 | 36 | 1 | 211 | 2 | 2 | 3 | –*) | 3 | 4 | 4 | 6 | 2 | 2 | 3 | 5 |
| Seq_1 | 37 | 1 | 286 | 2 | 3 | 3 | 3 | 3 | 3 | 3 | 4 | 2 | 3 | 3 | 3 |
| Apex3_7 | 39 | 1 | 227 | 3 | 4 | 4 | 5 | 4 | 5 | 6 | 7 | 3 | 4 | 4 | 5 |

*) – too long computation time

Table 3 shows the comparison results of the minimum number of blanket $\beta_G$ blocks for all methods for examples converted to truth table format (required by method from [18]). The results were obtained for decompositions with 3, 4, 5, and 6 input variables in set $V$. Results obtained by the decomposition with the systematic search are optimal in the sense of the number of blocks of $\beta_G$. The method based on the evolutionary algorithm despite of its heuristic character produces results similar to the systematic method.

It is very difficult to describe large multi-output systems with truth tables. Such examples are usually presented in espresso format, which in most cases is not truth table format. Table 4 present the minimum number of blocks of blanket $\beta_G$ obtained by method based on the evolutionary algorithm for large examples. The comparison with other two methods was impossible due to unacceptably long computation time for systematic method and due to the fact that method from [18] accepts only truth table format.

Table 4

The number of blocks in blanket $\beta_G$ obtained by heuristic method based on evolutionary algorithm for different size of set $V$

| | Size | | | Heuristic based on evolutionary algorithm | | | |
|---|---|---|---|---|---|---|---|
| | inputs | outputs | terms | 3 | 4 | 5 | 6 |
| duke2 | 22 | 29 | 405 | 4 | 5 | 7 | 8 |
| misex2 | 25 | 18 | 102 | 2 | 2 | 2 | 2 |
| seq | 41 | 35 | 3137 | 4 | 5 | 5 | 5 |
| apex1 | 45 | 45 | 1440 | 4 | 5 | 6 | 7 |
| apex3 | 54 | 50 | 1036 | 4 | 5 | 7 | 8 |
| e64 | 65 | 65 | 327 | 4 | 5 | 5 | 7 |
| apex5 | 117 | 88 | 2849 | 1 | 3 | 4 | 3 |

Table 5 presents the comparison of estimated computation time of the systematic method and computation time of the heuristic method based on the evolutionary algorithm for different sizes of set $V$. For large functions, this method is many times faster than the systematic method. The difference in processing time between these two methods grows very fast with the function size. For the largest functions we tried, the heuristic method is many thousands times faster. It has to be stressed that the multilevel decomposition consists of many single serial decomposition steps. Thus, application of the heuristic methods can speed up the multi-level decomposition process dramatically.

Figures 5a and 5b present the influence of such parameters as the population size and the number of generations on results obtained by presented method and on computation time. These two parameters allow for trade-off between the quality of solutions and computation time. It is worth noticing that in most cases decrease in the size of population and the number of generations allowed for much faster computation while keeping the quality of solution very close to optimal.

Table 5

Comparison of computation time of systematic method and heuristic method based on evolutionary algorithm for different sizes of set $V$

| | Systematic method* | | | | Heuristic based on evolutionary algorithm [s] | | | |
|---|---|---|---|---|---|---|---|---|
| | 3 | 4 | 5 | 6 | 3 | 4 | 5 | 6 |
| duke2 | 31 s | 2 m 40 s | 10 m 58 s | 34 m 56 s | 37.7 | 38.9 | 40.4 | 58.5 |
| misex2 | 10 s | 40 s | 4 m 4 s | 13 m 52 s | 10.2 | 12.4 | 14.9 | 24.9 |
| seq | > 2 h | > 1 day | > 8 days | > 59 days | 1656.8 | 1692.9 | 1704 | 1712.9 |
| apex1 | > 1 hour | > 12 hours | > 4 days | > 39 days | 463.3 | 506.3 | 506 | 524.6 |
| apex3 | > 1 hour | > 16 hours | > 8 days | > 81 days | 324 | 316.5 | 325 | 328.7 |
| e64 | 31 m 53 s | > 8 hours | > 5 days | > 68 days | 136.5 | 137.1 | 79 | 191.2 |
| apex5 | > 6 days | > 185 days | > 11 years | > 221 years | 2849 | 3772.6 | 3799.5 | 3901.8 |

*) estimated time

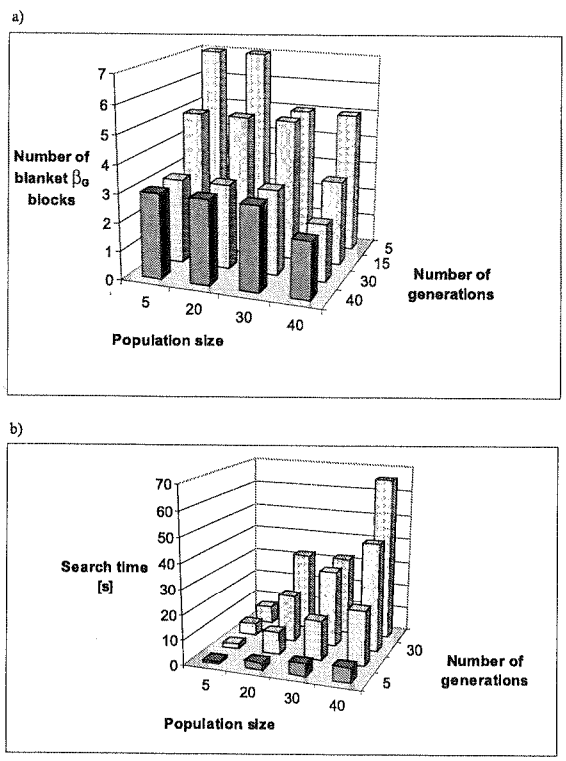


Fig. 5. The influence of the population size and the number of generations on a) the number of blanket $\beta_G$ blocks, b) computation time

All experiments presented in this section were preformed on the computer with 512 Mbytes of RAM and AMD Athlon XP 3200.

## 5. CONCLUSIONS

The proposed heuristic method of the variable partitioning based on evolutionary algorithm is very efficient. The method delivers results of similar or comparable quality to results obtained from the systematic method, but does it many times faster. For the largest benchmarks that we tried the systematic method requires unacceptably long computation time. The method based on the evolutionary algorithm is thousands times faster than the systematic method and allows finding solution of optimal or near optimal quality. The algorithm parameters (the number of generations and the size of population) can be used to control the trade-off between the search time and the quality of solutions.

These features make the proposed heuristic method very useful for decomposition-based synthesis of large systems.

## 6. REFERENCES


1. J.A. Brzozowski, T. Łuba: *Decomposition of Boolean Functions Specified by Cubes, Part 1: Theory of Serial Decompositions Using Blankets*. Research Report CS-97-01, University of Waterloo, Waterloo, Canada, 1997; REVISED October 1998.
2. M. Burns, M. Perkowski, L. Józwiak: *An Efficient Approach to Decomposition of Multi-Output Boolean Functions with Large Set of Bound Variables*. EUROMICRO'98 Conference, Vasteras, Sweden, 1998.
3. S.C. Chang, M. Marek-Sadowska, T.T. Hwang: *Technology Mapping for TLU FPGAs Based on Decomposition of Binary Decision Diagrams*. IEEE Trans. on CAD, vol. 15, No. 10, October, 1996, pp. 1226-1236.
4. C. Files, M. Perkowski: *Multi-Valued Functional Decomposition as a Machine Learning Method*, ISMVL'98, Fukuoka, Japan, 1998, pp. 173-178.
5. J.F. Frenzel: *Application of Genetic Algorithms to Pattern Theory*. Final Report for Summer Faculty Research Program, Wright Laboratory, Sponsored by Air Force Office of Scientific Research, Bolling Air Force Base, DC and Wright Laboratory, July 1993.
6. J.H. Holland: *Adaptation in Natural and Artificial Systems: An Introductory Analysis with Applications to Biology, Control, and Artificial Intelligence*. 1975 and 1992, MIT Press.
7. L. Józwiak: *Information Relationships and Measures: An Analysis Apparatus for Efficient Information System Synthesis*. 23rd EUROMICRO Conference, Budapest, Hungary, Sept. 1-4, 1997, pp. 13-23.
8. S. Khuri: *An Evolutionary Approach to Combinatorial Optimization Problems*. Proceedings of CSC, Phoenix, Arizona. March 1994.
9. Y.T. Lai, K.R.R. Pan, M. Pedram: *OBDD-Based Functional Decomposition: Algorithm and Implementation*. IEEE Trans. on CAD, vol. 15, No 8, August, 1996, pp. 977-990.
10. T. Luba, H. Selvaraj, M. Nowicka, A. Kraśniewski: *Balanced multilevel decomposition and its applications in FPGA-based synthesis*. G.Saucier, A.Mignotte (ed.), Logic and Architecture Synthesis, Chapman&Hall, 1995.
11. T. Luba, H. Selvaraj: *A General Approach to Boolean Function Decomposition and its Applications in FPGA-based Synthesis*. VLSI Design, Special Issue on Decompositions in VLSI Design, vol. 3, No. 3-4, 1995, pp. 289-300.

12. T. Luba: *Decomposition of Multiple-Valued Functions.* 25th International Symposium on Multiple-Valued Logic, Bloomington, Indiana, 1995, pp. 256-261.
13. Z. Michalewicz: *Genetic Algorithms + Data Structures = Evolution Programs.* Springer-Verlag, Berlin, third edition, 1996.
14. M.J. Noviskey, T.D. Ross, D.A. Gadd, M. Axtell: *Application of Genetic Algorithms to Functional Decomposition in Pattern Theory.* Report WL-TR-94-1015, Wright Laboratory, WL/AART-2. WPAFB, OH 4533-5543. Jan 1994.
15. M. Perkowski: *A Survey of Literature on Function Decomposition.* Final Report for Summer Faculty Research Program, Wright Laboratory, Sponsored by Air Force Office of Scientific Research, Bolling Air Force Base, DC and Wright Laboratory, September 1994.
16. M. Perkowski, M. Marek-Sadowska, L. Jóźwiak, T. Łuba, S. Grygiel, M. Nowicka, R. Malvi, Z. Wang, S. Zhang: *Decomposition of Multiple-Valued Relations.* International Symposium on Multiple-Valued Logic, Antigonish, Nova Scotia, Canada 1997, pp. 13-18.
17. M. Rawski, L. Jóźwiak, M. Nowicka, T. Luba: *Non-Disjoint Decomposition of Boolean Functions and Its Application in FPGA-oriented Technology Mapping.* Proc. of the EUROMICRO'97 Conference, Budapest, Hungary, Sept. 1-4, 1997, pp. 24-30, IEEE Computer Society Press.
18. M. Rawski, L. Jóźwiak, T. Łuba: *Efficient Input Support Selection for Sub-functions in Functional Decomposition Based on Information Relationship Measures.* EUROMICRO'99 Conference, Milan, Italy, 1999.
19. M. Rawski, L. Jóźwiak, T. Łuba: *The Influence of the Number of Values in Sub-functions on the Effectiveness and Efficiency of the Functional Decomposition.* EUROMICRO'99 Conference, Milan, Italy, 1999.
20. M. Rawski, H. Selvaraj, P. Morawiecki: *Efficient Method of Input Variable Partitioning in Functional Decomposition Based on Evolutionary Algorithms.* DSD 2004, Proc. Euromicro Symposium on Digital System Design, Architectures, Methods and Tools, IEEE Computer Society, Selvaraj H. (Editor), Rennes, France, August 31 – September 3, 2004, pp. 136-143.
21. T. Ross, M. Noviskey, T. Taylor, D. Gadd: *Pattern Theory: An Engineering Paradigm for Algorithm Design.* Final Technical Report, Wright Laboratories, WL/AART/WPAFB, 1991.
22. T. Sasao: *FPGA design by generalised functional decomposition.* Logic Synthesis and Optimisation, pp. 231-258, Kluwer Academic Publishers, 1993.
23. B. Steinbach, M. Stokert: *Design of Fully Testable Circuits by Functional Decomposition & Implicit Test Pattern Generation.* IEEE VLSI Test Symposium Proceedings, 1994, pp. 22-27.
24. W. Wan, M. Perkowski: *A New Approach to the Decomposition of Incompletely Specified Multi-Output Functions Based on Graph Coloring and Local Transformations and its Application to FPGA Mapping.* Proceedings of the IEEE European Design Automation Conference, September 7-10, Hamburg, 1992.
25. B. Zupan, M. Bohanec: *Experimental Evaluation of Three Partition Selection Criteria for Decision Table Decomposition.* Research Report, Department of Intelligent Systems, Josef Stefan Institute, Ljubljana, Slovenia, Oct. 1966.
26. B. Zupan, M. Bohanec: *Learning Concept Hierarchies from Examples by Functional Decomposition.* Research Report, Department of Intelligent Systems, Josef Stefan Institute, Ljubljana, Slovenia, Sept. 1966.
27. Collaborative Benchmarking Laboratory, Department of Computer Science at North Carolina State University, http://www.cbl.ncsu.edu/

ELECTRONICS AND TELECOMMUNICATIONS QUARTERLY, 2007, 53, no 1, pp. 83–95

# Design of 2-D FIR filters with real and complex coefficients using two approximation criteria

FELICJA WYSOCKA-SCHILLAK

*Institute of Telecommunications,*
*University of Technology and Life Sciences*
*Prof. S. Kaliskiego 7, 85-796 Bydgoszcz, Poland*
*felicja@mail.atr.bydgoszcz.pl*

*Otrzymano 2005.11.14*
*Autoryzowano 2006.10.20*

In the paper, a method for designing two-dimensional finite impulse response linear phase digital filters is presented. The method can be applied for designing filters with both real and complex impulse response. In the method, two approximation criteria are used, i.e., the equiripple error criterion in the passband and the least-squared (LS) error criterion in the stopband. The design problem is solved by means of its transformation into an equivalent bicriterion optimization problem. A column vector $\mathbf{Y}$ of filter coefficients is defined and two objective functions $X_1(\mathbf{Y})$ and $X_2(\mathbf{Y})$ are introduced. The function $X_1(\mathbf{Y})$ has the global minimum equal to zero when the amplitude error is equiripple in the passband. The LS error in the stopband is used as the second objective function $X_2(\mathbf{Y})$. The bicriterion optimization problem is converted into a single criterion one using the weighted sum strategy. Optionally, a constraint on the maximum permissible error in the passband can also be added and easily incorporated into the optimization problem. The obtained constrained minimization problem is solved using the penalty function algorithm. Unconstrained minimization is performed by means of a conjugate gradient method. Three design examples illustrating the application of the proposed method are given. The results are compared with those obtained using the equiripple and the LS approaches.

*Keywords:* two-dimensional filters, finite impulse response filters, optimization

## 1. INTRODUCTION

Two-dimensional (2-D) finite impulse response (FIR) digital filters have many applications. They are widely used in image processing, and radar, sonar and seismic signal processing [1]. They are also applied in nonseparable filter banks [2, 3]. 2-D

FIR filters can have exactly linear-phase response and they are free from stability problems [1].

Several techniques have been proposed for designing 2-D FIR filters that meet desired specifications in the frequency domain [1, 4–12]. These techniques are usually based either on least-square (LS) or on minimax error criteria. In case of the minimax design, the maximum error is smaller than in case of the LS design. However, the minimax design is complicated and computationally intensive. In many cases, the design based on the equiripple error criterion in the passband and LS criterion in the stopband is much more appropriate than the pure minimax or LS design. A detailed discussion on this problem can be found in [12, 13].

In the paper, a new approach for the design of 2-D linear-phase 2-D FIR filters with real- and complex-valued coefficients is proposed. This approach is based on the equiripple error criterion in the passband and the LS criterion in the stopband. In this approach, the approximation problem is transformed into an equivalent bicriterion optimization problem that is converted into a single criterion problem using the weighted sum strategy. Additional constraints, as eg., a constraint on the maximum allowable approximation error in the passband can also be included in the problem. Three design examples are presented to illustrate the proposed technique.

## 2. FORMULATION OF THE PROBLEM

A 2-D FIR filter with an impulse response $h(m,n)$ has a complex frequency response of the general form given by [5, 7]:

$$H(e^{j\omega_1}, e^{j\omega_2}) = \sum_{m=0}^{M_1-1} \sum_{n=0}^{N_1-1} h(m,n) e^{-j\omega_1 m} e^{-j\omega_2 n} \tag{1}$$

where $h(m,n)$ is rectangularly sampled impulse response of the filter, $M_1$ and $N_1$ are integers representing the lengths of the filter, and $\omega_1$ and $\omega_2$ are the horizontal and vertical frequencies, respectively.

The impulse response $h(m,n)$ can be real or complex. In case of a complex-valued impulse response: $h(m,n) = h_R(m,n) + jh_I(m,n)$, where $h_R(m,n)$ and $h_I(m,n)$ denote the real and imaginary parts, respectively.

If $h(m,n)$ meets the conjugate symmetry [5]

$$h(m,n) = h^*(M_1 - 1 - m, N_1 - 1 - n) \tag{2}$$

where the superscript $^*$ denotes the complex conjugate, then (1) gives a linear-phase frequency response.

The frequency response of a linear-phase filter can be expressed as [5]:

$$H(e^{j\omega_1}, e^{j\omega_2}) = e^{-j\left(\frac{M_1-1}{2}\omega_1 + \frac{N_1-1}{2}\omega_2\right)} H(\omega_1, \omega_2) \tag{3}$$

where the purely real function $H(\omega_1, \omega_2)$ is the zero-phase frequency response and it represents the magnitude response A of the filter ($A = |H(\omega_1, \omega_2)|$). The complex exponential part in the above equation denotes the linear-phase characteristic of the filter.

In case of the complex-valued impulse response, the function $H(\omega_1, \omega_2)$ has four types of expressions depending on different combinations of odd and even filter lengths $M_1$ and $N_1$. For odd $M_1$ and $N_1$, which are only considered in this paper, the zero-phase frequency response $H(\omega_1, \omega_2)$ of a linear phase 2-D FIR filter can be written in the form [7]:

$$H(\omega_1, \omega_2) = \sum_{m=0}^{L_1} \sum_{n=0}^{L_2} a(m,n) \cos(m\omega_1) \cos(n\omega_2) + \sum_{m=0}^{L_1} \sum_{n=1}^{L_2} b(m,n) \cos(m\omega_1) \sin(n\omega_2) +$$
$$+ \sum_{m=1}^{L_1} \sum_{n=0}^{L_2} c(m,n) \sin(m\omega_1) \cos(n\omega_2) + \sum_{m=1}^{L_1} \sum_{n=1}^{L_2} d(m,n) \sin(m\omega_1) \sin(n\omega_2). \tag{4}$$

The coefficients $a(m,n)$, $b(m,n)$, $c(m,n)$, and $d(m,n)$ can be expressed in terms of the impulse response $h(m,n)$. The suitable formulas can be found eg., in [5].

A linear-phase filter with a real-valued impulse response has a centro-symmetric magnitude response. In this case, the zero-phase frequency response $H(\omega_1, \omega_2)$ satisfies the condition [1]:

$$H(\omega_1, \omega_2) = H(-\omega_1, -\omega_2) \tag{5}$$

The impulse response $h(m,n)$ of the centro-symmetric filter has twofold symmetry, so only approximately half of the points in $h(m,n)$ are independent. The region of support of a zero-phase impulse response $h(m,n)$ consists of three mutually exclusive regions: the origin (0,0), $R^+$ and $R^-$. Regions $R^+$ and $R^-$ are flipped with respect to the origin. As a result, a zero-phase frequency response of a centro-symmetric filter can be expressed as [1]:

$$H(\omega_1, \omega_2) = h(0,0) + \sum_{(m,n) \in R^+} \sum 2h(m,n) \cos(m\omega_1 + n\omega_2) \tag{6}$$

If $h(m,n)$, in addition, meets the constraint [8]:

$$h(m,n) = h(M_1 - 1 - m, n) = h(m, N_1 - 1 - n) \tag{7}$$

then the filter has quadrantally symmetric magnitude response. The zero-phase frequency response $H_s(\omega_1, \omega_2)$ of a quadrantally symmetric filter can be written in the form [1]

$$H_s(\omega_1,\omega_2)=\sum_{m=0}^{M}\sum_{n=0}^{N}a(m,n)\cos(n\omega_1)\cos(m\omega_2) \tag{8}$$

where $M=(M_1-1)/2$ oraz $N=(N_1-1)/2$.

For odd $M_1$ and $N_1$ the coefficients $a(m,n)$ are defined as follows:

$$a(m,n)=\begin{cases}4h(m,n), & \text{for} \quad m\neq 0 \text{ i } n\neq 0,\\ 2h(m,n), & \text{for} \quad m=0,\ n\neq 0 \text{ i } m\neq 0 \text{ i } n=0,\\ h(0,0) & \text{for} \quad m=0 \text{ i } n=0,\end{cases} \tag{9}$$

The 2-D FIR filter design problem is to determine the impulse response $h(m,n)$ so that the zero-phase frequency response of the filter is the best approximation of the desired zero-phase frequency response $H_d(\omega_1,\omega_2)$ in the given sense.

Let $\mathbf{Y}$ be a vector of filter coefficients defined as follows:

– in case of a filter with complex-valued coefficients: $\mathbf{Y}=[y_1,y_2,...,y_K]^T$, where:

$$y_i=h_R(m,n)\ ,\quad i=1,2,...,K/2;\quad m=0,1,...,(M_1-1)/2;\ n=0,1,...,N_1-1 \tag{10}$$

$$y_i=h_I(m,n)\ ,\quad i=K/2+1,\ K/2+2,...,K\quad m=0,1,...,(M_1-1)/2;\ n=0,1,...,N_1-1 \tag{11}$$

– in case of a centro-symmetric filter: $\mathbf{Y}=[y_1,y_2,...,y_{L+1}]^T$, where:

$$y_1=h(0,0), \tag{12}$$

$$y_i=h(m,n),\qquad i=2,3,...,(L+1);\quad m,\ n\in R^+ \tag{13}$$

– in case of a quadrantally symmetric filter: $\mathbf{Y}=[y_1,y_2,...,y_{(M_1+1)(N_1+1)}]^T$, where:

$$y_i=a(m,n)\ ,\quad i=1,2,...,(M_1+1\ )(N_1+1);\ m=0,1,...,M_1;\ n=0,1,...,N_1. \tag{14}$$

Let $H(\omega_1,\omega_2,\mathbf{Y})$ denote the zero-phase frequency response of the 2-D FIR filter obtained by putting into equation (4), (6) or (8), respectively, the coefficients given by vector $\mathbf{Y}$. The desired zero-phase frequency response $H_d(\omega_1,\omega_2)$ of the 2-D filter is:

$$H_d(\omega_1,\omega_2)=\begin{cases}1, & \text{for } (\omega_1,\omega_2) \text{ in the stopband } P,\\ 0, & \text{for } (\omega_1,\omega_2) \text{ in the passband } S.\end{cases} \tag{15}$$

Assume that the continuous $(\omega_1,\omega_2)$ – plane is discretized by using a $K_1\times K_2$ rectangular grid defined by [5, 9]:

$$\omega_{1k} = \frac{2\pi k}{K_1 - 1} - \pi, \quad k = 0, 1, ..., K_1 - 1, \tag{16}$$

$$\omega_{2l} = \frac{2\pi l}{K_2 - 1} - \pi, \quad l = 0, 1, ..., K_2 - 1. \tag{17}$$

In case of the proposed method, the approximation error is defined differently in the passband and in the stopband. In the passband $P$, the approximation is to be equiripple, and the error function $E(\omega_{1k}, \omega_{2l}, \mathbf{Y})$ is:

$$E(\omega_{1k}, \omega_{2l}, \mathbf{Y}) = H(\omega_{1k}, \omega_{2l}, \mathbf{Y}) - H_d(\omega_{1k}, \omega_{2l}), \quad \omega_{1k}, \omega_{2l} \in P. \tag{18}$$

In the stopband $S$, the LS error $E_2(\mathbf{Y})$o be minimized is:

$$\begin{aligned} E_2(\mathbf{Y}) &= \sum_{\omega_{1k} \in S} \sum_{\omega_{2l} \in S} [H(\omega_{1k}, \omega_{2l}, \mathbf{Y}) - H_d(\omega_{1k}, \omega_{2l})]^2 = \\ &= \sum_{\omega_{1k} \in S} \sum_{\omega_{2l} \in S} [H(\omega_{1k}, \omega_{2l}, \mathbf{Y})]^2 \end{aligned} \tag{19}$$

The filter design problem can be formulated as follows: For desired zero-phase frequency response $H_d(\omega_{1k}, \omega_{2l})$ defined on the rectangular grid $K_1 \times K_2$ and given integers $M_1$ and $N_1$, find a vector $\mathbf{Y}$ for which the error function $E(\omega_{1k}, \omega_{2l}, \mathbf{Y})$ is equiripple in the passband and, simultaneously, the LS error $E_2$ is minimized in the stopband.

Optionally, a following constraint can be added:

$$\underset{\omega_{1k}, \omega_{2l} \in P}{\forall} |H(\omega_{1k}, \omega_{2l}, \mathbf{Y}) - H_d(\omega_{1k}, \omega_{2l})| \leqslant \delta_p. \tag{20}$$

where $\delta_p$ is the maximum allowable approximation error in the passband.

Note that in case of the centro-symmetric filter, we need to perform calculations only in the region $R^+$ and at the origin (0,0). In case of a quadrantally symmetric filter, it is necessary to perform calculations only in the first quadrant of the $(\omega_1, \omega_2)$ – plane. Besides, the advantage of using the symmetry constraints is that the number of independent coefficients to optimize is significantly reduced in comparison with (1).

## 3. TRANSFORMATION OF THE PROBLEM

The design problem formulated in the previous section can be transformed into an equivalent bicriterion optimization problem. In order to do this, two objective functions $X_1(\mathbf{Y})$ and $X_2(\mathbf{Y})$ should be introduced. Assume that the function $X_1(\mathbf{Y})$ has the minimum equal to zero when the error function $E(\omega_{1k}, \omega_{2l}, \mathbf{Y})$ is equiripple in the passband. The error function $E(\omega_{1k}, \omega_{2l}, \mathbf{Y})$ is equiripple in the passband when the absolute values $\Delta E_i(\mathbf{Y})$, $i = 1, 2, ..., J$, of all the local extrema of the function $E(\omega_{1k}, \omega_{2l}, \mathbf{Y})$ in the

passband as well as the maximum value $\Delta E_{J+1}(\mathbf{Y})$ of $E(\omega_{1k}, \omega_{2l}, \mathbf{Y})$ at the passband edge are equal, i.e.:

$$\Delta E_i(\mathbf{Y}) = \Delta E_k(\mathbf{Y}), \quad i,k = 1,2,..,J+1, \tag{21}$$

In order to find a vector $\mathbf{Y}$, for which the conditions (21) hold, we introduce an objective function $X_1(\Delta E_1, \Delta E_2, ..., \Delta E_{J+1})$ defined as follows:

$$X_1(\mathbf{Y}) = \sum_{i=1}^{J+1} \left( \Delta E_i(\mathbf{Y}) - \tfrac{1}{J+1} \sum_{j=1}^{J+1} \Delta E_j(\mathbf{Y}) \right)^2 \tag{22}$$

The function $X_1$ is non-negative function of $\Delta E_1, \Delta E_2, ..., \Delta E_{J+1}$ and it is equal to zero if and only if $\Delta E_1 = \Delta E_2 = ... = \Delta E_{J+1}$. As $\Delta E_1, \Delta E_2, ..., \Delta E_{J+1}$ are the functions of the vector $\mathbf{Y}$, the function $X_1$ can be used as the first objective function in our bicriterion optimization problem. As the second objective function $X_2$ we use the LS error $E_2$ defined by equation (19), so $X_2(\mathbf{Y}) = E_2(\mathbf{Y})$.

Using the weighted sum strategy, which converts the bicriterion optimization problem into a single criterion one, the equivalent optimization problem can be stated as follows: For given filter specifications and weighting coefficients $\beta_1$ and $\beta_2$ find a vector $\mathbf{Y}$ such that the function

$$X(\mathbf{Y}, \beta_1, \beta_2) = \beta_1 \sum_{i=1}^{J+1} (\Delta E_i(\mathbf{Y}) - \tilde{S})^2 + \beta_2 \sum_{\omega_{1k} \in S} \sum_{\omega_{2l} \in S} [H(\omega_{1k}, \omega_{2l}, \mathbf{Y})]^2 \tag{23}$$

is minimized
where

$$\tilde{S} = \frac{1}{J+1} \sum_{i=1}^{J+1} \Delta E_i(\mathbf{Y}) \tag{24}$$

Optionally, the additional constraint (20) can also be given.

The above formulated optimization problem can be solved using standard minimization methods. The obtained solution depends on the choice of the weighting coefficients $\beta_1$ and $\beta_2$. In order to obtain the equiripple passband and in the same time to minimize the LS error in the stopband, the weighting coefficients $\beta_1$ and $\beta_2$ should be chosen so that the initial values of the two terms in (23) are approximately the same.

The initial values of the coefficients of the vector $\mathbf{Y}$, used as the starting point in the considered optimization problem, are determined by solving an appropriate LS approximation problem.

## 4. DESIGN EXAMPLES

Two computer programs based on the described design procedure have been developed in Fortran 77. These programs F2RE and F2CO enable designing 2-D linear-phase FIR filters with real- and complex-valued coefficients, respectively. Using the program F2RE, it is possible to design centro-symmetric and quadrantally symmetric filters. In both programs, the constrained minimization is performed using the penalty function method [14, 15]. The unconstrained minimization problem is solved using the modified procedure GSPR1EM based on the Polak-Ribiere version of the conjugate gradient algorithm [15].

In order to illustrate the application of the proposed approach, we will design three filters with different symmetries, i.e., quadrantally and centro-symmetric low-pass filters and a filter with complex coefficients, with additional constraints on the maximum permissible error $\delta_p$ in the passband. In all designs, a square grid of $101 \times 101$ is used for discretizing the $(\omega_1, \omega_2)$ – plane. The prescribed magnitude is 1 in the passband $P$, 0 in the stopband $S$, and varies linearly in the transition band $Tr$. The weighting coefficients are $\beta_1 = 2 \times 10^4$ and $\beta_2 = 1$.

As the first example, we consider the design of a quadrantally symmetric diamond shaped filter. The desired magnitude specification of the filter is shown in Fig. 1. The filter is designed with $N_1 = M_1 = 19$, $A = 0.68\pi$, and $B = 0.86\pi$. The calculations were performed for $\delta_p = 0.027$ and $\delta_p = 0.050$. The resulting magnitude responses $A = |H(\omega_{1k}, \omega_{2l}, \mathbf{Y})|$ are shown in Fig. 2 and 3, respectively. In these and all subsequent figures: $x = \omega_1/\pi$ and $y = \omega_2/\pi$. Note that in case of the proposed approach it is possible to obtain different values of $\delta p$ in the passband.

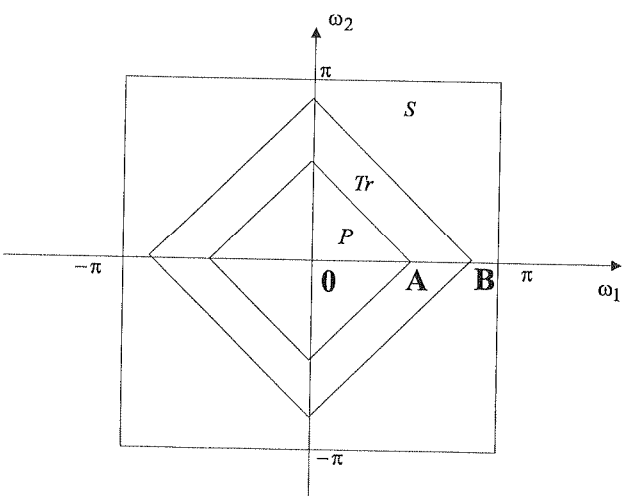


Fig. 1. Magnitude specification of a quadrantally symmetric filter

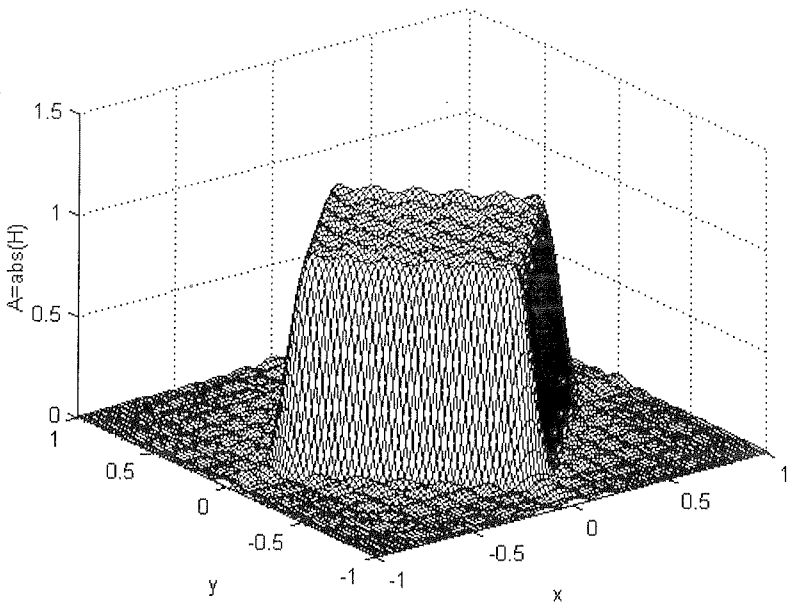


Fig. 2. Magnitude response of the filter designed in the first example with $M_1 = N_1 = 19$ and $\delta_p = 0.027$

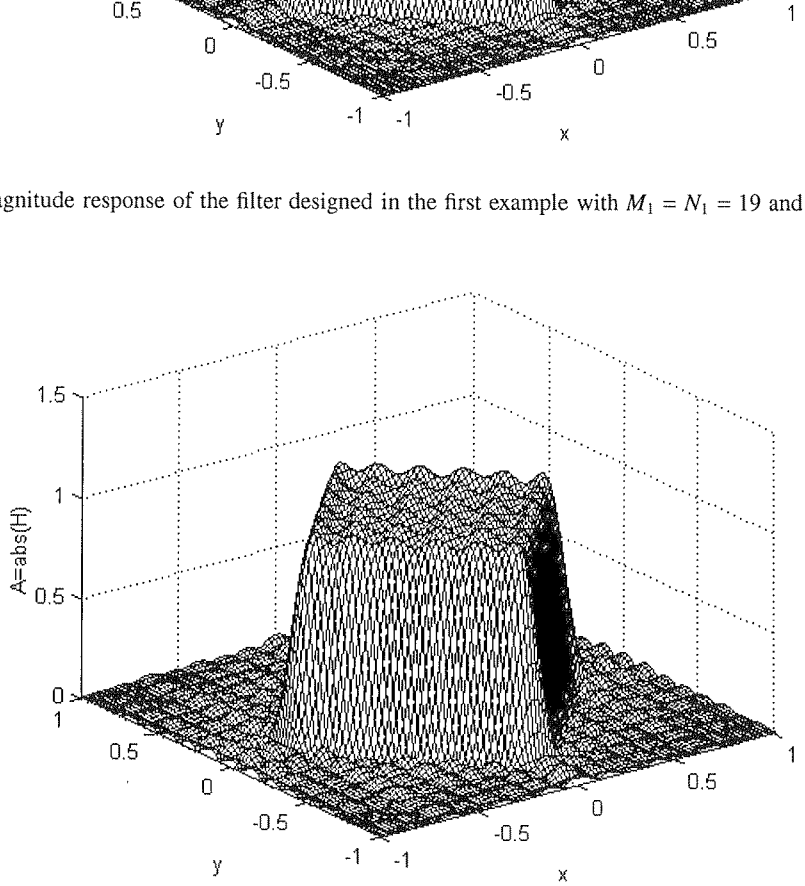


Fig. 3. Magnitude response of the filter designed in the first example with $M_1 = N_1 = 19$ and $\delta_p = 0.05$

In order to compare the obtained magnitude response with a magnitude response equiripple both in the passband and in the stopband, an equiripple filter was designed for the same specifications using a method presented in [16]. In case of the equiripple filter, the ripples are $\delta = 0.034$ both in the passband and in the stopband. In case of the proposed approach, for $\delta_p = 0.027$ the maximum magnitude error in the stopband equals $\delta_s = 0.062$.

Note that in case of the proposed approach, it is possible to obtain smaller ripples $\delta_p$ in the passband than the ripple $\delta$ in case of the equiripple design. In the significant part of the stopband, the magnitude error obtained using the proposed approach is also smaller than $\delta$. However, the maximum magnitude error $\delta_s$, which occurs at the stopband edge, is greater than the ripple $\delta$ in case of the equiripple design.

In order to compare the resulting filter with the filter obtained using the LS approach, the LS filter was designed for the same specifications. For the LS filter, the maximum errors in the magnitude response are: in the passband $\delta_p = 0.045$, and in the stopband $\delta_s = 0.060$. In case of the proposed approach, the maximum error in the passband is considerably smaller and equals $\delta_p = 0.027$. In the stopband, the obtained maximum error is approximately the same as in case of the LS design.

As the second example, we consider the design of a 2-D centro-symmetric filter [17]. The desired magnitude specification is shown in Fig. 4. The passband of the filter is an elliptic region with a rotation angle of 30°. The major and minor axes of the passband edge are $0.45\pi$ and $0.225\pi$. The major and minor axes of the stopband edge are $0.65\pi$ and $0.375\pi$. The filter is designed with $N_1 = M_1 = 19$ and $\delta_p = 0.0365$. The resulting magnitude response $A = |H(\omega_1 k, \omega_2 l, \mathbf{Y})|$ is shown in Fig. 5. The maximum errors in the magnitude response are: in the passband $\delta_p = 0.0365$ and in the stopband $\delta_s = 0.0442$.

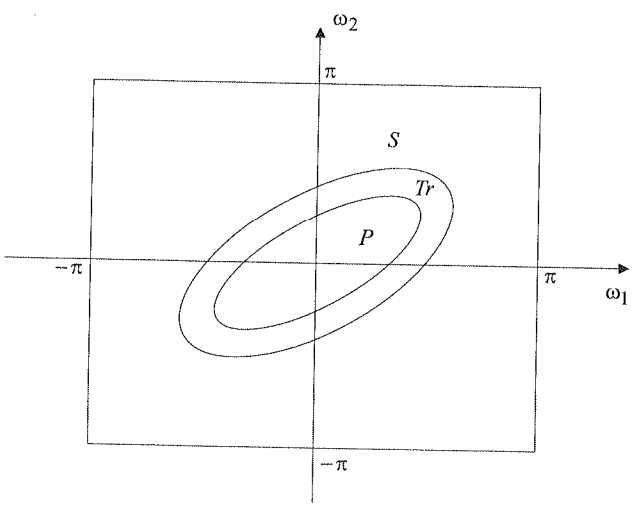


Fig. 4. Magnitude specification of a centro-symmetric filter

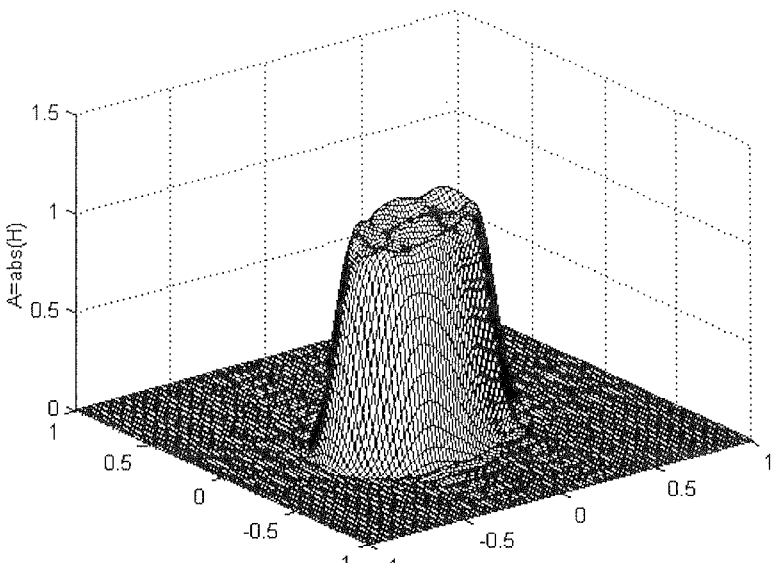


Fig. 5. Magnitude response of the filter designed the second example with $M_1 = N_1 = 19$ and $\delta_p = 0.0365$

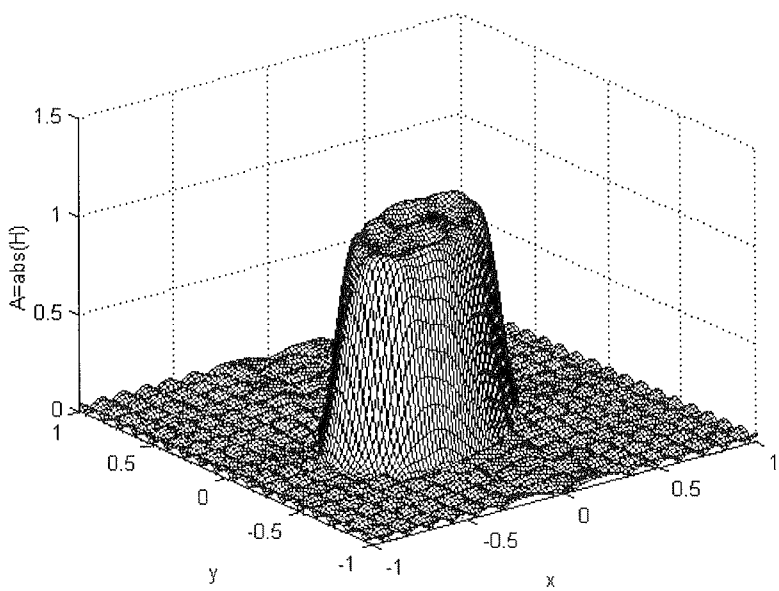


Fig. 6. Magnitude response of the equiripple filter designed in the second example with $M_1 = N_1 = 19$

In order to compare the resulting filter with the LS and equiripple filters, these filters were designed for the same specifications as in case of the proposed approach. The magnitude response A of the equiripple filter is shown in Fig. 6. The obtained ripple is $\delta = 0.0365$ both in the passband and in the stopband. The ripple $\delta$ is the same as $\delta_p$ in case of the proposed approach, but it is a bit smaller than the maximum error $\delta_s$ at the stopband edge. However, the magnitude error obtained using the proposed approach is smaller than $\delta$ in the significant part of the stopband.

For the LS filter, $\delta_p = 0.066$ and $\delta_s = 0.050$. Note that they are greater than the maximum errors of the magnitude response in the passband and in the stopband in case of the proposed approach.

In order to present the results obtained using the program F2CO with additional constraints on the maximum permissible error $\delta_p$ in the passband, we design a linear-phase 2-D FIR filter with complex coefficients and with the same specifications as in [7]. The desired magnitude specification is shown in Fig. 7. The passband is a circular region centred at $(-0.26\pi,\ 0.1\pi)$ with a radius of $0.3\pi$. The width of the transition band is $0.16\pi$. The filter is designed with $N_1 = M_1 = 21$. The maximum permissible error is $\delta_p = 0.032$. The resulting magnitude response $A = |H(\omega_1 k, \omega_2 l, \mathbf{Y})|$ is shown in Fig. 8. The maximum errors of the magnitude response in the passband and in the stopband are: $\delta_p = 0.032$ and $\delta_s = 0.043$. It difficult to compare the results obtained using the proposed method with the results reported in [7], because the values of the maximum stopband and passband errors are not provided in [7].

In order to compare the resulting filter with the filter obtained using the LS approach, the LS filter was designed for the same filter specifications. For the LS filter, the maximum errors of the magnitude response in the passband and in the stopband are: $\delta_p = 0.064$ and $\delta_s = 0.044$. Note that in case of the proposed approach, the maximum error in the passband is considerably smaller than in case of the LS design. In the stopband, the obtained maximum error is approximately the same as in case of the LS design.

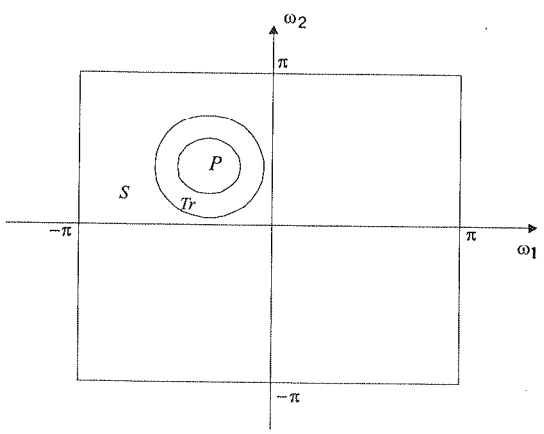


Fig. 7. Magnitude specification of a 2-D filter in the third example

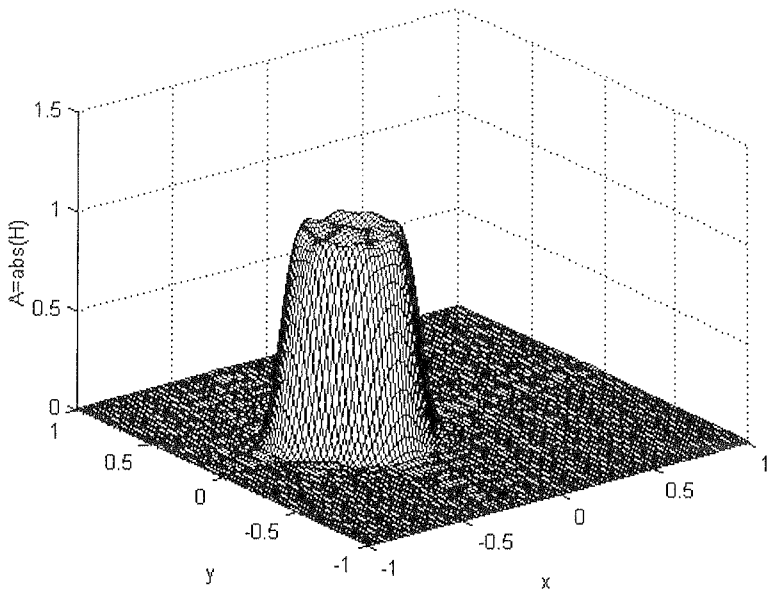


Fig. 8. Magnitude response of the filter designed in the third example with $M_1 = N_1 = 21$ and $\delta_p = 0.032$

## 5. CONCLUSIONS

In the paper, a technique for the design of 2-D linear-phase FIR filters with the equiripple passband and LS stopband has been proposed. A constraint on the maximum permissible error $\delta_p$ in the passband has also been included into the design problem. The proposed technique is general and can be used for the design of 2-D FIR filters with different symmetries, with both real- and complex-valued coefficients.

The design examples show that using the proposed approach, it is possible to obtain filters with magnitude responses, which are the trade-off between the equiripple passband and the LS stopband. The advantage of the proposed approach is the possibility of obtaining smaller maximum error $\delta_p$ in the passband than in case of the equiripple design. Using the proposed method it is also possible to obtain other prescribed values of $\delta_p$ in the passband. It is necessary to underline that for given $M_1$ and $N_1$ defining the number of the filter coefficients, there is some minimum value $\delta_p = \delta_{p\min}$. In order to obtain $\delta_p$ smaller than $\delta_{p\min}$, it is necessary to increase $M_1$ and/or $N_1$.

The proposed method requires shorter computational time than the equiripple design. It is also simple to implement The resulting optimization problem can be solved using standard constrained optimization methods, and efficient implementations

of these methods are available in different program libraries. The proposed method is also very flexible and additional linear and/or nonlinear constraints, e.g., regarding the magnitude response, can be included into the optimization problem.

## 6. REFERENCES


1. J. Lim: *Two-dimensional signal and image processing.* Englewood Cliffs, NJ, Prentice-Hall, 1990.
2. W.-S. Lu, A. Antoniou, H. Xu: *A direct method for the design of 2-D nonseparable filter banks.* IEEE Trans. Circuits and Syst.- II: Analog and Digital Signal Processing, 1998, vol. 45, no 8, pp. 1146-1150.
3. S.-I. Park, M.J.T. Smith, R.M. Mersereau: *Improved structures of maximally decimated directional filter banks for spatial image analysis.* IEEE Trans. Image Processing, 2004, vol. 13, no 11, pp. 1424-1431.
4. W.-S. Lu: *A unified approach for the design of 2-D digital filters via semidefinite programming.* IEEE Trans. Circuits and Syst.- I: Fundamental Theory and Applications, 2002, vol. 49, no 6, pp. 814-826.
5. W.-P. Zhu, M.O. Ahmad, M.N. Swamy: *A closed-form solution to the least-square design problem of 2-D linear-phase FIR filters.* IEEE Trans. Circuits and Syst.- II: Analog and Digital Signal Processing, 1997, vol. 44, no 12, pp. 1032-1039.
6. W.-P. Zhu, M.O. Ahmad, M.N. Swamy: *A least-square design approach for 2-D FIR filters with arbitrary frequency response.* IEEE Trans. Circuits and Syst.- II: Analog and Digital Signal Processing, 1999, vol. 46, no 8, pp. 1027-1034.
7. S.C. Pei, J.J. Shyu: *Fast design of 2-D linear-phase complex digital filters by analytical least squares method,* IEEE Trans. Signal Proc., 1996, vol. 44, no 12, pp. 3157-3161.
8. W.-P. Zhu, M.O. Ahmad, M.N. Swamy: *Realization of 2-D linear-phase filters by using singular-value decomposition.* IEEE Trans. Signal Processing, 1999, vol. 47, no 8, pp. 1349-1358.
9. T.-B. Deng, E. Saito, E. Okamoto: *Efficient design of SVD-based 2-D digital filters using specification symmetry and order-selecting criterion.* IEEE Trans. Circuits and Syst.- I: Fundamental Theory and Applications, 2003, vol. 50, no 2, pp. 217-256.
10. M.T. Hanna: *A singular value decomposition derivation in the discrete frequency domain of optimal noncentro-symmetric 2-D FIR filters.* IEEE Trans. Signal Processing, 1998, vol. 46, no 5, pp. 1397-1402.
11. E. Gislason, M. Johansen, K. Conradsen, B.K. Ersboll, S.K. Jacobsen: *Three different criteria for the design of two-dimensional zero phase FIR digital filters.* IEEE Trans. Signal Processing, 1993, vol. 41, no 10, pp. 3070-3074.
12. M. Lang, I.W. Selesnick, C.S. Burrus: *Constrained least squares design of 2-D FIR filters.* IEEE Trans. Signal Processing, 1996, vol. 44, no 5, pp. 1234-1241.
13. J.W. Adams, J.L. Sullivan: *Peak-constrained least-squares optimization.* IEEE Trans. Signal Processing, 1998, vol. 46, No 2, pp. 306-320.
14. J. Nocedal, S.J. Wright: *Numerical optimization.* Berlin Heidelberg New York, Springer-Verlag, 1999.
15. T. Kręglewski, T. Rogowski, A. Ruszczyński, J. Szymanowski: *Optimization methods in FORTRAN,* Warszawa, PWN, 1984 (in Polish).
16. F. Wysocka-Schillak: *Design of 2-D linear-phase FIR filters with equiripple magnitude response.* Proc. of IEEE EUROCON 2003, Computer as a Tool, Ljubljana (Slovenia) Sept. 2003, pp. 76-79.
17. F. Wysocka-Schillak: *Design of 2-D FIR centro-symmetric filters with equiripple passband and least-squares stopband.* Proc. of the European Conference on Circuit Theory and Design ECCTD 2003, Cracow, September 2003, paper III-113-116.

# INFORMATION FOR AUTHORS OF E.T.Q.

An article published in other magazines can not be submitted for publishing in E.T.Q. TThe size of an article can not exceed 30 pages, 1800 character each, including figures and tables.

**Basic requirements**

The article should be submitted to the editorial stuff as a one side, clear, black and white computer printout in two copies. The article should be prepared in English. Floppy disc with an electronic version of the article should be enclosed. Preferred wordprocessors: WORD 6 or 8.

Layout of the article.

- Title.
- Author (first name and surname of author/authors).
- Workplace (institution, adress and e-mail).
- Concise summary in a language article is prepared in (with keywords).
- Main text with following layout:
  - Introduction
  - Theory (if applicable)
  - Numerical results (if applicable)
  - Paragraph 1
  - Paragraph 2
  - .....
  - .....
  - Conclusions
  - Acknowledgements (if applicable)
  - References
- Summary in additional language:
  - Author (firs name initials and surname)
  - Title (in Polish, if article was prepared in English)
  - Extensive summary, hawever not exceeching 3600 characters (along with keywords) in Polish, if artide was prepared in English). The summary should be prepared in a way allowing a reader to obtaoin essential information contained in the artide. For that reason in the summary author can place numbers of essential formulas, figures and tables from the article.

Pages should have continues numbering.

**Main text**

Main text cannot contain formatting such as spacing, underlining, words written in capital letters (except words that are commonly written in capital letters). Author can mark suggested formatting with pencil on the margin of the article using commonly accepted adjusting marks.

Text should be written with double line spacing with 35 mro left and right margin. Titles and subtitles should be written with small letters. Titles and subtitles should be numberd using no mor than 3 levels (i.e. 4.1.1.).

**Tables**

Tables with their titles should be places on separate page at the end of the article. Titles of rows and columns should be written in small letters with double line spacing. Annotations concerning tables should be placed directly below the table. Tables should be numbered with Arabic numbers on the top of each table. Table can contain algorithm and program listings. In such cases original layout of the table will be preserved. Table should be cited in the text.

**Mathematical formulas**

Characters, numbers, letters and spacing of the formula should be adequate to layout of main text. Indexes should be properly lowered or raised above the basic line and clearly written. Special characters such as lines, arrows, dots

should be placed exactly over symbols which they ar attributed to. Formulas should be numbered with Arabic numbers place in brackets on the right side of the page. Units of measure, letter and graphic symbols should be printed according to requirements of IEE (International Electronical Commission) and ISO (International Organisation of Standardisation).

**References**

References should be placed at the and of the main text with th subtitle „References". Refrences should be numbered (without brackets) adequately to references placed in the text. Examples of periodical [@], non-periodical [2] and book [3] references:

1. F. Valdoni: A new milimetre wave satelite. E.T.T. 1990, vol. 2, no 5, pp. 141–148
2. K. Anderson: A resource allocation framework. XVI International Symposium (Sweden). May 1991. paper A 2.4
3. Y.P. Tvidis: Operation and modeling of the MOS transistors. Nw York. McGraw-Hill. 1987. p. 553

**Figures**

Figures should be clearly drawn on plain or milimetre paper in the format not smaller than $9 \times 12$ cm. Figures can be also printed (preferred editor – CorelDRAW). Photos or diapositives will be accepted in black and whit format not gratd than $10 \times 15$ cm. On th margin of each drawing and on th back side of each ohoto authorp name and abbreviation of the title of article should be placed. Figure's captures should be given in two languages (first in the language the article is writtes in and then in additional language). Figure's captures should be also listed on separate page. Figures should be cited in the text.

**Additional information**

On the separate page following information should be placed:

- mailing address (home or office),
- phone (home or/and office),
- e-mail.

Author is entiled to free of charge 20 copies of article. Additional copies or the whole magazine can be ordered at publisher at th one's expense.

Author is obliged to perform the author's correction, which should be accomplished within 3 days starting from the date of receiving the text from the editorial stuff. Corrected text should be returned to the editorial stuff personally or by mail. Correction marks should be placed on th margin of copies received from the editorial stuff or if needed on separate pages. In the case when the correction is not returned within said time limit, correction will be performed by technical editorial stuff of the publisher.

In case of changing of workplace or home address Authors are asked to inform the editorial stuff.